Evaluating 3D In Vitro Models for Translational Relevance: From Spheroid Architecture to Clinically Relevant Potency

By

Yiyin Chen

BA, Case Western Reserve University, May 2024

Thesis

Submitted in partial fulfillment of the requirements for the Degree of Master of Science in the Graduate Program of Biotechnology at Brown University

PROVIDENCE, RHODE ISLAND

May 2026

This thesis by Yiyin Chen is accepted in its present form by the Graduate Program in Biotechnology as satisfying the thesis requirements for the degree of Master of Science

Date_____ Signature: _____

Dr. Anubhav Tripathi, Advisor

Date_____ Signature: _____

Dr. Sean Lawler, Reader

Date_____ Signature: _____

Dr. Theresa Raimondo, Reader

Approved by the Graduate Council

Date_____ Signature: _____

Dr. David P. Lindstrom, Dean of the Graduate School

Vita

Yiyin Chen received a Bachelor of Science in Biochemistry from Case Western Reserve University in May 2024. During undergraduate studies, he focused on noncanonical post-translational modification of IL-17/Act1 pathway with 2D culture model validation. At Brown University, he pursued a Master of Science in Biotechnology, conducting research in 3D cell culture and tissue culture systems and therapeutic evaluation frameworks under the supervision of Dr. Anubhav Tripathi. His work integrates experimental and conceptual approaches to improve the interpretation of in vitro models for translational applications.

Acknowledgements

I would like to express my deepest gratitude to the Tripathi Lab for providing an intellectually stimulating and supportive environment throughout the duration of this research. The collective expertise and camaraderie within the lab have been instrumental in shaping my development as a researcher. I also wish to thank Professor Jacquelyn Schell and Professor Adam Crego for their invaluable guidance from the Biotechnology program.

I am profoundly grateful to Professor Anubhav Tripathi for his exceptional mentorship, vision, and unwavering guidance. His insights were fundamental to the conceptualization and execution of this project. My special and sincere thanks also go to Sarah Planchak, whose dedicated support and technical expertise from the very beginning were indispensable to the progress of this work.

This work was further strengthened by the support of my thesis committee. I am incredibly thankful to Professor Sean Lawler and Professor Theresa Raimondo for their vital roles in overseeing this research and providing the perspective necessary for this thesis.

I also would like to thank Alejandra Hernandez Moyers and Owen Lockwood for their incredible and essential support in laboratory work and manuscript writing.

Finally, this work would not have been possible without the essential funding, resources, and technical partnership provided by Revvity.

Table of Contents

Table of Tables

Table of Figures

Chapter 1—General Introduction

Preclinical in vitro models occupy a central position in modern biomedical research because they offer controlled, scalable, and mechanistically tractable systems for studying disease biology and therapeutic response. Yet their utility depends not only on convenience or throughput, but on how faithfully they preserve the biological constraints that shape function in human tissues[1]. Conventional two-dimensional (2D) cultures remain indispensable for early screening because they are standardized, inexpensive, and well suited for quantifying molecular and early phenotypic responses under controlled exposure conditions[2]. However, by flattening cells onto plastic, they remove many of the spatial, architectural, and microenvironmental features that influence cellular behavior in vivo[2,3]. As a result, the same system that performs well for reductionist measurement may perform poorly when the scientific question depends on tissue structure, diffusion, extracellular matrix, or multicellular interaction[2].

This problem is especially important in fields where biological function is inseparable from higher-order tissue organization. In hepatic research, the physiological relevance of a model depends on whether hepatocyte-like cells can maintain architecture, metabolic activity, and synthetic function in a way that better approximates native tissue[4,5]. In cancer therapeutics, especially for modern biologics and RNA-based interventions, the critical question is often not simply whether a target can be modulated in isolated cells, but whether that activity survives the barriers imposed by three-dimensional (3D) tumor architecture, heterogeneous exposure, extracellular matrix, and local immune or stromal context[3,6,7]. In both settings, 2D systems remain useful as first-line tools, but they often under-represent the rate-limiting constraints that determine whether a biological effect is likely to remain meaningful beyond the dish[2,4].

These limitations have driven growing interest in 3D in vitro systems, including spheroids, patient-derived organoids, and organoid-based co-culture or microfluidic platforms[2,3,8]. Such models can restore features lost in monolayer culture, including radial gradients, cell-cell and cell-matrix interactions, and, in some cases, clinically relevant heterogeneity or multicompartment signaling[2,3,9]. For hepatocyte-like

cultures, 3D spheroids can improve functions such as albumin production and other physiologically relevant outputs compared with planar culture[4,10]. For tumor models, spheroids and organoids can make delivery barriers, local exposure heterogeneity, and architectural resistance mechanisms experimentally visible in ways that 2D assays cannot[2,3,7]. At the same time, current organoid-based RNA potency workflows are often used as selective confirmation or filtering layers after 2D screening rather than as primary, fully standardized potency-defining systems[8,11,12]. Taken together, these features and current deployment patterns have led to a widespread but often oversimplified assumption that "3D" is inherently more relevant than "2D," but the reality is more complicated.

A central premise of this thesis is that 3D model architecture is not a neutral technical detail. Models that are all described as spheroids or organoids may differ substantially in geometry, aggregation mechanics, diffusion behavior, reproducibility, throughput, and biological output[2,13]. In current HepG2 literature, even the term *spheroid* is used loosely across platforms that yield markedly different structures, making direct comparison difficult and limiting reproducibility[14–16]. Likewise, in the tumor-organoid literature, organoids, cell-line spheroids, air-liquid interface cultures, and microfluidic systems are often grouped together under the broad label of 3D culture despite probing very different aspects of biology[2,3,8]. A model is therefore not informative merely because it is more complex. It is informative when its architecture preserves the specific barriers or interactions that are actually relevant to the question being asked.

This thesis addresses that problem from two complementary directions. The first is experimental and focuses on HepG2 spheroid culture as a model-system design question. In Chapter 2, five commonly used spheroid-generation methods were systematically compared across seeding density and culture duration: 35- and 96-microwell agarose gels, microwell and single-well ultra-low attachment plates, and hanging drop. The study was motivated by the observation that 3D HepG2 models are widely used but insufficiently standardized, and that method-dependent variation may itself influence the biological conclusions drawn from these systems. The results showed that the culture platform strongly affected spheroid morphology and function. In particular, 35-microwell agarose gels produced the most circular

spheroids; among the multi-spheroid formats functionally assessed, they also yielded the strongest albumin and ATP outputs. Meanwhile, no single method simultaneously maximized throughput, repeatability, and functional robustness. Taken together, these findings argue that the choice of 3D culture method can materially shape the behavior being measured and therefore the interpretation of model performance.

The second direction is conceptual and concerns how biologic activity should be interpreted once clinically relevant constraints are reintroduced. Chapter 3 examines organoid-based potency assays for RNA therapeutics in solid tumors and develops the framework of **clinically relevant potency**. Under this framework, potency is not treated as a single universal number, but as a layered relationship between dose and mechanism-appropriate functional response. Molecular potency captures target engagement and proximal signaling effects; cellular or phenotypic potency captures downstream cellular outcomes such as viability, apoptosis, or invasion; and clinically relevant potency captures the same dose-response behavior under conditions that preserve the barriers and interactions that are rate-limiting for therapeutic performance. For RNA therapeutics, these may include 3D diffusion distances, extracellular matrix, heterogeneous tissue exposure, and, when present, immune or stromal constraints. This framework moves the field beyond a simplistic 2D-versus-3D binary by asking a more rigorous question: when does additional model complexity produce decision-relevant information rather than technical cost alone?

Although the two chapters address different biological systems, they converge on the same thesis-level argument. The HepG2 study demonstrates experimentally that different 3D platforms are not interchangeable even when they nominally model the same cell type. The RNA-organoid review extends that insight by arguing that model selection should be governed by mechanism and by the specific failure modes one is trying to reveal. In other words, biological relevance is not conferred by complexity alone, but by matching model architecture to the mechanistic bottleneck under investigation. A compact cell-line spheroid may be sufficient as a first-pass filter for diffusion-limited delivery failure; a patient-derived organoid may be more suitable for probing patient-linked epithelial heterogeneity; and an immune- or stromal-constrained organoid may be needed when therapeutic function depends on multicellular

microenvironmental interactions. Conversely, when the central question is sequence activity or proximal target modulation under uniform exposure, simpler 2D assays may remain the most appropriate system.

Viewed together, these chapters support a broader methodological principle for translational bioengineering and preclinical model design. The goal is not simply to replace 2D assays with 3D systems, nor to treat organoids and spheroids as inherently superior proxies of in vivo biology. Rather, the goal is to develop a more disciplined logic for selecting, building, and interpreting in vitro models according to the biological constraints that matter for the experimental endpoint. From this perspective, model architecture becomes an experimental variable in its own right: one that shapes morphology, function, assay readout, and ultimately translational inference. This thesis therefore argues for a shift from model adoption by convention to model selection by mechanistic relevance. In doing so, it links a concrete experimental comparison in hepatic spheroid culture with a general framework for evaluating clinically relevant potency in tumor organoid systems, providing both a practical and conceptual basis for more rigorous use of 3D in vitro models.

References—Chapter 1

1. Loewa, A., Feng, J. J. & Hedtrich, S. Human disease models in drug development. *Nat Rev Bioeng* **1**, 545–559 (2023).

2. Jubelin, C. *et al.* Three-dimensional in vitro culture models in oncology research. *Cell Biosci* **12**, 155 (2022).

3. Polak, R., Zhang, E. T. & Kuo, C. J. Cancer organoids 2.0: modelling the complexity of the tumour immune microenvironment. *Nat Rev Cancer* **24**, 523–539 (2024).

4. Godoy, P. *et al.* Recent advances in 2D and 3D in vitro systems using primary hepatocytes, alternative hepatocyte sources and non-parenchymal liver cells and their use in investigating mechanisms of hepatotoxicity, cell signaling and ADME. *Arch Toxicol* **87**, 1315–1530 (2013).

5. Cox, C. R., Lynch, S., Goldring, C. & Sharma, P. Current Perspective: 3D Spheroid Models Utilizing Human-Based Cells for Investigating Metabolism-Dependent Drug-Induced Liver Injury. *Front. Med. Technol.* **2**, 611913 (2020).

6. Liu, C. *et al.* mRNA-based cancer therapeutics. *Nat Rev Cancer* **23**, 526–543 (2023).

7. Gonzalez, J. C. *et al.* Nano Approaches to Nucleic Acid Delivery: Barriers, Solutions, and Current Landscape. *WIREs Nanomed Nanobiotechnol* **17**, e70010 (2025).

8. Park, B. *et al.* Advances in organoid-on-a-chip for recapitulation of human physiological events. *Materials Today* **84**, 75–94 (2025).

9. Luo, Z. *et al.* Reconstructing the tumor architecture into organoids. *Advanced Drug Delivery Reviews* **176**, 113839 (2021).

10. Fey, S. J. & Wrzesinski, K. Determination of Drug Toxicity Using 3D Spheroids Constructed From an Immortal Human Hepatocyte Cell Line. *Toxicological Sciences* **127**, 403–411 (2012).

11. Wang, Q., Yuan, F., Zuo, X. & Li, M. Breakthroughs and challenges of organoid models for assessing cancer immunotherapy: a cutting-edge tool for advancing personalised treatments. *Cell Death Discov.* **11**, 222 (2025).

12. Tong, L. *et al.* Patient-derived organoids in precision cancer medicine. *Med* **5**, 1351–1377 (2024).

13. Park, S. Y., Hong, H. J. & Lee, H. J. Fabrication of Cell Spheroids for 3D Cell Culture and Biomedical Applications. *BioChip J* **17**, 24–43 (2023).

14. Hurrell, T., Ellero, A. A., Masso, Z. F. & Cromarty, A. D. Characterization and reproducibility of HepG2 hanging drop spheroids toxicology in vitro. *Toxicology in Vitro* **50**, 86–94 (2018).

15. Hirschhaeuser, F. *et al.* Multicellular tumor spheroids: An underestimated tool is catching up again. *Journal of Biotechnology* **148**, 3–15 (2010).

16. Härmä, V. *et al.* A Comprehensive Panel of Three-Dimensional Models for Studies of Prostate Cancer Growth, Invasion and Drug Responses. *PLoS ONE* **5**, e10431 (2010).

Chapter 2—Comparative Evaluation of HepG2 Spheroid Generation Methods for Toxicology

Note: This Chapter is adapted from Planchak, S., Hernandez Moyers, A., Chen, Y. *et al.* Comparative Evaluation of HepG2 Spheroid Generation Methods for Toxicology. *Cel. Mol. Bioeng.* (2026). Some changes have been made to fit Master's thesis style.

Introduction

The liver's primary role in processing external compounds and pathologies makes it a critical target for sophisticated *in vitro* models. A wide range of agents, including antibiotics, other drugs, herbs, and toxins, have been shown to harm the liver[1]. Drug-induced liver injury (DILI), the major cause of acute liver injury in the US accounts for up to 50% of acute hepatic failures from commercially approved drugs[2–5]. Liver cancers, including hepatoblastoma and hepatocellular carcinoma, remain the sixth leading cause of cancer-related deaths worldwide[6]. The lack of accurate preclinical drug evaluation platforms has led to approved drug withdrawals, impacting patients and pharmaceutical companies[7]. This highlights the need for accurate models to study treatments for liver pathologies and xenobiotic genotoxicity.

When xenobiotics enter the gastrointestinal tract, they undergo first-pass metabolism in the liver, where hepatocytes transform xenobiotics and secrete many of their conjugates into bile, while separately detoxifying ammonia via the urea cycle for renal excretion[8,9]. Hepatic cells, primarily hepatocytes, play a key role in metabolic processes (i.e., glycogenolysis, amino acid metabolism, beta-oxidation, synthesis of ketone bodies), synthesis and secretion of serum proteins (i.e., albumin and coagulation factors), and the expression of enzymes (CYP450) necessary for eliminating toxic elements[7,10,11]. Therefore, hepatic cells are a physiologically and clinically relevant target to examine xenobiotic-induced toxicity, including genotoxicity or anticancer drug treatments.

Primary human hepatocytes (PHHs) are widely regarded as a gold-standard in vitro model for hepatic xenobiotic metabolism and toxicology studies because they retain a more physiologically relevant hepatic gene-expression profile and metabolic enzyme activity than transformed liver cell lines[11–14].

However, these hepatic functions progressively decline in culture as hepatocytes dedifferentiate, and substantial inter-donor variability can further complicate study interpretation[11,13,14]. Despite recent advances in dissociation methods[15], these cells are also difficult to isolate, scarce in availability, non-expandable in culture, and quickly begin to dedifferentiate, compromising key hepatic functions[16,17]. As a result, models that minimize the use of primary, patient-derived cells accommodate standardized and reproducible experimentation while maintaining physiologically relevant function, providing a balance between biological fidelity and experimental practicality. HepG2 cells, a human liver cancer-derived or hepatoblastoma cell line, offer an attractive alternative due to their unlimited growth potential, availability, and manageability in experiments.

In vitro models offer a compelling alternative to animal models, overcoming limitations such as species-differences, cost, time, ethical concerns, and predictivity issues. HepG2 spheroids are increasingly popular tools for comprehensively assessing not only genotoxic effects and potential for DILI, but also for broadening understanding of complex liver pathologies. HepG2 models have aided the investigation of liver cancers (e.g., hepatoblastoma, hepatocellular carcinoma), viral infections (e.g., hepatitis), and metabolic liver diseases (e.g., MASH, MetALD)[18–24]. Thus, HepG2 cells provide a versatile, physiologically relevant platform for advancing liver research, understanding disease pathogenesis, and ensuring safer drug development.

Conventional two-dimensional (2D) HepG2 monolayers retain viability and some stress-response transcription (e.g., Nrf2-regulated programs), but they display low or variably expressed drug-metabolizing enzymes with poor inducibility compared with primary human hepatocytes—most notably CYP3A4, CYP2D6 and several UGTs/SULTs—which constrains metabolic competence and toxicology predictivity[11,14,25–29]. Although xenobiotic receptors, such as PXR and CAR, are present, their downstream transcriptional activation of phase-I/II enzymes and transporters is often blunted in 2D, yielding muted induction phenotypes[13,14]. In parallel, planar culture fails to establish hepatocyte architecture, including apical–basolateral polarity, bile-canaliculus formation, and robust cell–cell/ECM cues, which alters

transporter localization (e.g., BSEP/MRP2) and signaling, further reducing in vivo relevance[11,23]. Collectively, these features explain why 2D HepG2 is useful for screening but underperforms against 3D/PHH systems for mechanism-anchored metabolism and DILI prediction[26–29].

3D models show more promising results, reflecting *in vivo* conditions more accurately. HepG2 3D spheroids demonstrate close cell-to-cell and cell-to-matrix contacts[28,29], better cell turnover[30], and some methods have exhibited upregulation of toxicity-responsive genes and CYP450 enzyme expression compared to 2D cultures[27–29,31,32]. Because they more accurately replicate physiological conditions, HepG2 cells in 3D models exhibit many *in vivo* metabolic functions, such as higher production of proteins (i.e., albumin), glutamate, urea synthesis, absorption of branched-chain amino acids, and increased cytochrome expression[11,33]. Given that multiple cell types collaborate in the body to respond to xenobiotics, coculture is frequently proposed as a method to enhance existing models. However, integrating multiple cell lines makes experimental analysis and interpretation of cellular behavior challenging[7]. Thus, 3D HepG2 models are well-suited for both comprehensive drug testing, including assessing DILI cytotoxicity, and for investigating the fundamental behavior and progression of liver-related diseases [7,11,27–29,33,34].

However, the term spheroid is loosely defined and is applied to various methods that yield vastly different 3D models. This includes characterizing loosely packed cells as spheroids, which leads to inconsistencies in cell-to-cell interactions and behaviors[5,35]. In prostate cell lines, four distinct morphologies were characterized but their morphological characteristics could not be directly compared to those observed in hanging drops, a method where gravitational forces promote cell aggregation[36,37]. Thus, while 3D models offer a more physiologically accurate alternative to 2D, the lack of standardization, characterization, and reproducibility across available models prevents consistent results in 3D HepG2 models, hindering their reliable application for investigating liver pathogenesis and xenobiotic toxicity[38,39].

Previous research has examined methods available for 3D models[40]. Comprehensive reviews have compared current spheroid-formation methods for 3D culture, including discussions of standardization and evaluations across a variety of cell lines[31,41]. However, these analyses were not centered on HepG2 cells.

Breslin and colleagues reviewed hanging-drop, forced-floating, agitation-based, and microfluidic approaches for HepG2 cells. However, because the field still lacks controlled comparisons performed under consistent conditions across methods, it remains difficult to determine which platform is most suitable for genotoxicity studies or liver disease modeling[42]. While experimental attempts have characterized HepG2 properties relevant to toxicity studies and disease progression, the reliance on a single spheroid formation method impedes direct comparison for optimizing these methods[27,28].

This study involves a controlled experiment where we examine current methods for 3D spheroid formation with HepG2 cells, directly comparing their results. Therefore, this paper aims to enhance understanding in the field by systematically comparing commonly used methods for 3D spheroid formation from HepG2 cells—namely hanging drop, microwell plates, ultra-low attachment (ULA) plates, and agarose gels **(Figure 1)**—and evaluating their effects on viability, morphology, and hepatocyte-like function. We chose these methods for spheroid generation because they collectively represent the most widely used and mechanistically distinct strategies for 3D culture: agarose microtissue gels provide inert, non-adhesive surfaces that promote uniform aggregation; ULA plates offer a high-throughput, reproducible platform; and hanging drops enable gravity-driven, scaffold-free assembly that minimizes external interference with cell–cell interactions. Together, these approaches capture the range of physical forces and material interactions that govern spheroid formation, enabling a systematic evaluation of their morphological and functional outcomes.

For functional analysis, we selected assays that capture complementary aspects of hepatic physiology: human-specific ELISA for albumin secretion as a measure of hepatocyte synthetic function, and the CellTiter-Glo 3D assay for intracellular ATP as an indicator of metabolic activity and viability[38,43–45]. Circularity was emphasized as a key morphological descriptor because spheroid geometry directly influences nutrient and oxygen diffusion; computational models demonstrate that more circular and compact spheroids maintain physiologic oxygen gradients and develop hypoxic cores, thereby better replicating *in vivo* tumor microenvironments relevant to drug screening[46]. Functional assays were restricted

to multi-spheroid formats to ensure sufficient analyte volume, reproducibility, and statistical power, while single-spheroid formats were excluded due to limited sampling volume, and low signal generation.

By systematically dissecting how each method shapes spheroid structure and function, this study establishes a framework for selecting and optimizing 3D HepG2 culture systems tailored to specific applications—from drug toxicity screening to liver disease modeling—thereby advancing the reproducibility, scalability, and physiological relevance of *in vitro* hepatic models.

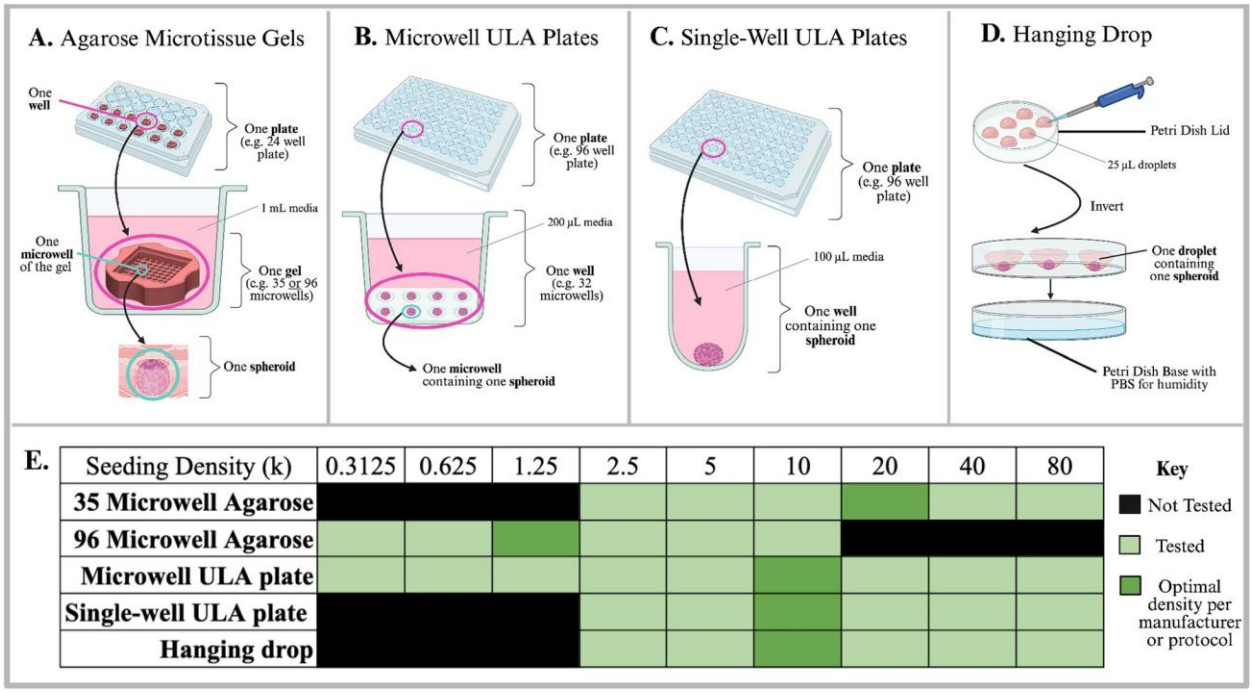

Figure 1. Diagrams representing various HepG2 spheroid generation platforms.

Agarose microtissue gels (A), Microwell ULA plate (B), Single-well ULA plate (C), and Hanging Drop (D). Table showing different seeding densities per spheroid across 3D culture methods, with a key on the right (E). Figure made using BioRender.

Methods

HepG2 Cell Culture

Human hepatocellular carcinoma cells (HepG2, ATCC HB-8065) were obtained from the American Type Culture Collection (ATCC, Manassas, VA) and expanded in T-75 flasks using Eagle's Minimum Essential Medium (EMEM) supplemented with 10% fetal bovine serum (FBS) and 1% penicillin–streptomycin[47,48]. Cultures were maintained under standard conditions (37 °C, 5% CO_2), with media changes every other day and passaging performed weekly. Cells were used for experiments between passages 4 and 10. Upon reaching ~ 80% confluence, at around 7 days after seeding, cultures were washed with 5 mL phosphate-buffered saline (PBS) and incubated with 5 mL of 0.25% trypsin for 5 min to detach the monolayer from the culture flask. Trypsinization was quenched by adding 5 mL of pre-warmed media, and the resulting cell suspension was collected into 15 mL conical tubes and centrifuged at 180 × g for 5 min. The supernatant was aspirated, and the pellet was resuspended in 3 mL of media, followed by gentle pipette mixing to disaggregate any clumps. Cells were stained with Acridine Orange/Propidium Iodide (ViaStain™ AOPI staining solution, Revvity, Waltham, MA) and counted using the Cellaca MX imaging cytometer (Revvity, Waltham, MA). Following counting, a fresh T-75 flask was seeded with 1.25 million cells in 15 mL of complete media, gently rocked to ensure even distribution, and returned to the incubator for continued culture under standard conditions (37 °C, 5% CO2). Following counting, cells that were not seeded in T-75 flasks were used for seeding spheroids. Spheres for all methods were incubated under standard culture conditions without further media changes to ensure consistency between different spheroid generation methods. All cell culture work, spheroid seeding, or sphere handling/processing was carried out in aseptic conditions in a biosafety cabinet. Cell counts are hereafter expressed as A × 10B cells. For convenience, when B = 3, we denote this as A k cells (e.g., 1.25 k cells = 1.25×10^3 cells). Furthermore, seeding densities hereafter refer to the approximate number of cells seeded per spheroid, unless otherwise specified.

Spheroid Generation Methods

Agarose Microtissue Gels

3D agarose microtissue gels (**Figure 1A**) were fabricated using 3D Petri Dish® molds (Microtissues, Inc., Providence, RI) designed for small (24–96 format) and large (24–35 format) spheroids[49,50]. Molten 2% ultrapure agarose (dissolved in PBS) was pipetted into each mold (casted) and allowed to solidify at room temperature. Once fully gelled, agarose constructs were removed (demolded) from the molds and transferred to individual wells of a 24-well tissue culture plate. Each well was filled with 1 mL of serum-free media and incubated under standard conditions for at least 24 h to equilibrate the gels. For seeding, cell suspensions were prepared in complete media and seeded directly into the microwells in a volume of 70 µL per gel. Following seeding, gels were allowed to rest undisturbed for 30 min to permit cell settling into microwells, after which 1 mL of pre-warmed complete media was gently added to each well. Small spheroid gels containing 96 microwells per gel were seeded with 960 k, 480 k, 240 k, 120 k, 60 k, and 30 k cells per gel, corresponding to approximately 10 k, 5 k, 2.5 k, 1.25 k, 0.625 k and 0.3125 k cells per microwell **(Figure 1E)**, respectively. Large spheroid gels containing 35 microwells per gel were seeded with 2800 k, 1400 k, 700 k, 350 k, 175 k, and 87.5 k cells per gel, corresponding to approximately 80 k, 40 k, 20 k, 10 k, 5 k, and 2.5 k cells per microwell **(Figure 1E)**, respectively.

Microwell ULA Plates

AggreWell™ HT 96-well plates (STEMCELL Technologies, Vancouver, Canada)[51], containing 32 microwells per well, were utilized **(Figure 1B)**. Each well was first treated with 75 µL of Anti-Adherence Rinsing Solution (STEMCELL Technologies), reverse pipetted to minimize bubble formation, and incubated at room temperature for 5 min. The solution was then aspirated, and wells were washed with 200 µL of serum-free media. After washing, serial dilutions of cells were seeded at 2560 k, 1280 k, 640 k, 320 k, 160 k, 80 k, 40 k, 20 k, and 10 k cells per well in a final volume of 200 µL, corresponding to

approximately 80 k, 40 k, 20 k, 10 k, 5 k, 2.5 k, 1.25 k, 0.625 k and 0.3125 k cells per microwell **(Figure 1E)**, respectively.

Single-Well ULA Plates

CellCarrier™ Spheroid Ultra-Low Attachment (ULA) 96-well plates (Revvity, Waltham, MA)[52] were used for formation of one spheroid per well **(Figure 1C)**. Serial dilutions of 80 k, 40 k, 20 k, 10 k, 5 k, and 2.5 k cells per well **(Figure 1E)** were seeded directly into individual wells in complete media at a final volume of 100 µL per well. Each well supported the formation of a single spheroid.

Hanging Drop

The hanging drop method **(Figure 1D)** was used to generate single spheroids in suspension[32,53]. Petri dishes were prepared with sterile PBS in the base to maintain humidity. Twenty-five microliter droplets of cell suspensions were pipetted onto the inner surface of the dish lid, and the lid was immediately inverted over the PBS-filled base. Drops containing 80 k, 40 k, 20 k, 10 k, 5k, and 2.5 k cells **(Figure 1E)** per 25 µL were used. Each droplet produced a single spheroid by gravity-mediated aggregation.

Methods for Result Analysis

Brightfield Microscopy and ImageJ Analysis

Brightfield imaging was conducted using the EVOS M5000 Imaging System (ThermoFisher Scientific, Waltham, MA) for spheroids formed in agarose microtissue gels, microwell ULA plates, and single-well ULA plates. Hanging drop spheroids were imaged using an ECLIPSE Ti fluorescence microscope (Nikon, Tokyo, Japan) equipped with a motorized stage, direct illumination LED (Thorburn), a multichannel light source (Lumencor Spectra-X), cMOS camera (Andor Neo), and a × 4 objective (Nikon Plan Fluor, NA = 0.13) [34,54]. For imaging, Petri dish lids containing hanging drops were carefully,

aseptically transferred to a clean, PBS-free base and re-inverted to orient the droplets downward on the imaging surface. After imaging, lids were returned to the original PBS-filled base to maintain humidity. Images were taken on days 1, 3, 5, and 7 after initial seeding.

Brightfield images of HepG2 spheroids were segmented by INSIDIA 2.0, an ImageJ Macro developed by Perimi et al. (https://valentinapalmieri.wixsite.com/insidia/nature)[55]. INSIDIA 2.0 was also used to measure each sphere's geometric parameters, such as radius and circularity, which can function as proxies of sphericity from 2D images. To quantify the average radius in image analysis, INSIDIA 2.0 measured the best-fit ellipse of the segmented spheroid, defined as the ellipse that most accurately matched the spheroid shape using least-squares fitting. The radius measured was half of the major axis of that ellipse.

ELISA for Human Albumin

Following the final day (day 7) of brightfield imaging, the supernatant was extracted for analysis. Human albumin secretion was quantified using the Human Albumin ELISA Kit (ThermoFisher Scientific, Waltham, MA, Cat.# EHALB), following the manufacturer's instructions[56]. For spheroids generated in agarose microtissue gels, 1 mL of culture supernatant per condition was harvested for analysis. For spheroids formed in microwell ULA plates, 30 µL of supernatant per well was collected.

Samples and standards were prepared according to the kit protocol, added to antibody-coated 96-well plates, and incubated with the detection antibody and streptavidin–HRP conjugate. After washing steps, substrate solution was applied, and absorbance was measured at 450 nm using a microplate reader. A standard curve was generated from serial dilutions of recombinant human albumin provided in the kit. Luminescence was measured using a BioTek Cytation 5 plate reader (Agilent, Santa Clara, CA).

Two technical repeats were performed per seeding density. Raw absorbance values were blank-subtracted and converted to concentrations (ng/mL) using the standard curve. To account for culture format and cell input, albumin secretion values were normalized by dividing by the initial cell seeding density. Final results were expressed as total albumin per sample (ng), calculated by multiplying the concentration

by the corresponding assay volume (1 mL for agarose microtissue gels and 30 µL for microwell ULA spheroids, shown in **Table 1**).

CellTiter-Glo® 3D Cell Viability Assay

Cell viability of spheroid cultures was assessed using the CellTiter-Glo® 3D Cell Viability Assay (Promega, Madison, WI), following the manufacturer's protocol[38]. After supernatant extraction, spheroids **(Table 1)** were carefully transferred to a white opaque-walled 96-well assay plate (Corning). An equal volume of CellTiter-Glo® 3D reagent was added directly to each well, and spheroids were mixed gently to ensure complete lysis. Plates were incubated at room temperature for 30 min on an orbital shaker to allow ATP release and luminescent signal stabilization. Luminescence was measured using a BioTek Cytation 5 plate reader.

Two technical repeats were performed for each seeding density and culture method. Blank wells containing culture medium and reagent were used for background subtraction. Data processing and normalization followed the same procedure as described for the ELISA assay: values were blank-subtracted, normalized by dividing by the initial cell seeding density, and converted to total signal by accounting for the assay volume.

Statistical Analysis and Data Visualization

Morphological and functional data were analyzed using GraphPad Prism 10 (GraphPad Software, San Diego, CA) and Python (v3.11, pandas 2.2, statsmodels 0.14). For spheroid morphology, changes in radius and circularity across spheroid age (days 1, 3, 5, and 7), seeding density, and culture method were evaluated using analysis of variance (ANOVA). Specifically, a linear model of the form: **"response ~ C(method) + $\log_{10}$(density) + C(day) + C(method):$\log_{10}$(density) + C(method):C(day)"** was fit to test main and interaction effects. Type II ANOVA tables were generated, and significance was defined at $p < 0.05$. Up to 18 biological replicates were analyzed per condition, although some conditions contained fewer

replicates due to limitations in image segmentation. Statistical outputs from multiple comparisons were not visualized due to the large number of pairwise interactions.

For ELISA assays, standard curves were generated using nonlinear regression with the Sigmoidal, 4-parameter logistic (4PL), X is concentration model in Prism 10. The accuracy of calculated concentrations was verified by simple linear regression of calculated versus known input concentrations. Comparisons of albumin secretion across spheroid age and seeding density were performed using two-way ANOVA followed by Tukey's multiple-comparisons test. Two technical replicates were included per condition, and pairwise outputs were not displayed for clarity.

For CellTiter-Glo 3D assays, standard curves were similarly generated with a 4PL nonlinear regression model and validated by linear regression of calculated versus known values. Comparisons of viability across spheroid age and seeding density were analyzed using two-way ANOVA with Tukey's post hoc test. Two technical replicates were included per condition, and individual pairwise outputs were not visualized.

Method	**35 Microwell Agarose**	**96 Microwell Agarose**	**Microwell ULA plate**	**Single-well ULA plate**	**Hanging drop**
# of Microwells	35	96	32	1	1
Volume of media per well/drop (µL)	1070	1070	200	100	25
Volume per ELISA well (µL)	1000	1000	30	n/a	n/a
# of spheres per CellTiter-Glo well	35	96	32	n/a	n/a
Diameter used to contain one sphere (µm)	800	400	900	6350 > FOV	Variable > FOV

Table 1. Comparison of spheroid-generation methods across key platform and assay parameters.

Abbreviations: n/a, not applicable, for methods in which each spheroid forms in an individual well or droplet rather than in microwells; FOV, field of view of microscopes; "> FOV" indicates that the spheroid diameter exceeded the field of view of the microscope used.

Results

Each spheroid formation method was evaluated across a range of seeding densities from 0.3125 k to 80 k cells per spheroid **(Table 1)** over 7 days of culture. Day 7 served as the primary focus for morphological comparisons, corresponding to the timepoint of functional assays[38,44,45]. As shown in Figure 2A, some seeding densities in the 96-microwell agarose, 35-microwell agarose, and microwell ULA plates were limited by the physical dimensions of their wells **(Table 1)**. In the 96-microwell agarose format, spheroids seeded at 2.5 k cells per well occasionally formed confluent cell sheets spanning adjacent wells. Although many wells produced discrete spheroids as intended, the microwell ULA plates exhibited a similar overgrowth effect at 40 k and 80 k cells per well, where cells merged between neighboring wells to create continuous layers **(Figure 2A)**. This phenomenon was less prevalent in the 35-microwell agarose but occasionally occurred at higher densities. Quantitative analysis confirmed that, on day 7, spheroid radius generally increased with seeding density for all methods except the 96-microwell agarose **(Figure 2B)**. In that format, spheroid size was restricted by the well geometry and reached a consistent maximum radius at all densities by day 7. ANOVA results showed a strong main effect of seeding density ($p < 0.001$) and method ($p < 0.0001$) on radius, with significant Method×Density and Method×Day interactions (both $p < 0.0001$), confirming that both the rate and extent of size change depended on culture format.

Analysis of circularity across seeding densities revealed that methods with fixed well geometries—the agarose gels and ULA plates—maintained relatively consistent circularities across their density ranges **(Figure 2C)**. In contrast, the hanging-drop method, which lacks physical confinement and relies solely on surface tension and gravity, exhibited pronounced variability in circularity across densities. Microwell ULA plates consistently yielded the lowest and most uniform circularity values, likely due to their square–pyramidal well design, which constrains aggregates into slightly angular shapes. To compare spheroid behavior over time, all methods were analyzed at 10 k cells per spheroid—a density spanning all five methods and representing the optimal range for three of them **(Figure 1E)**. Across methods, spheroid area decreased between days 1 and 7 **(Figure 3A)**, consistent with progressive compaction during 3D

aggregation. Quantitative radius measurements supported this observation, showing either stable or modestly decreasing values over time **(Figure 3B)**. This reduction is likely due to structural compaction rather than cell death, as visual inspection revealed darker, denser cores forming from day 3 onward (particularly in the microwell ULA plates and 35-microwell agarose format), while spheroid borders became smoother after day 1.

Circularity at 10 k cells varied across both method and time **(Figure 3C)**. The 35-microwell agarose method, characterized by circular wells, demonstrated a marked increase in circularity after day 1 and maintained the highest circularity overall. Two-way ANOVA confirmed that this method produced spheroids of significantly higher circularity than all others ($p < 0.0001$), whereas pairwise comparisons among the remaining methods revealed no significant differences. Although circularity represents a useful 2D metric of boundary regularity, it should be distinguished from true 3D sphericity, which was not directly measured here.

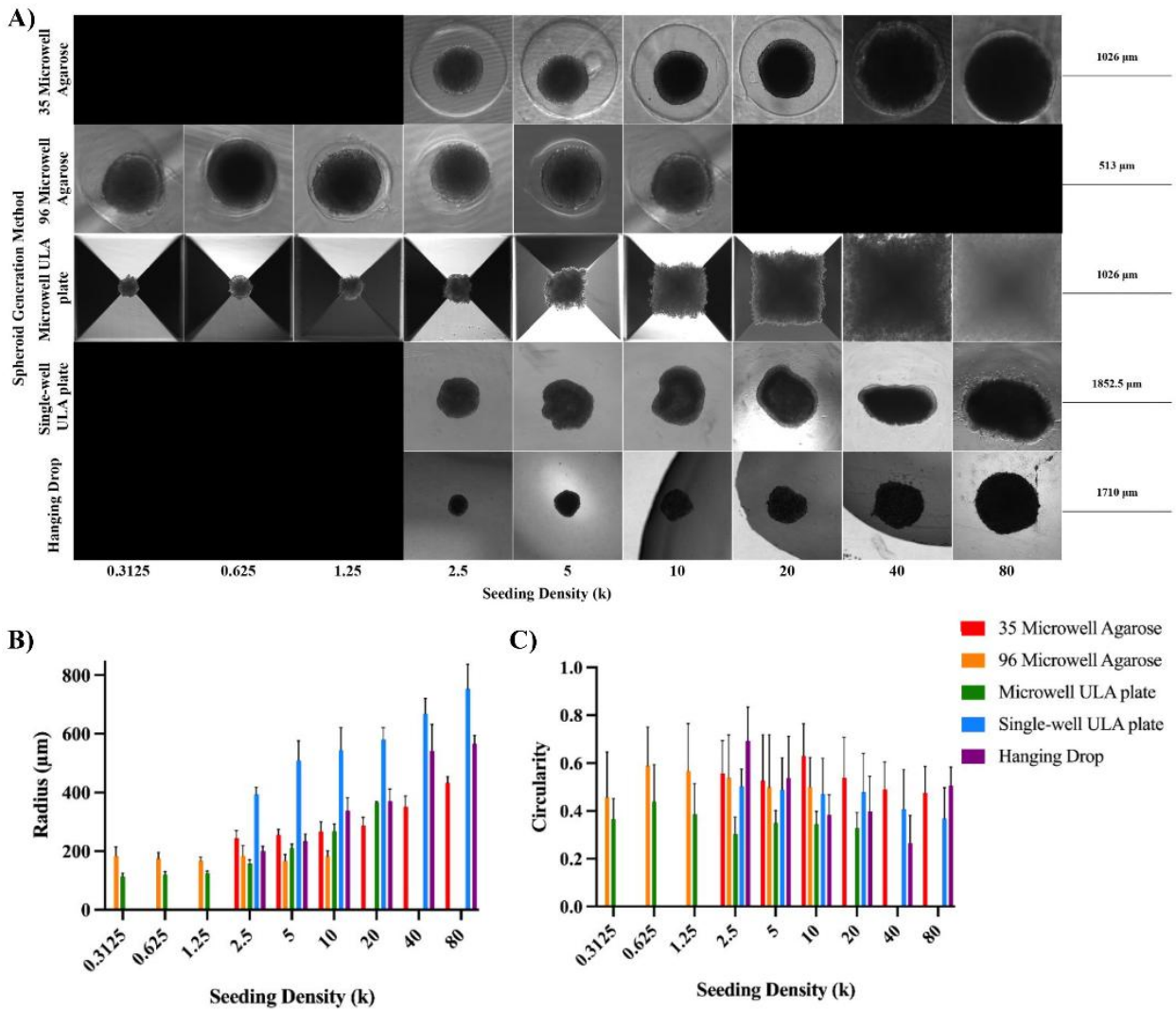

Figure 2. Morphological comparison of HepG2 spheroid culture platforms at Day 7.

(A) Visual overview of each culturing method after 7 days of culturing, as well as **(B)** the quantified average radius and **(C)** circularity taken from the ImageJ INSIDIA 2.0 macro's output. For circularity: "0" equals to "noncircular" whereas "1" equals to "perfectly circular".

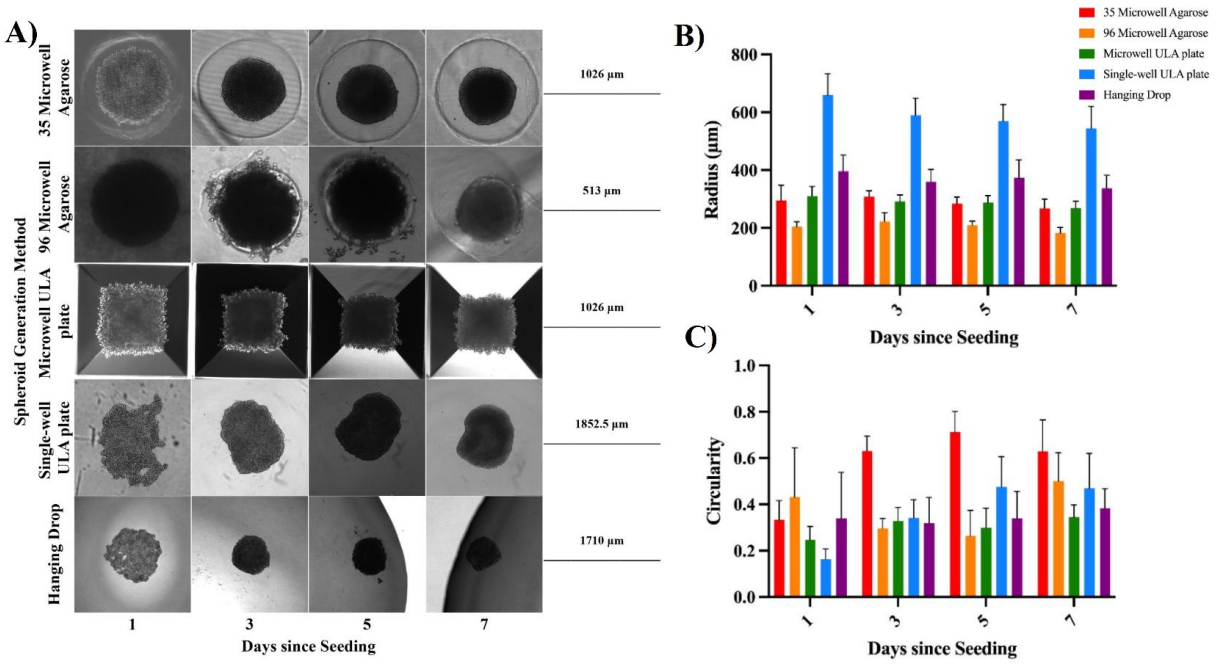

Figure 3. Morphological comparison of HepG2 spheroid culture platforms at 10 k Seeding Density per sphere.

(A) Visual overview of the progressive growth of spheroids from five platforms from Days 1-7 at an initial seeding density of 10 k. Quantified average radius **(B)** and circularity **(C)** of each method were also compared from the output from the ImageJ INSIDIA 2.0 macro.

To evaluate hepatocyte-like function and metabolic activity, albumin secretion (ELISA) and intracellular ATP (CellTiter-Glo) were quantified. These functional assays were limited to multi-spheroid formats to ensure sufficient analyte volume and reproducible measurements. ELISA calibration reported strong agreement between measured albumin and input albumin, indicating reliability of baseline calibrations **(Figure 4A)**. Calibration for the CellTiter-Glo assay was slightly weaker but remained acceptable for comparative analysis **(Figure 4C)**. Two-way ANOVA indicated that culture method significantly affected albumin production ($p < 0.0001$), while seeding density had no significant effect ($p =$

0.985, **Figure 4A, 4B**). Specifically, albumin secretion per HepG2 spheroid was higher in 35-microwell agarose than in either 96-microwell agarose or microwell ULA plate, at seeding densities of 1.25 k cells per spheroid and above. In addition, albumin secretion increased with seeding density in 35-microwell agarose, whereas it remained relatively constant in the other two methods. Notably, albumin yield per spheroid in microwell ULA plates remained low, with spheroids seeded at 0.3125 k, 0.625 k, 1.25 k, and 5 k cells unable to be quantified **(Figure 4B)**.

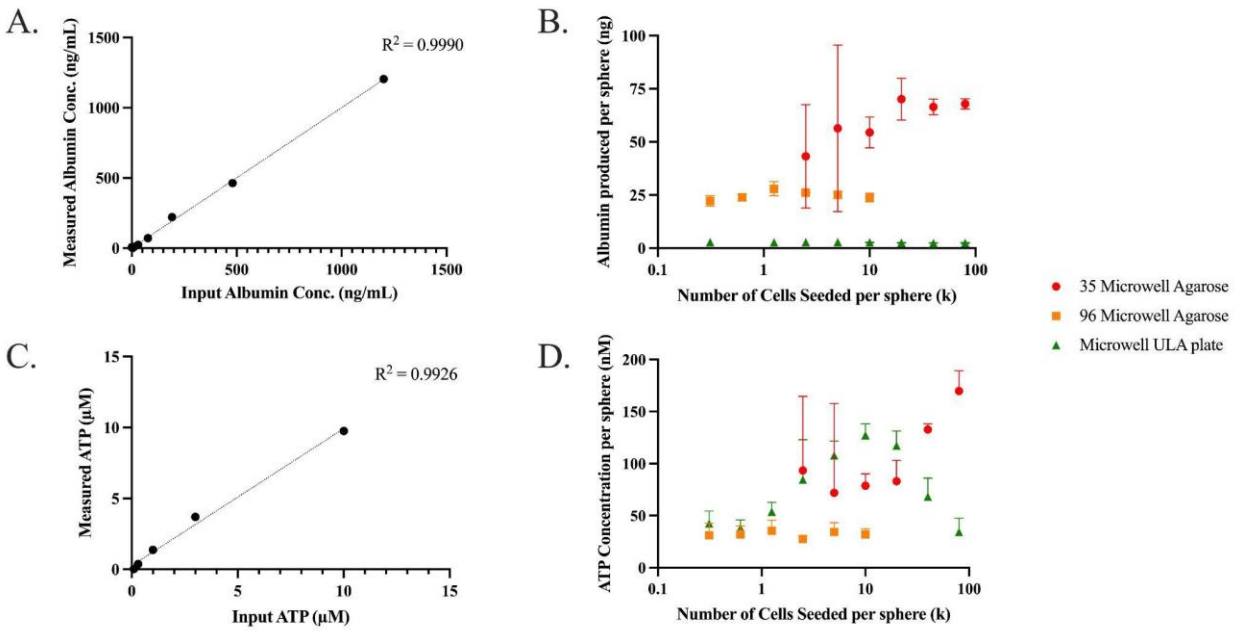

Figure 4. Quantitative analysis of normalized albumin secretion and ATP production from multi-spheroid culture platforms.

(A) Linearity of the albumin ELISA: measured albumin (ng/mL) versus nominal input (ng/mL) for ELISA calibration. The dotted line represents (y = x). **(B)** Albumin per spheroid (ng) versus seeding density (k cells/sphere) across culture methods. **(C)** Linearity of CellTiter-Glo Assay: measured ATP level (µM) versus input ATP level (µM) for CellTiter-Glo Assay calibration. The dotted line represents (y = x). **(D)** ATP produced per HepG2 spheroid (nM) versus seeding density (k cells/sphere) across multi-spheroid culture methods.

A two-way ANOVA on the CellTiter-Glo Assay found that culturing methods had a significant effect on the spheroids' overall metabolic activity ($p < 0.05$), and no significant effect on seeding density ($p = 0.83$) on ATP produced by HepG2 spheroids. Spheroids cultured in 35-microwell agarose were observed to yield higher ATP as their seeding density increased incrementally from 2.5 k cells per sphere to 80 k cells per sphere, with the exception of spheroids at 2.5 k cells per sphere: the average ATP yield was 93.4 μM. On the other hand, spheroids seeded at 0.3125 k, 0.625 k densities and cultured in the microwell ULA plate yielded 50 μM ATP on average **(Figure 4D)**. As the seeding density of spheres in microwell ULA plates increased incrementally from 1.25 k cells per sphere, ATP yields from these spheres continued to increase until culminating at 127 μM **(Figure 4D)**. Lastly, spheroids cultured in 96-microwell agarose were observed to yield approximately 30 μM ATP across all seeding densities ranging from 0.3125 k cells per sphere to 10 k cells per sphere. It is noteworthy that the ATP yield from HepG2 spheroids cultured in 96-microwell agarose was the lowest compared to other two methods regardless of seeding density. Collectively, these results revealed that among the HepG2 spheroids cultured in these three methods, 35-microwell agarose most effectively supported hepatocyte-like function (albumin secretion) and metabolic activity (ATP) over the tested range of cell densities per sphere.

Discussion

With the rapid expansion of drug discovery and advances in cell and molecular medicine, the development of reliable *in vitro* testing platforms has become essential. This study aimed to evaluate several well-established methods for spheroid formation under controlled experimental conditions to provide a comprehensive assessment of their respective advantages and limitations. Agarose gels provide a theoretically high-throughput format capable of accommodating multiple seeding densities. However, their practical limitations are substantial. Preparation is a multistep, technique-dependent process that is both time-consuming and relatively inefficient. Gel equilibration must be judged qualitatively, creating a risk of misestimation. Gel equilibration is assessed qualitatively via visual inspection, introducing subjectivity that may lead to the misclassification of malformed gels as viable or the erroneous rejection of functional gels due to optical artifacts. Casting further complicates the procedure as bubble formation, lack of settling, or merging of microwells frequently results in structural defects such as ruptured gels, leakage of seeded cells, or aggregation into large multicellular clusters. Demolding presents an additional challenge as the gel structure around each well must be preserved to maintain uniform geometry. The workflow requires several hours of hands-on time followed by an additional 24-h equilibration period, yet many gels fail to meet the quality standards for seeding. Since agarose gel quality, and thus spheroid outcomes, are heavily reliant on technical skill, efficiency and reproducibility are limited.

In contrast, microwell ULA plates offer a more practical alternative. These plates enable highly repeatable, high-throughput (per well, and overall) spheroid production with minimal time and resource investment. The procedure involves only three steps—treating wells with an anti-adherence solution, washing with serum-free medium, and seeding cells—making the platform straightforward and consistent. Single-well ULA plates provide an even simpler approach, requiring only cell seeding. Relative to agarose gels, both methods significantly improve reproducibility, throughput, and overall efficiency.

The hanging drop method has gained attention in the literature as a cost-effective and accessible strategy. Unlike gel or plate-based techniques, it requires only basic laboratory materials, including Petri

dishes, medium, PBS, and cells, making it broadly adaptable. Spheroid formation occurs through natural cell aggregation within droplets, where gravity, surface tension, and intrinsic cell–cell interactions drive assembly in suspension. The absence of external forces acting on the developing spheroids allows the method to better approximate physiological conditions. Despite these advantages, the technique poses several limitations: it supports lower seeding densities than gels or ULA plates, complicates imaging because spheroids cannot be visualized as easily (droplet formats on the lid of a dish), and prevents supernatant extraction/analysis due to small droplet sizes. These restrictions limit its suitability for high-throughput screening or multi-assay workflows. Furthermore, a small slip or movement when moving plates could result in the movement or merging of drops, and thus spheres; whereas it would take a relatively large error to accidentally move spheroids between microwells, and an extremely large issue to accidentally transfer spheroids between wells.

Overall, while agarose gels demand extensive preparation with low efficiency, and hanging drops have lower throughput and limited scalability, ULA plates offer reproducibility, high throughput, and simplicity. However, the hard plastic, despite ULA coating materials, disrupts the physiological relevance of the models. The results further suggest a more nuanced picture. Agarose gels produced spheroids with the highest circularity, generating structures theoretically closest to an ideal sphere. This was most evident in the 35-well agarose format, where spheroids were more circular, smooth, and often displayed dark cores, characterizing a high degree of cellular condensation and increased optical thickness common in mature, compact spheroids **(Figure 3)**. Functional assays further suggested that spheroids cultured in 35-well agarose gels yielded the highest albumin and ATP compared to other microwell formats. Single-well ULA and hanging drop spheroids could not be analyzed in these assays due to limited analyte volume, high variability, and low albumin/ATP yields. Thus, while agarose gels are technically demanding, they appear to produce spheroids with the most favorable morphology and functional readouts. An additional consideration for microwell-based spheroid formation is the potential for residual single cells to escape the wells during early medium addition and subsequently attach to the surrounding tissue culture plastic. While

routine imaging did not reveal obvious monolayer overgrowth in our experiments, low-level 2D attachment cannot be fully excluded and could contribute modestly to measured secretory or metabolic readouts. This possibility highlights a general methodological consideration in microwell systems, where careful handling or plate transfer strategies may further minimize contributions from non-spheroid cell populations.

Comparison with previously reported HepG2 spheroid studies suggests that the morphological and functional outputs observed here fall broadly within reported ranges while highlighting important methodological differences. For example, spheroids formed in ULA plates by Pingitore et al. seeded with 2 k cells exhibited radii of~160–180 μm during early culture, substantially smaller than the ~ 380–400 μm radii observed in our single-well ULA conditions at slightly higher seeding densities (2.5 k), while agarose microwell spheroids in our study more closely matched those smaller reported sizes[43]. Similarly, albumin secretion levels reported by Tutty et al. for HepG2 spheroids in ULA plates were generally lower than those measured in our microwell systems, possibly reflecting differences in culture duration, feeding schedules, or material interactions with secreted proteins[44]. Namely, they observed between 0.1–0.4 ng per sphere on day 3, and 0.4–0.8 ng on day 7 (for 5 and 10 k seeding densities respectively); compared with our ~ 2.7 ng of albumin across all microwell ULA plate seeding densities, and > 25 ng for agarose gel methods. This could indicate superior anti-adherence properties of agarose compared with treated plates. Reported circularity values such as the ~ 0.94 roundness (3 k seeding density, day 6) described by Eilenberger et al. also exceed those observed in similar ULA conditions (0.5 circularity for 2.5 k seeding density, day 7); however, both studies showed very comparable radii of 400 μm[38]. Furthermore, Tutty et al. found that their spheres secreted 1.68 μg/mL of albumin over 6 days using the ULA plate, our comparable spheres on day 7 produced 0.028 and 0.52 μg/mL for microwell ULA plates and 35 microwell gels respectively[45]. Finally, while ATP levels are difficult to compare directly across studies due to normalization differences, values reported in other spheroid systems (e.g., Lazzari et al. using PANC-1 cells) fall within a broadly comparable order of magnitude[46]. Collectively, these comparisons support the conclusion that platform choice

substantially influences spheroid size, morphology, and functional outputs and reinforce the importance of considering culture method when interpreting hepatocyte spheroid data.

Brightfield imaging confirmed that seeding density strongly influenced morphology. Across methods, spheroids seeded at 10 k cells generally appeared optimal, forming compact aggregates with progressively darker cores from days 1 to 7. Exceptions were seen in the 96-well agarose format, where spheroids remained small and less structured. The maximum spheroid size was also constrained by each method's physical environment **(Figure 1E)**. For example, spheroids in single-well ULA plates reached the largest radii due to greater well space and media volume per sphere (100 µL, as opposed to e.g. 1 mL/35 spheres= 28.6 µL). Hanging drops also offer more physical space, but with less constraints and subsequently less 'guidance' for the cells causing the irregularities seen. These results highlight how both well geometry and available media shape spheroid growth.

In functional assays, albumin secretion was highest in 35-well agarose spheroids rather than in 96-well agarose spheroids, despite our initial hypothesis that smaller, better-oxygenated spheroids in the 96-well format may yield stronger hepatocyte-like function. Some ULA plate spheroids seeded at < 10 k cells exceeded the upper limit of quantification (ULOQ) for the ELISA, even at 1:100 dilution. While this confirms robust secretion in these conditions, it precluded precise comparative normalization for those specific high-density groups. Morphologically, ULA spheroids above 5 k cells per well often flattened against the well edge ('pancaked' instead of spherical), potentially constraining function. These observations are consistent with reports that HepG2 spheroids secrete insufficient collagen I to maintain structural integrity and function[57–59], and that hypoxia or necrosis at higher densities reduces albumin output[60].

CellTiter-Glo assays showed trends similar to ELISA. In 35-well agarose gels, ATP per spheroid rose steadily with seeding density, peaking at 80 k cells. By contrast, ATP levels in 96-well agarose spheroids remained consistently low, consistent with crowding and nutrient competition among multiple spheroids in the same well sharing limited medium. Prior work has shown that greater inter-spheroid

spacing supports higher albumin secretion[61], aligning with our observation that 35-well agarose spheroids outperformed the denser 96-well format. In ULA plates, ATP levels increased up to 10 k cells seeded per spheroid, then declined at higher densities—potentially reflecting wall contact, loss of circularity, and reduced viability.

Together, these results indicate that culture method—not seeding density—was the dominant factor shaping per spheroid outputs. After per-spheroid normalization, 35-well agarose consistently produced the highest albumin and ATP. By contrast, 96-well agarose spheroids underperformed across assays, while ULA plates were prone to ELISA saturation effects at low–mid densities and viability decline at high densities. These findings support 35-well agarose as the most functionally robust platform, though its low efficiency and high technical burden limit its scalability. None of the tested methods simultaneously achieved scalability and functional robustness, highlighting the need for hybrid approaches that integrate the strengths of both agarose- and plate-based platforms.

Our study was not without its limitations. ELISA readouts were constrained by upper detection limits, with values exceeding the range even after 1:100 dilution being set to the top standard, which artifactually depressed normalized per-spheroid secretion. CellTiter-Glo was not subject to this limitation, though variability in luminescence reduced precision. Functional assays were restricted to multi-spheroid formats due to volume and sensitivity limitations, and overall sample sizes were small due to methodological differences. Because of the high cost of functional assays, only a limited number of technical and biological replicates could be performed, even when constrained to multi-spheroid formats. Consequently, the resulting data should be interpreted with caution given the reduced statistical power and reproducibility. Image analysis using INSIDIA 2.0 improved throughput and reduced operator bias but introduced systematic errors, particularly in misidentifying well borders or shadows as spheroids, requiring manual preprocessing and occasional exclusion of images. Despite these limitations, automated segmentation was preferable to manual analysis for consistency and speed.

We attempted to visualize internal spheroid architecture using confocal microscopy; however, these results were primarily limited to the superficial volume due to technical constraints. The resulting images exhibited significant laser light scattering at the spheroid periphery, with signal attenuation obscuring the expected necrotic core, a common limitation in non-cleared tissues where light penetration rarely exceeds 150–200 μm. Furthermore, immunofluorescence for Type-I collagen was unsuccessful, consistent with reports that HepG2 spheroids possess limited intrinsic ECM and may lack the structural scaffolding required to maintain a perfectly rigid spherical geometry[62–64]. Despite these imaging constraints, 3D surface-plots derived from the accessible z-stacks revealed a 'cap' morphology that suggests an approximation of spherical symmetry, yet with evidence of oblate deformation. Given the average spheroid radius of 370 μm (for 20 k seeding density on day 7, **Figure 2B**), the observed curvature in the measured section appears lower than theoretically expected for a perfect sphere. We attribute this subtle flattening to low tissue surface tension and a lack of vertical compaction, likely exacerbated by gravitational loading and wetting against rigid substrates upon transfer from hanging drops. This results in an oblate profile where the spheroid's height is depressed relative to its lateral diameter.

Future work could focus on advanced imaging techniques such as light-sheet microscopy or tissue clearing, to overcome the light-scattering limitations observed in this study and visualize the internal architecture of large (>500 μm) spheroids. To distinguish handling-induced artifacts from intrinsic mechanics, future work could compare cell lines with distinct biophysical signatures; for instance, Huh7 cells, which naturally form more compact aggregates, could serve as a benchmark against the softer, more deformable HepG2 phenotype[65]. Taken together, our results underscore that while agarose gels, particularly the 35-well format, produced the most morphologically and functionally favorable spheroids, their low efficiency, high technical burden, and incompatibility with high-throughput workflows restrict broader application. ULA plates provide scalability and reproducibility but may introduce artifacts at low and high densities. Hanging drops remain valuable for accessibility and physiological relevance but lack compatibility with many downstream assays.

Future studies should also build on these findings by combining the throughput and reproducibility of plate-based methods with the functional performance of agarose formats, thereby developing hybrid platforms that balance scalability with physiological relevance. For example, methodology for coating small wells (e.g. 384 well plate) in a thin layer of agarose would simplify the workflow while retaining the material benefits of the agarose gels. To more fully assess each method's translational potential, it will be important to expand functional benchmarking beyond albumin and ATP. One key direction is to test xenobiotic-response competence, for example by assessing CYP3A induction with rifampicin and appropriate controls using complementary readouts such as P450-Glo activity[66,67], CYP3A4 transcript and protein levels[68,69], and testosterone hydroxylation by LC–MS/MS[70]. A second avenue is to evaluate drug sensitivity across formats by exposing spheroids to agents such as acetaminophen or lenvatinib[3] and measuring concentration–response effects on viability, function, and stress-response pathways, providing insight into each method's suitability for toxicology and disease-modeling workflows[11,71,72].

An additional consideration not directly measured in this study is the mechanical environment associated with different spheroid formation strategies. Both substrate stiffness during aggregation and the evolving mechanical properties of the spheroids themselves can influence cell phenotype, extracellular matrix deposition, and functional maturation. Previous work has demonstrated that spheroid stiffness reflects cellular compaction, cytoskeletal tension, and matrix production, linking mechanical properties to tissue-like behavior and disease modeling applications[64,73,74]. Differences between hanging drop, agarose microwell, and ultra-low attachment platforms likely expose cells to distinct mechanical constraints during aggregation, potentially affecting spheroid compaction and long-term function. For example, more compact spheroids may better recapitulate fibrotic or tumor-like microenvironments, whereas less compact aggregates may resemble healthy hepatic tissue states[73,75–77]. Although mechanical characterization was beyond the scope of this comparative study, integrating stiffness measurements in future work could provide additional insight into how spheroid formation methods influence physiological relevance and disease modeling potential.

Future work could also address how well spheroids generated by each method can be dissociated into viable single cells, enabling downstream single-cell sequencing and multi-omics applications[15]. Durations longer than 7 days would be beneficial for future experiments to further investigate time-based differences, particularly when combined with media exchange studies, to investigate their impacts on spheroid formation. Together, these directions would establish not only which spheroid culture formats perform best under baseline conditions, but also which can most effectively model adaptive metabolism, drug response, and integration with emerging single-cell technologies. Finally, the progression to co-culture spheroids, patient-derived spheres, or organoids, combined with the future directions above, would increase the physiological relevance and reliability of the results further.

Conclusion

Our systematic comparison of HepG2 spheroid culture methods revealed clear method-dependent differences in morphology, albumin secretion, and metabolic activity. While 35-well agarose formats consistently produced spheroids with the highest circularity, albumin secretion, and ATP yield, they remain technically demanding to produce and low-throughput. Microwell ULA plates offered greater reproducibility and ease of use but showed functional limitations at both low and high densities, whereas 96-well agarose formats underperformed across functional assays, likely due to crowding effects and nutrient competition. Hanging drops and single-well ULA formats, although accessible and low-cost, were unsuitable for quantitative functional assays due to small culture volumes and high variability. These findings highlight that no single method fully balances scalability, reproducibility, and functional robustness. Instead, each approach offers distinct advantages and disadvantages, and the optimal choice will depend on the intended application and constraints, such as assay compatibility, cost, throughput, or the need for physiological function. While some of our assays remain preliminary, this study establishes a framework for method selection in the field of cell spheroid formation and underscores that culture format is a critical determinant of experimental outcome. Future work should refine these methods and explore hybrid approaches that combine the throughput of plate-based systems with the functional performance of agarose formats, tailoring spheroid models more precisely to specific research and translational goals.

References

1. David, S. & Hamilton, J. P. Drug-induced Liver Injury. *US Gastroenterol Hepatol Rev.* **6**, 73–80 (2010).

2. Ostapowicz, G. *et al.* Results of a Prospective Study of Acute Liver Failure at 17 Tertiary Care Centers in the United States. *Ann Intern Med* **137**, 947–954 (2002).

3. Wang, T. *et al.* Comparative analysis of sorafenib and lenvatinib on HepG2 cells and human umbilical vein endothelial cells: Involvement of transforming growth factor-β signaling in their molecular effects. *Hepatology Research* **54**, 921–930 (2024).

4. Kola, I. & Landis, J. Can the pharmaceutical industry reduce attrition rates? *Nat Rev Drug Discov* **3**, 711–716 (2004).

5. Hurrell, T., Ellero, A. A., Masso, Z. F. & Cromarty, A. D. Characterization and reproducibility of HepG2 hanging drop spheroids toxicology in vitro. *Toxicology in Vitro* **50**, 86–94 (2018).

6. Bray, F. *et al.* Global cancer statistics 2022: GLOBOCAN estimates of incidence and mortality worldwide for 36 cancers in 185 countries. *CA A Cancer J Clinicians* **74**, 229–263 (2024).

7. Cox, C. R., Lynch, S., Goldring, C. & Sharma, P. Current Perspective: 3D Spheroid Models Utilizing Human-Based Cells for Investigating Metabolism-Dependent Drug-Induced Liver Injury. *Front. Med. Technol.* **2**, 611913 (2020).

8. Gissen, P. & Arias, I. M. Structural and functional hepatocyte polarity and liver disease. *Journal of Hepatology* **63**, 1023–1037 (2015).

9. Treyer, A. & Müsch, A. Hepatocyte Polarity. in *Comprehensive Physiology* (ed. Prakash, Y. S.) 243–287 (Wiley, 2013). doi:10.1002/cphy.c120009.

10. Ren, Z., Chen, S., Qin, X., Li, F. & Guo, L. Study of the roles of cytochrome P450 (CYPs) in the metabolism and cytotoxicity of perhexiline. *Arch Toxicol* **96**, 3219–3231 (2022).

11. Godoy, P. *et al.* Recent advances in 2D and 3D in vitro systems using primary hepatocytes, alternative hepatocyte sources and non-parenchymal liver cells and their use in investigating mechanisms of hepatotoxicity, cell signaling and ADME. *Arch Toxicol* **87**, 1315–1530 (2013).

12. Harris, A. J., Dial, S. L. & Casciano, D. A. Comparison of basal gene expression profiles and effects of hepatocarcinogens on gene expression in cultured primary human hepatocytes and HepG2 cells. *Mutation Research - Fundamental and Molecular Mechanisms of Mutagenesis* **549**, 79–99 (2004).

13. LeCluyse, E. L. Human hepatocyte culture systems for the in vitro evaluation of cytochrome P450 expression and regulation. *European Journal of Pharmaceutical Sciences* **13**, 343–368 (2001).

14. Gerets, H. H. J. *et al.* Characterization of primary human hepatocytes, HepG2 cells, and HepaRG cells at the mRNA level and CYP activity in response to inducers and their predictivity for the detection of human hepatotoxins. *Cell Biol Toxicol* **28**, 69–87 (2012).

15. Planchak, S. *et al.* Innovative Method for Fully Automated, Enzyme-Free Tissue Dissociation and Preparation for Single-Cell Analysis. *Cel. Mol. Bioeng.* **18**, 251–269 (2025).

16. Wang, Z. *et al.* HepaRG culture in tethered spheroids as an *in vitro* three-dimensional model for drug safety screening. *J of Applied Toxicology* **35**, 909–917 (2015).

17. Drewitz, M. *et al.* Towards automated production and drug sensitivity testing using scaffold-free spherical tumor microtissues. *Biotechnology Journal* **6**, 1488–1496 (2011).

18. Zuchowska, A., Kwapiszewska, K., Chudy, M., Dybko, A. & Brzozka, Z. Studies of anticancer drug cytotoxicity based on long-term HepG2 spheroid culture in a microfluidic system. *Electrophoresis* **38**, 1206–1216 (2017).

19. Royo, F. *et al.* Three-Dimensional Hepatocyte Spheroids: Model for Assessing Chemotherapy in Hepatocellular Carcinoma. *Biomedicines* **12**, 1200 (2024).

20. Bchini, R., Capel, F., Dauguet, C., Dubanchet, S. & Petit, M. A. In vitro infection of human hepatoma (HepG2) cells with hepatitis B virus. *J Virol* **64**, 3025–3032 (1990).

21. Lee, G. S., Purdy, M. A. & Choi, Y. Cell Culture Systems for Studying Hepatitis B and Hepatitis D Virus Infections. *Life* **13**, 1527 (2023).

22. Yamamoto, G. *et al.* DHCR7 inhibition ameliorates MetALD and HCC in mice and human 3D liver spheroids. *JHEP Reports* **7**, 101415 (2025).

23. Chen, J. *et al.* An in vitro 3D spheroid model with liver steatosis and fibrosis on microwell arrays for drug efficacy evaluation. *Journal of Biotechnology* **399**, 153–163 (2025).

24. Pastore, M., Giachi, A., Spínola-Lasso, E., Marra, F. & Raggi, C. Organoids and spheroids: advanced in vitro models for liver cancer research. *Front. Cell Dev. Biol.* **12**, 1536854 (2025).

25. Tuschl, G., Lauer, B. & Mueller, S. O. Primary hepatocytes as a model to analyze species-specific toxicity and drug metabolism. *Expert Opinion on Drug Metabolism & Toxicology* **4**, 855–870 (2008).

26. Kyffin, J. A. *et al.* Impact of cell types and culture methods on the functionality of in vitro liver systems – A review of cell systems for hepatotoxicity assessment. *Toxicology in Vitro* **48**, 262–275 (2018).

27. Štampar, M., Tomc, J., Filipič, M. & Žegura, B. Development of in vitro 3D cell model from hepatocellular carcinoma (HepG2) cell line and its application for genotoxicity testing. *Arch Toxicol* **93**, 3321–3333 (2019).

28. Štampar, M., Breznik, B., Filipič, M. & Žegura, B. Characterization of In Vitro 3D Cell Model Developed from Human Hepatocellular Carcinoma (HepG2) Cell Line. *Cells* **9**, 2557 (2020).

29. Štampar, M., Žabkar, S., Filipič, M. & Žegura, B. HepG2 spheroids as a biosensor-like cell-based system for (geno)toxicity assessment. *Chemosphere* **291**, 132805 (2022).

30. Kelm, J. M. & Fussenegger, M. Microscale tissue engineering using gravity-enforced cell assembly. *Trends in Biotechnology* **22**, 195–202 (2004).

31. Kelm, J. M., Timmins, N. E., Brown, C. J., Fussenegger, M. & Nielsen, L. K. Method for generation of homogeneous multicellular tumor spheroids applicable to a wide variety of cell types. *Biotech & Bioengineering* **83**, 173–180 (2003).

32. Shah, U.-K. *et al.* A three-dimensional in vitro HepG2 cells liver spheroid model for genotoxicity studies. *Mutation Research/Genetic Toxicology and Environmental Mutagenesis* **825**, 51–58 (2018).

33. Fey, S. J. & Wrzesinski, K. Determination of Drug Toxicity Using 3D Spheroids Constructed From an Immortal Human Hepatocyte Cell Line. *Toxicological Sciences* **127**, 403–411 (2012).

34. Kim, J. *et al.* Collective Transitions from Orbiting to Matrix Invasion in 3D Multicellular Spheroids. Preprint at https://doi.org/10.1101/2025.02.10.636936 (2025).

35. Hirschhaeuser, F. *et al.* Multicellular tumor spheroids: An underestimated tool is catching up again. *Journal of Biotechnology* **148**, 3–15 (2010).

36. Härmä, V. *et al.* A Comprehensive Panel of Three-Dimensional Models for Studies of Prostate Cancer Growth, Invasion and Drug Responses. *PLoS ONE* **5**, e10431 (2010).

37. Kenny, P. A. *et al.* The morphologies of breast cancer cell lines in three-dimensional assays correlate with their profiles of gene expression. *Molecular Oncology* **1**, 84–96 (2007).

38. Eilenberger, C., Rothbauer, M., Ehmoser, E.-K., Ertl, P. & Küpcü, S. Effect of Spheroidal Age on Sorafenib Diffusivity and Toxicity in a 3D HepG2 Spheroid Model. *Sci Rep* **9**, 4863 (2019).

39. Vinken, M. & Hengstler, J. G. Characterization of hepatocyte-based in vitro systems for reliable toxicity testing. *Arch Toxicol* **92**, 2981–2986 (2018).

40. Gómez-Lechón, M. J., Tolosa, L. & Donato, M. T. Cell-based models to predict human hepatotoxicity of drugs. *Rev. Toxicol* **31**, (2014).

41. Park, S. Y., Hong, H. J. & Lee, H. J. Fabrication of Cell Spheroids for 3D Cell Culture and Biomedical Applications. *BioChip J* **17**, 24–43 (2023).

42. Breslin, S. & O'Driscoll, L. Three-dimensional cell culture: the missing link in drug discovery. *Drug Discovery Today* **18**, 240–249 (2013).

43. Leung, M. *et al.* Chitosan-Alginate Scaffold Culture System for Hepatocellular Carcinoma Increases Malignancy and Drug Resistance. *Pharm Res* **27**, 1939–1948 (2010).

44. Pingitore, P. *et al.* Human Multilineage 3D Spheroids as a Model of Liver Steatosis and Fibrosis. *IJMS* **20**, 1629 (2019).

45. Tutty, M. A., Vella, G. & Prina-Mello, A. Pre-clinical 2D and 3D toxicity response to a panel of nanomaterials; comparative assessment of NBM-induced liver toxicity. *Drug Deliv. and Transl. Res.* **12**, 2157–2177 (2022).

46. Lazzari, G. *et al.* Multicellular spheroid based on a triple co-culture: A novel 3D model to mimic pancreatic tumor complexity. *Acta Biomaterialia* **78**, 296–307 (2018).

47. Zein-Sabatto, A. *et al.* Multi-assay assessment of cytotoxicity reveals multiple mechanisms of action in 3D microtissues. *Sci Rep* **15**, 3090 (2025).

48. Whitehead, K. *et al.* Cell2Read: an automated workflow to generate sequencing-ready DNA libraries from human cell suspensions. *Biology Methods and Protocols* **10**, bpaf091 (2025).

49. Dean, D. M. & Morgan, J. R. Cytoskeletal-Mediated Tension Modulates the Directed Self-Assembly of Microtissues. *Tissue Engineering Part A* **14**, 1989–1997 (2008).

50. Huang, B., Yu, Z., Cui, D. & Du, F. MAPKAP1 orchestrates macrophage polarization and lipid metabolism in fatty liver-enhanced colorectal cancer. *Translational Oncology* **45**, 101941 (2024).

51. Lopez-Cavestany, M. *et al.* Superhydrophobic Array Devices for the Enhanced Formation of 3D Cancer Models. *ACS Nano* **18**, 23637–23654 (2024).

52. Vera, A. O. *et al.* Protective antigen–mediated delivery of an anti-CRISPR protein for precision genome editing. *Proc. Natl. Acad. Sci. U.S.A.* **122**, e2426960122 (2025).

53. Shri, M., Agrawal, H., Rani, P., Singh, D. & Onteru, S. K. Hanging Drop, A Best Three-Dimensional (3D) Culture Method for Primary Buffalo and Sheep Hepatocytes. *Sci Rep* **7**, 1203 (2017).

54. Kim, Y., Kim, H. & Kim, Y. Advancing hepatotoxicity assessment: current advances and future directions. *Toxicol Res.* **41**, 303–323 (2025).

55. Perini, G. *et al.* INSIDIA 2.0 High-Throughput Analysis of 3D Cancer Models: Multiparametric Quantification of Graphene Quantum Dots Photothermal Therapy for Glioblastoma and Pancreatic Cancer. *IJMS* **23**, 3217 (2022).

56. Gurevich, I. *et al.* iPSC-derived hepatocytes generated from NASH donors provide a valuable platform for disease modeling and drug discovery. *Biology Open* bio.055087 (2020) doi:10.1242/bio.055087.

57. Yamane, K. *et al.* Cell type-specific regulation of the TGF-β-responsive α2(I) collagen gene by CpG methylation. *Journal Cellular Physiology* **202**, 822–830 (2005).

58. Maseko, T. E. *et al.* Collagen I Increases Palmitate-Induced Lipotoxicity in HepG2 Cells via Integrin-Mediated Death. *Biomolecules* **14**, 1179 (2024).

59. Kamm, D. R. & McCommis, K. S. Hepatic stellate cells in physiology and pathology. *The Journal of Physiology* **600**, 1825–1837 (2022).

60. Anada, T., Fukuda, J., Sai, Y. & Suzuki, O. An oxygen-permeable spheroid culture system for the prevention of central hypoxia and necrosis of spheroids. *Biomaterials* **33**, 8430–8441 (2012).

61. Kang, S., Kim, D., Lee, J., Takayama, S. & Park, J. Y. Engineered Microsystems for Spheroid and Organoid Studies. *Adv Healthcare Materials* **10**, 2001284 (2021).

62. Song, Y. *et al.* Activated hepatic stellate cells play pivotal roles in hepatocellular carcinoma cell chemoresistance and migration in multicellular tumor spheroids. *Sci Rep* **6**, 36750 (2016).

63. Nguyen, R. Y. *et al.* Cytoskeletal dynamics regulates stromal invasion behavior of distinct liver cancer subtypes. *Commun Biol* **5**, 202 (2022).

64. Efremov, Y. M. *et al.* Mechanical properties of cell sheets and spheroids: the link between single cells and complex tissues. *Biophys Rev* **13**, 541–561 (2021).

65. Song, Y. *et al.* Identification of hepatic fibrosis inhibitors through morphometry analysis of a hepatic multicellular spheroids model. *Sci Rep* **11**, 10931 (2021).

66. Stipp, M. C. & Acco, A. Involvement of cytochrome P450 enzymes in inflammation and cancer: a review. *Cancer Chemother Pharmacol* **87**, 295–309 (2021).

67. Ueyama, T., Tsuji, S., Sugiyama, T. & Tada, M. Fluorometric evaluation of CYP3A4 expression using improved transgenic HepaRG cells carrying a dual-colour reporter for CYP3A4 and CYP3A7. *Sci Rep* **7**, 2874 (2017).

68. Jin, J., Tawfik, S. M., Nguyen, L. T. G., Armanios, B. & Zhong, X. Visualization of CYP3A4 expression at both mRNA and protein levels simultaneously at single cell resolution in various conditions using RNAscope combined with immunofluorescence. *Drug Metabolism and Disposition* **53**, 100123 (2025).

69. El-Sayed, R. *et al.* Single-Walled Carbon Nanotubes Inhibit the Cytochrome P450 Enzyme, CYP3A4. *Sci Rep* **6**, 21316 (2016).

70. Escobar-Wilches, D. C. *et al.* Analysis of testosterone-hydroxylated metabolites in human urine by ultra high performance liquid chromatography-Mass Spectrometry. *Analytical Biochemistry* **597**, 113670 (2020).

71. Marotta, F. *et al.* study on the mechanisms of action of a novel phytotherapeutic compound against human hepatoma cells. *Annals of Hepatology* **6**, 111–116 (2007).

72. Xie, H. *et al.* Targeting Lactate Dehydrogenase-A Inhibits Tumorigenesis and Tumor Progression in Mouse Models of Lung Cancer and Impacts Tumor-Initiating Cells. *Cell Metabolism* **19**, 795–809 (2014).

73. Shah, S. & D'Souza, G. G. M. Modeling Tumor Microenvironment Complexity In Vitro: Spheroids as Physiologically Relevant Tumor Models and Strategies for Their Analysis. *Cells* **14**, 732 (2025).

74. Breideband, L. *et al.* Gravitational forces and matrix stiffness modulate the invasiveness of breast cancer cells in bioprinted spheroids. *Materials Today Bio* **31**, 101640 (2025).

75. Hu, X. *et al.* Organoid as a promising tool for primary liver cancer research: a comprehensive review. *Cell Biosci* **14**, 107 (2024).

76. Zhuang, P., Chiang, Y.-H., Fernanda, M. S. & He, M. Using Spheroids as Building Blocks Towards 3D Bioprinting of Tumor Microenvironment. *IJB* **7**, 444 (2024).

77. Wong, C.-W., Han, H.-W., Tien, Y.-W. & Hsu, S. Biomaterial substrate-derived compact cellular spheroids mimicking the behavior of pancreatic cancer and microenvironment. *Biomaterials* **213**, 119202 (2019).

Chapter 3—From Molecular, Cellular, to Clinically Relevant Potency: When and Why Organoids Inform RNA Therapeutic Development in Solid Tumors

1. Overview and Motivation

Modern RNA therapeutics for solid tumors demand potency assays that report not only molecular target engagement but also whether those effects survive the barriers of three-dimensional tumor architecture and the TME. Conventional 2D assays remain the workhorse for RNA interference strategies (siRNA/miRNA/piRNA/ASO) and mRNA/circRNA vaccines and exogenous payloads: they are standardized, high-throughput, and well suited to quantify "molecular potency" (knockdown or expression changes by qPCR or western blot) and classic viability-based IC_{50}/EC_{50} metrics under controlled exposure conditions. However, 2D monolayers strip away diffusion distances, extracellular matrix, and stromal and immune organization, and therefore cannot answer whether a formulation that looks potent on plastic will remain effective in the 3D context of a solid tumor.

This review focuses on organoid-based potency assays for RNA therapeutics in solid tumors and asks in which concrete situations organoids provide more informative or clinically relevant readouts than 2D, and why they are not yet used as routine potency platforms. We summarize how current studies deploy tumor spheroids, patient-derived organoids, and other organoid-based platforms to evaluate siRNA/RNAi nanocomplexes, non-coding RNA mimics, and mRNA and circRNA payloads. In practice, organoids are used in three main roles: (i) cell line-derived spheroids as early 3D phenotypic tests for delivery-sensitive siRNA formulations; (ii) patient-derived organoids as a 3D viability "filter" layered on top of 2D pharmacology; and (iii) more specialized organoid co-cultures that read out immune or stromal functions.

Across modalities, the conceptual advantages of organoids are clear with patient-linked heterogeneity, 3D architecture, and the option to add immune and stromal compartments, but most implementations fall short of true potency assays. 3D readouts are often single-dose and qualitative or semi-quantitative. 3D dose-response curves and IC_{50}/GR metrics are rarely reported, and target knockdown or

pathway modulation is usually confirmed only in 2D. We argue for a layered strategy in which 2D assays continue to define molecular potency and screen conditions, while organoids are used deliberately to test 3D delivery, patient-specific resistance, and immune or stromal constraints. We outline practical paths toward more standardized organoid-based potency workflows, including immune-competent and stromal co-culture systems, plate-based and microfluidic platforms, and integration of imaging and multi-omics, with the goal of making organoid assays quantitatively useful, rather than decorative, in RNA drug development for solid tumors.

This review provides the first integrated potency-framework analysis across all major RNA therapeutic classes in solid tumors, proposing "clinically relevant potency" as the organizing principle that unifies molecular, cellular, and tissue-level readouts, and systematically evaluating for each RNA modality and organoid platform class precisely when 3D models add clinically relevant information beyond conventional 2D assays and when they do not.

Box 1 | Our definition of potency in solid-tumor RNA therapeutics

In biologics regulation, potency is interpreted as a product's specific ability to achieve an intended effect, supported by appropriate laboratory assays and, in some contexts, controlled clinical data[34]. In practice, potency for solid-tumor biologics is not a single number but a mapping between dose/exposure and a mechanism-appropriate functional endpoint, evaluated under the *rate-limiting constraints* that determine clinical performance. We therefore distinguish three nested layers. **Molecular potency** quantifies target engagement and proximal pathway modulation (e.g., knockdown, expression, or signaling changes). **Cellular/phenotypic potency** quantifies downstream cellular outcomes (e.g., growth inhibition, apoptosis, invasion) using dose-response metrics such as IC_{50}/EC_{50} or growth-rate-adjusted (GR) readouts when appropriate[11,35–37]. **Clinically relevant potency** quantifies the same dose-response relationship *when clinically relevant barriers and interactions are preserved*, such that the measured endpoint reports whether the therapeutic mechanism survives constraints like 3D diffusion distances, ECM, spatial heterogeneity, and, when included, immune/stromal interactions. Under this framework, different model systems interrogate different steps of a therapeutic cascade; an assay is informative only insofar as it captures the step(s) that are rate-limiting for the candidate modality.

2. Potency testing for modern cancer biologics, and our focus on RNA

Cancer, especially solid tumors, remains a leading cause of mortality worldwide despite decades of advances in surgery, radiotherapy, chemotherapy, and targeted small molecule agents[1]. Yet fewer than 10% of oncology drug candidates entering clinical development ultimately achieve regulatory approval[2], and many that perform well in preclinical models fail to demonstrate meaningful clinical benefit, reflecting persistent limitations in how current models predict human response[3]. Whereas many traditional agents are designed to inhibit a defined molecular target within cancer cells, a growing fraction of new oncology drug candidates are complex biologics, such as cell-based immunotherapies, oncolytic viruses, protein therapeutics, and RNA-based drugs[2,4,5]. Some act mainly on tumor-intrinsic pathways, but many derive their activity from how they engage or reprogram immune and stromal compartments of the dynamic, heterogeneous tumor microenvironment (TME) to overcome resistance niches, and sustain anti-tumor activity within solid tumors[6–8]. For these biologics, potency is no longer adequately summarized by a 2D proliferation assay or a tumor-volume curve in mice. It becomes an emergent property of a multi-step cascade—delivery to the right cells, target engagement, and durable reprogramming of the TME—and whether those changes persist in the three-dimensional architecture and dynamically complex microenvironments of solid tumors[4]. Potency assays therefore need to report not only that a target is modulated, but that this modulation produces durable functional effects in a context that meaningfully approximates human tumors.

Conventional preclinical testing relies for drug potency on a combination of 2D cell-based assays and animal models[2,9]. 2D monolayer cultures using immortalized lines or short-lived primary cells are efficient for defining *molecular potency* and *cellular potency*—target knockdown, pathway modulation, and IC_{50} readouts under well-controlled exposure **(BOX 1)**[10,11]. However, they progressively lose key features of patient tumors, including stable genotype, three-dimensional architecture, and microenvironmental constraints, and therefore overestimate how easily a candidate drug can reach and act on its targets[10]. On the other hand, animal models remain a mainstay of preclinical development for

integrating pharmacokinetics, pharmacodynamics, safety, and disease biology in an intact organism[2,12]. Yet for solid tumors, their ability to predict human response is limited. Cross-species differences in tumor physiology and immunity, shortened lifespans, and practical constraints on sampling and dosing mean that many RNA and other biologics that appear potent in mice fail to demonstrate clinical benefit, particularly in the setting of marked inter-patient and intra-tumoral heterogeneity[12–14]. Together, these limitations motivate additional in vitro systems that can bridge the gap between reductionist 2D potency assays and whole-animal studies[13,15].

Three-dimensional culture systems—including tumor spheroids and organoids—were developed to restore aspects of tissue architecture that are lost in 2D. Tumor organoids are self-organizing 3D epithelial structures derived from patient tumors or engineered lines, typically embedded in an extracellular matrix (ECM) scaffold[7,10]. They recapitulate key features of solid tumors, including cell-cell and cell-matrix contacts, gradients of nutrients and oxygen, and at least part of the clonal and phenotypic heterogeneity seen in patients. However, it is imperative to note that organoids introduce new sources of variability, cost, and technical complexity[16,17]. They still omit important components of the TME—such as vasculature, immune cells, and stromal compartments—unless these are added deliberately through co-culture or microphysiological designs[7,15]. Nevertheless, for modern biologics in solid tumors, organoid systems offer a way to test delivery, penetration, and resistance mechanisms that are largely invisible in classical 2D potency assays and difficult to dissect mechanistically in animal models. These features of organoids, whether advantages or limitations, render them practical platforms to probe what we term *clinically relevant potency* **(BOX 1)**. Clinically relevant potency refers to the dose-response relationship between a therapeutic candidate and a mechanism-appropriate functional endpoint, and this relationship is measured under models that preserve clinically-relevant constraints manifesting as rate-limiting steps for the therapeutic candidate's mechanism of action. In other terms, clinically relevant potency asks not "how a drug candidate influences the 3D tissue culture models", but asks "what the quantifiable functional effects of this drug candidate are when clinically and physiologically relevant barriers and interactions are present". We believe this

definition is helpful and necessary for investigating the potency of new anti-tumoral biologics, especially when they are targeting components in the TME.

Although many biologic modalities are now pursued in oncology, antibodies remain the dominant therapeutic chassis in biopharmaceutical development and commercialization, supported by mature engineering, manufacturing, and approval pipelines[18–20]. Meanwhile, RNA therapeutics have emerged as a highly programmable platform—with the potential for rapid design iterations and scalable production in the case of mRNA-based and circRNA-based constructs—while enabling access to targets and mechanisms that are difficult to reach with proteins alone[4,21–24]. For both antibodies and RNA therapeutics, however, clinically relevant potency in solid tumors is shaped by constraints that classical in vitro assays only partially capture. For tumor-targeting antibodies, these include tumor-wide determinants such as antigen density and heterogeneity, intratumoral penetration and distribution, and dynamic antigen modulation or loss[25,26]; for immuno-modulating antibodies, these tumor-side factors are further compounded by the composition, activation state, and spatial organization of immune cells in the TME[27–31]. For RNA therapeutics, clinically relevant potency is more often limited by the ability to achieve sufficient intracellular exposure with appropriate cell-type specificity across heterogeneous 3D tissues—constraints governed by delivery, uptake, endosomal escape, and local microenvironmental context that 2D systems under-represent[23]. Together, these considerations galvanize potency assays that go beyond molecular and cellular readouts in 2D and explicitly quantify dose-response behavior under clinically relevant barriers and interactions—the clinically-relevant potency layer that organoid and organoid-based tumor models are well positioned to probe.

While antibody-based immuno-oncology has also been extensively reviewed, including in 3D and organoid contexts, the RNA-organoid space remains comparatively under-standardized as a potency framework[32,33]. Accordingly, this review centers on RNA therapeutics as active agents in solid tumors, and treats antibody and other biologic modalities only as contextual comparators where they sharpen shared principles. This review does not cover antibodies in general, endogenous RNAs as biomarkers or disease

drivers, or RNA components used solely as delivery aids for non-RNA drugs. Against this background, we ask a practical question: for RNA therapeutics in solid tumors, in which specific situations do tumor organoids provide more informative or clinically relevant potency readouts than conventional 2D cell-based assays, and what practical or technical barriers currently prevent their use as routine potency platforms? In the sections that follow, we first outline RNA therapeutic modalities and conventional 2D potency assays. Next, we examine how tumor organoids and organoid-based models are actually deployed for these drugs and compare their contributions to 2D assays and, where data exist, to patient response and translational outcome. Finally, we highlight key gaps and future directions for making organoid-based potency assays quantitatively useful rather than merely illustrative.

RNA modality	**Core therapeutic logic**	**Dominant potency readouts**	**What clinically relevant potency asks**	**Tumor organoid fit**
siRNA / shRNA	Sequence-directed silencing of defined targets	Target knockdown; viability, proliferation, apoptosis, invasion, sensitization	Does silencing remain effective under 3D delivery barriers, heterogeneous exposure, and ECM constraints?	Useful as downstream contextual platforms
ASOs	Transcript depletion or splice modulation	Knockdown, splice switching, isoform correction, growth effects	Do transcript / splice effects remain functional in heterogeneous 3D tissues?	Useful as confirmation / stratification layers

miRNA mimics / inhibitors	Reprogram multi-gene tumor networks	Target-network modulation; growth, apoptosis, invasion, chemoresponse	Does network-level reprogramming survive 3D architecture and patient heterogeneity?	Moderately useful, often semi-quantitative
Emerging piRNA agents	Experimental modulation of PIWI-associated circuits	Early molecular effects and simple antitumor phenotypes	Does activity persist in patient-linked 3D models?	Mostly conceptual at present
mRNA cancer vaccines	Encode antigens to prime antitumor immunity	APC activation / presentation; antigen-specific T-cell priming and expansion	Does the construct reach the right immune compartments and generate effective priming?	Poor as primary platform; useful only downstream as tumor challenge systems
mRNA local payloads	Express therapeutic proteins locally in tumor / TME	Payload expression; local tumor, immune, or stromal effects	Is expression tumor-restricted and functionally effective in 3D tissue context?	Good conceptual fit, but still early
circRNA cancer vaccines	Circularized antigen-expression constructs for immune priming	Antigen expression durability; APC activation and T-cell priming	Does the construct achieve effective immune-compartment expression and priming?	Poor as primary platform; mainly downstream challenge use

circRNA local payloads	Circularized local effector-protein expression in tumor / TME	Payload expression durability; downstream functional effects	Does expression persist and remain spatially effective in 3D heterogeneous tissue?	Plausible fit, but evidence remains sparse

Table 2. Major RNA therapeutic modalities in solid tumors and their dominant potency logic.

Conceptual summary of the main RNA therapeutic classes discussed in this review. For each modality, the table highlights the core therapeutic logic, the dominant potency readouts, what clinically relevant potency means in practice, and whether classical epithelial tumor organoids are a natural first-line platform or mainly a downstream contextual platform.

3. Therapeutic RNA platforms in solid tumors and what "potency" means in these platforms

RNA therapeutics in oncology span several mechanistic classes, from inhibitory RNAs that silence tumor-intrinsic targets to mRNA and circRNA constructs that encode immunostimulatory or therapeutic proteins. Although they share common challenges in delivery and stability, the meaning of "potency" differs between these classes: for some, it is dominated by tumor-cell knockdown and phenotypic effects; for others, by the ability to prime or sustain immune responses in an appropriate tissue context. In this section, we outline the main RNA modalities currently explored in solid tumors and clarify what molecular, cellular, and clinically relevant potency mean for each, setting the stage for how organoid-based models are used in later sections **(Table 2)**.

3.1 RNA interference and antisense strategies (siRNA, miRNA mimics/inhibitors, ASOs, emerging piRNA agents)

RNA interference (RNAi) and related antisense strategies aim to suppress defined RNA targets in tumor cells or other compartments by sequence-directed degradation, splicing modulation, or translational inhibition. In oncology, these modalities include small interfering RNAs (siRNAs), short hairpin RNAs (shRNAs), microRNA (miRNA) mimics or inhibitors, chemically modified antisense oligonucleotides (ASOs), and more recently, experimental PIWI-interacting RNA (piRNA)[38–40] **(Table 2)**. Most current applications of RNA therapeutics in solid tumors remain tumor-intrinsic: silencing oncogenic drivers, survival pathways, or resistance mechanisms in cancer cells, sometimes in combination with chemotherapy or targeted agents[38]. A smaller but growing literature explores interference with non-tumor compartments, for example modulating macrophage checkpoints or stromal signaling[41,42].

For these inhibitory and antisense therapeutics, molecular potency is classically defined by the efficiency and durability of target suppression at the RNA and protein levels, for example, the percentage knockdown by qPCR and western blot at a given dose and time[4] **(Figure 5A)**. Cellular and phenotypic potency are typically assessed in 2D monolayer cultures as effects on viability, proliferation, apoptosis,

invasion, or migration under controlled exposure[4,43] **(Figure 5A)**. When multi-dose designs are used, these responses can be summarized by IC_{50}/EC_{50} or growth-rate-adjusted (GR) metrics[35]. These early assay layers remain central to lead optimization, although regulatory expectations for biologic potency are framed more broadly around quantitative measures of mechanism-relevant biological activity rather than purely historical small-molecule paradigms[34]. ASOs and siRNA duplexes, in particular, fit this framework well: they act on one or a small number of primary transcripts, and the relationship between target knockdown and phenotypic readouts can often be parameterized in classical pharmacology terms[4,23].

Therapeutic miRNA mimics and inhibitors occupy a similar mechanistic space but act at a broader network level. Endogenous miRNAs are loaded into RISC and, via a short seed region, partially repress dozens to hundreds of mRNA targets, so potency is defined by both modulation of key direct targets and shifts in downstream pathway and phenotypic programs[44,45]. Emerging piRNA-based agents are conceptually related but less mature, acting through PIWI-associated pathways originally characterized in the germline; dysregulated piRNA-PIWI axes have been implicated in oncogenic and immune-regulatory circuits across several solid tumors[40]. In both cases, current therapeutic designs in oncology remain early-stage compared with siRNA and ASO, and standardized potency frameworks, especially dose-response metrics in 3D models, are far less developed[45]. Thus, in this review we treat miRNA- and piRNA- based therapeutic agents as part of the broader inhibitory small RNA family, while highlighting only selected organoid applications where they have been tested as active agents.

In solid tumors, however, the clinically relevant potency of many inhibitory small-RNA therapeutic strategies is strongly shaped by whether sufficient intracellular exposure is achieved at relevant sites within a heterogeneous 3D tissue[22–24]. Formulations must traverse abnormal vasculature, ECM, and elevated interstitial pressure, then bind, be internalized, and escape endosomes in the right cell populations[22–24]. In standard 2D monolayer systems, many of these constraints are minimized: tumor cells are arranged as a thin sheet with short diffusion distances, negligible matrix, and uniform exposure to media[10]. As a result, 2D potency assays are highly sensitive to sequence and chemistry, but relatively insensitive to delivery and

tissue-architecture failure modes that can dominate in vivo[22]. For RNAi, miRNA- and ASO-based strategies, and likely emerging piRNA-based therapeutic approaches in solid tumors, clinically relevant potency therefore not only hinges on whether a sequence can silence a target under ideal exposure, but more on whether that silencing can be reproduced across relevant regions and cell types in a 3D tumor. In later sections, we examine how organoid-based 3D systems are used, though often imperfectly, to interrogate this clinically relevant layer.

3.2 mRNA therapeutics: vaccines and local payloads

mRNA-based therapeutics in oncology can be broadly divided into two functional categories **(Table 2)**. The first comprises cancer vaccines, in which mRNA encodes tumor-associated or neoantigenic antigens, often alongside adjuvant features, to drive antigen expression, presentation, and priming of tumor-reactive T-cell responses via professional antigen-presenting cells (APCs)[21]. The second comprises local or tumor-directed payload constructs, in which exogenous mRNA is delivered directly to the tumor or its microenvironment to drive expression of cytokines, costimulatory ligands, bispecific engagers, or other therapeutic proteins within the lesion itself[21]. Operationally, these local payloads can be grouped into three broad classes: secreted factors that act on nearby immune or stromal cells (for example cytokines or engager-type proteins), membrane-displayed ligands that alter cell-cell signaling at the tumor site, and intracellular proteins that directly reprogram tumor-cell state. This distinction matters for potency testing, because the relevant molecular readout may be secretions into the supernatant, surface display on transfected cells, or intracellular protein accumulation, and the downstream functional readouts differ accordingly[21,46,47]. Both vaccines and local payloads rely on transient translation of an RNA template, but they differ in where their critical biology occurs and therefore what "potency" means **(Table 2) (Figure 5B, 5C).**

For mRNA cancer vaccines, molecular potency is usually defined by the level and duration of antigen expression in dendritic cells (DCs) or other APCs, along with innate sensing and costimulatory

signatures[48]. Cellular and phenotypic potency are reflected in the magnitude, breadth, and functional quality of antigen-specific T-cell responses—typically measured in 2D systems as T-cell proliferation, cytokine production, cytotoxic activity, or tetramer-positive frequencies in co-culture or ex vivo assays[21,49]. In this case, clinically relevant potency is largely determined at the level of lymphoid and systemic immune organization: uptake by the right APCs in the right anatomical sites, trafficking to draining lymph nodes, and clonal expansion in an appropriate cytokine milieu[21,49]. Classical epithelial tumor organoids do not naturally recapitulate this priming cascade and are therefore not obvious primary platforms for vaccine potency per se[7,50].

In contrast, for intratumoral or local mRNA payloads, their potency is more tightly coupled to the tumor itself. Molecular potency corresponds to the efficiency of mRNA delivery and translation in target cells within the lesion[21,46]. Cellular/phenotypic potency includes changes in tumor-cell intrinsic behavior, such as apoptosis, immunogenic cell death, and in the behavior of local immune and stromal cells, including as enhanced T-cell cytotoxicity in response to a locally expressed cytokine or costimulatory ligand[21,46]. In contrast, clinically-relevant potency depends on penetration and distribution of the mRNA formulation through 3D tumor architecture, the cell-type specificity of expression, and the ability of local immune and stromal compartments to respond[46,51,52]. These are precisely the kinds of constraints that 2D assays under-represent and that 3D models can, in principle, be configured to probe[7,10].

3.3 Exogenous circRNA therapeutics: vaccines and local payloads in development

Exogenous circRNA therapeutics in oncology are often used as circularized RNA expression platforms that parallel linear mRNA therapeutics, particularly for vaccine constructs encoding antigens and local payload constructs encoding immunostimulatory or other therapeutic proteins[21,47,53,54] **(Table 2)**. Compared with linear mRNA, exogenous circRNA design places greater emphasis on circularization quality, cap-independent translation control, ORF and sequence optimization, durability of expression, and tuning innate immune sensing, because circRNAs are generally more resistant to exonuclease-mediated

decay and do not require a 5′ cap or poly(A) tail[53,54]. In anti-tumoral vaccine applications, this design still serves the same proximal goal as for mRNA vaccines: both aim for efficient antigen expression in professional APCs followed by antigen presentation and priming of tumor-reactive T cells[53,54]. In contrast, local payload constructs aim to express cytokines, costimulatory ligands, or other therapeutic proteins directly within the tumor or its TME[47,55,56].

The basic potency logic for both mRNA and circRNA therapeutics is broadly similar: molecular potency reflects the efficiency and durability of payload expression in target cells, and cellular/phenotypic potency reflects downstream immune or tumor-cell responses to that payload[21,47,53,54]. In addition, the clinically relevant potency of circRNA agents is similar to that of mRNA therapeutic agents: it depends on where and how they are expressed in vivo. For vaccine-like applications, the key events occur in professional APCs and lymphoid organs, so priming potency is largely governed by APC uptake, antigen presentation, and T-cell expansion in appropriate anatomical sites[53,54]. For local circRNA payloads delivered to tumors or their microenvironment, clinically relevant potency is instead tied to penetration and distribution through 3D architecture, cell-type specificity of expression, and the ability of local immune and stromal compartments to respond[47]. As with linear mRNA payloads, these local circRNA constructs may encode secreted immunomodulators, transmembrane proteins, or intracellular therapeutic proteins, and this encoded-protein class strongly influences which potency readouts are most informative[47,53,54,56]. These considerations mirror those for mRNA therapeutics, and in later sections we treat circRNA payloads alongside mRNA when discussing which aspects of potency can be meaningfully probed in 2D versus organoid-based models **(Table 2)**.

4. Conventional 2D Potency Assays for RNA therapeutics in solid tumors

For most RNA therapeutic programs discussed in this review, in vitro potency characterization still begins in conventional 2D monolayers. These systems are the primary workhorse for quantifying molecular potency and cellular/phenotypic potency under relatively uniform exposure conditions. In this section, we summarize the typical 2D assay workflows used to evaluate RNA drug candidates in solid tumors and highlight the main strengths and limitations of these workflows. This sets up our later comparison with organoid-based assays, which are designed to probe the clinically relevant potency layer that 2D monolayers largely cannot address **(Figure 5)**.

4.1 2D potency workflows for inhibitory and antisense RNAs (siRNA, miRNA mimics/inhibitors, ASOs, emerging piRNA agents)

For inhibitory and antisense RNA therapeutics, 2D monolayer cultures are the primary platform for defining molecular and early cellular/phenotypic potency before introducing any 3D models[4,43]. In most studies, tumor cell lines or short-term primary cancer cells are first transfected or exposed to the RNA candidate under controlled conditions, and molecular potency is quantified as the extent and durability of target modulation at the RNA and protein levels. Typical readouts include RT-qPCR for target and off-target transcripts; western blot, flow cytometry, or ELISA for protein expression and pathway markers, and in some cases reporter assays in which luciferase or fluorescent proteins are fused to target 3′UTRs or promoters[4,57]. These assays provide clean, sequence- and chemistry-dependent knockdown or modulation curves under near-uniform exposure **(Figure 5A)**.

The same 2D monolayer systems are then used to quantify cellular and phenotypic potency. Here, studies most often measure changes in viability or proliferation using tetrazolium- or ATP-based metabolic assays (such as MTT, WST, or CellTiter-Glo)[58–60], sometimes supplemented by apoptosis assays (such as Annexin V/PI staining, caspase activity)[4,58,61] and, when relevant, migration or invasion assays (such as wound-healing and Transwell assays)[60,62]. For tumor-cell-focused endpoints, studies commonly report

viability, proliferation, or apoptosis changes across one or several concentrations[4,43,59]; as in cell-based oncology workflows more broadly, multi-dose designs can be summarized by IC_{50}/EC_{50}-type values[35,37,63]. In the RNA-focused literature, however, many studies stop short of formal pharmacometric parameterization and instead report relative responses at fixed or limited dose ranges [64,65]. In the broader drug-response literature, GR or normalized drug-response metrics have been introduced to correct for proliferation confounders in cell-based screens[35,36]. They are conceptually applicable to RNA potency assays as well, although they are rarely applied explicitly in the RNA-focused studies reviewed here.

For inhibitory RNAs designed to modulate immune visibility or stromal interactions, additional 2D co-culture assays are layered on top. These systems measure functional endpoints such as macrophage phagocytosis, T-cell or NK-cell cytotoxicity, activation-marker expression, and cytokine production under still-idealized exposure conditions[4,57]. Readouts are often reported at one or a few doses rather than as formal IC_{50} curves, but they still belong to the cellular/phenotypic potency layer of Box 1 because they quantify reprogrammed cell behavior in flat culture. For example, Huang et al. used macrophage-tumor co-cultures to measure phagocytosis of labeled tumor cells after CD47 or calreticulin axis modulation in flat culture[42]. A recent study likewise used primary human Natural Killer (NK) cells transfected with Cish siRNA and co-cultured them with gastric cancer cells to quantify cytokine secretion, exhaustion-associated markers, and tumor-cell cytotoxicity in 2D culture settings[66]. In practice, target-centric agents such as siRNA and many ASOs fit especially well into these workflows, whereas miRNA and emerging piRNA therapeutics are assayed in similar 2D systems but interpreted at the level of pathway or program changes rather than single-gene IC_{50} relationships[4,40,67].

4.2 2D potency workflows for mRNA and circRNA therapeutics

As outlined in Section 2, exogenous mRNA and circRNA therapeutics in oncology often developed in two broad functional roles: (i) vaccines that prime anti-tumor immunity via professional APCs and lymphoid organs, and (ii) local payloads that act within tumors or their microenvironment. In practice, both roles rely heavily on conventional 2D assays to define molecular and cellular/phenotypic potency before any 3D or in vivo testing[21,53]. Here we summarize how those workflows are typically organized **(Figure 5B, 5C).**

For mRNA or circRNA cancer vaccines, 2D assays focus on APC and T-cell function[49,53]. Molecular potency is assessed by transfecting or exposing DCs or other professional APCs to the RNA construct, and measuring the level and duration of antigen expression and presentation. This is often complemented by detection of innate-sensing and maturation signatures: for example, surface co-stimulatory molecules, type I interferon-related genes, and cytokine secretion[49,68]. Cellular and phenotypic potency are then read out in co-culture or ex vivo systems that bring these antigen-loaded APCs together with T cells. Common endpoints include antigen-specific T-cell proliferation, expression of activation markers, cytokine production, and cytotoxic activity against peptide-pulsed or antigen-expressing targets[49,69]. These assays are typically performed in flat multiwell formats, where exposure to the vaccine formulation can be tightly controlled, and they define a first pass of "priming potency" under idealized conditions before in vivo studies are used to integrate trafficking to lymphoid organs and systemic immune orchestration. For circRNA vaccines, the same APC/T-cell workflows are generally used, with additional emphasis on the duration of antigen expression, cap-independent translation control, and innate immune sensing associated with the circular backbone[21,55].

For intratumoral or local mRNA/circRNA payloads, 2D workflows shift the emphasis to tumor cells and simple immune co-cultures[21,46,47]. Molecular potency corresponds to efficient delivery and translation of the payload in target cells—most often quantified as expression of the encoded cytokine, co-

stimulatory ligand, bispecific engager, or other therapeutic protein in tumor-cell monolayers or in relevant stromal or immune cell types[21,46,47]. The exact molecular readout depends on the encoded payload class: secreted proteins are often measured in supernatants by ELISA or related assays, transmembrane proteins by flow cytometry or immunostaining on transfected cells, and intracellular proteins by immunoblotting, microscopy-based expression analysis, or, in some platform-validation settings, reporter constructs[47,52,70,71]. In this setting, "delivery" refers primarily to cellular delivery into cultured target cells and successful translation of the encoded protein, rather than to tissue-level penetration through a solid tumor. Cellular and phenotypic potency include direct tumor-cell effects (such as apoptosis, immunogenic cell death markers, or changes in differentiation and proliferation); and examine indirect effects mediated through co-cultured immune cells (such as enhanced T-cell or NK-cell cytotoxicity, altered cytokine profiles, or changes in macrophage polarization)[21,46,47]. These experiments again use standard 2D plates and co-culture formats, and in some cases allow dose-response relationships to be constructed for expression and functional outputs under uniform exposure. In practice, such 2D assays serve as the main in vitro stage to verify that mRNA and circRNA constructs achieve their intended activities in the relevant cell types[21,46,47]. Only a subset of programs proceeds to organoid or more complex 3D models to test whether those activities survive the spatial and microenvironmental constraints of solid tumors[72,73].

4.3 Strengths of conventional 2D potency assays

Conventional 2D monolayer cultures remain the workhorse for in vitro potency testing in oncology because they make molecular and cellular readouts highly standardized, interpretable, and scalable. Cells are grown on flat plastic under well-controlled media conditions, so exposure to RNA therapeutics can be tightly defined in terms of dose, timing, and combination treatments, and basic assay parameters such as seeding density, confluence at treatment, and readout time are easy to harmonize across experiments and laboratories. This setting is naturally compatible with multiwell plates, automation, and high-throughput workflows, allowing large numbers of sequences, chemistries, and formulations to be screened quickly and at relatively low cost[9,10].

These features translate into clean pharmacology. Because each cell in a monolayer experiences a nearly uniform external concentration of the drug candidate, dose-response relationships between exposure and molecular or phenotypic endpoints can be parameterized with classical metrics such as IC_{50}/EC_{50}, GR, or normalized response measures[9,10]. Mechanistic perturbations—such as target overexpression or rescue constructs, mutant controls, or pathway inhibitors—can be layered in without the added complexity of spatial gradients or multi-compartment architectures[10]. As a result, 2D assays are well suited to separating sequence- and chemistry-driven differences in intrinsic activity from gross delivery failures, and they fit comfortably into established industrial expectations and into potency-testing habits that emphasize standardized dose-response and mechanism-linked in vitro readouts. In practice, this makes 2D monolayers the natural first stage for defining molecular and cellular potency of RNA therapeutics before more complex models are considered[9,10].

4.4 Where 2D potency assays fall short in solid tumors

At the same time, the very features that make 2D monolayers attractive for molecular and cellular potency also define their limits for solid tumors. Flattening cells onto plastic eliminates three-dimensional architecture, ECM, and realistic diffusion distances, so there are few physiologically meaningful gradients of oxygen, nutrients, or drug concentration and no physical barriers to penetration. Tumor cells grow as a relatively homogeneous sheet with little spatial structure, and stromal or immune cells, when included at all, are typically added in simple ratios without the organized niches, migration constraints, or spatial exclusion patterns seen in vivo[10]. Under these conditions, many delivery-sensitive failure modes for RNA—limited tissue penetration, sequestration in outer layers, or preferential uptake by non-target cell types—are largely masked by design[22].

2D systems also truncate tumor heterogeneity and microenvironmental dynamics. Established lines and short-lived primary cultures tend to lose rare subclones and patient-specific architectures, and they lack the evolving interactions with vasculature, fibroblasts, myeloid cells, and lymphocytes that shape drug

response in solid tumors[7,10]. Exposure regimens are non-physiologic: cells are bathed continuously in fixed concentrations of drug, with no realistic pharmacokinetic profiles, interstitial pressure, or convective flow[10,22]. As a result, many RNA formulations that look potent in 2D—achieving strong knockdown and IC_{50} shifts under idealized conditions—may fail once they must traverse 3D tissue, ECM, and complex TMEs[22].

Within the framework of Box 1, 2D assays are therefore excellent for defining molecular potency and cellular/phenotypic potency, but they contribute little to clinically relevant potency, because they do not preserve the clinically relevant barriers and interactions that are rate-limiting in solid tumors. The gap between what 2D can report and what matters in patients motivates additional in vitro systems that reintroduce aspects of 3D architecture, patient-linked heterogeneity, and immune or stromal compartments[7,9]. In the next sections, we examine how spheroids, patient-derived organoids, and organoid-immune co-culture systems attempt to fill this gap and to make clinically relevant potency measurable rather than inferred.

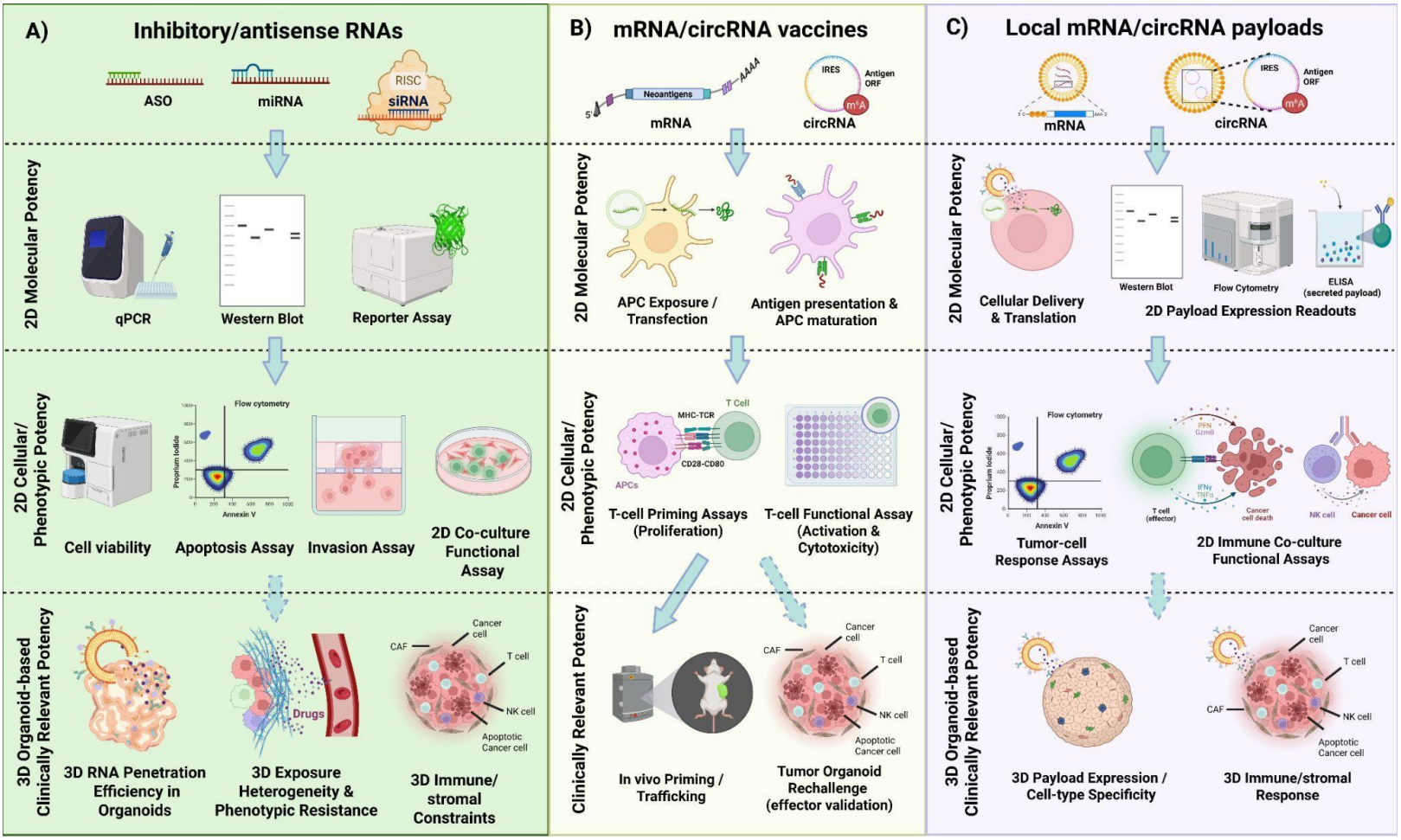

Figure 5. Typical 2D potency workflows for major RNA therapeutic classes in solid tumors, and where organoid-based models are layered in to probe clinically relevant potency.

For inhibitory/antisense RNAs **(A)** and local mRNA/circRNA payloads **(C)**, organoid-based models are introduced mainly to test whether molecular and phenotypic activity defined in 2D persists under 3D architectural and microenvironmental constraints; for local payloads, this contextual layer also includes 3D payload expression, cell-type specificity, and immune/stromal response. For mRNA/circRNA vaccines **(B)**, by contrast, primary potency is generally evaluated through APC- and T-cell-centered assays and in vivo priming models, while tumor organoids serve mainly as downstream tumor-side challenge systems rather than primary priming platforms. Figure made using BioRender.

5. Cancer-relevant organoids as platforms for potency testing

5.1 Definition of "organoid-based" potency assays

In this review, we use "organoid-based" as an operational umbrella term for 3D tumor culture systems that preserve key features of solid tumors and are deliberately used to impose clinically relevant 3D constraints on drug exposure and response[10] **(Figure 6A)**. These key features include epithelial architecture, cell-cell and cell-matrix contacts, and at least some patient-relevant heterogeneity[7,10]. Under this definition, patient-derived organoids (PDOs) are the canonical examples, while tumor spheroids are included when they are used to impose clinically relevant architectural and microenvironmental constraints on potency testing of RNA therapeutics[7,10,74]. It's worth noting that adjacent ex vivo models such as patient-derived tumor explants are not canonical organoids, but they can preserve native architecture and microenvironmental composition, and they have been used, albeit not frequent, in siRNA delivery studies[7,75].

This is intentionally broader than the traditional "organoid" definition in the strict developmental sense. PDOs derived from patient tumor biopsies or surgery samples and grown in ECM gels are the canonical example and remain the dominant 3D system in current oncology organoid work[7,76]. However, many preclinical drug-delivery and drug-response studies—including a growing number of nucleic-acid delivery programs—use highly standardized 3D spheroids formed from established tumor cell lines in ultra-low-attachment (ULA) plates or hanging drops[10,77–81]. These spheroids do not fully recapitulate organogenesis, but they introduce radial gradients of nutrients, oxygen, and drug, as well as simple cell-cell organization and, in some formats, cell-matrix architectures that are absent in 2D monolayers[77,81]. When such spheroids are used explicitly to test whether an siRNA nanocomplex or mRNA formulation can penetrate and act across a 3D tumor-like structure, we treat them as organoid-based clinically relevant potency platforms[10].

Beyond PDOs and standardized spheroids, we also consider more complex 3D platforms—such as organoid-on-chip (OOC), perfused microfluidic systems, and immune- or stromal-constrained organoids—when they are used to interrogate clinically relevant potency as defined in Box 1[7,10,15,82]. Other 3D culture methods, including micromolded agarose microwells and various hydrogels or scaffold systems, are well established for general drug and nanoparticle testing, and have also been used in some gene-delivery contexts[10,76,83]. However, in the RNA-oncology literature considered here, they appear more often as adjacent or enabling 3D techniques than as routine, standardized potency platforms.

By contrast, we do not classify small, irregular, or loosely compacted cell aggregates that do not establish stable assay-relevant 3D architectural or diffusion constraints, or 3D suspension cultures used solely for cell expansion, as organoid-based for the purposes of potency. Our focus in the following sections is on 3D systems where the culture geometry and microenvironment are part of the experimental question, which is "does the RNA therapeutic maintain its molecular, cellular/phenotypic, and clinically relevant potency, once realistic architectural and microenvironmental barriers are reintroduced?"

5.2 Types of organoid and organoid-based cultures relevant to RNA potency

Tumor cell line-derived spheroids and organoid-like 3D cultures

Spheroids derived from tumor cell lines are the simplest organoid-like systems used in RNA drug development. Tumor lines are seeded into ULA plates, hanging drops, or soft scaffolds to form compact 3D aggregates[84–86]. In some cases, they are embedded in Matrigel or collagen to introduce ECM components[87]. These spheroids do not reproduce the self-organization or patient-linked heterogeneity of canonical PDOs. Instead, they introduce radial gradients in oxygen, nutrients, and local drug exposure; simple 3D cell-cell organization; and, in some formats, cell-matrix architectures that are absent in 2D monolayers, while maintaining the logistical advantages of standardized cell lines and multiwell formats. In the RNA therapeutics literature we survey, such spheroids are often used as early 3D molecular or phenotypic potency tests, and in some cases as delivery-sensitivity assays **(Figure 6B)**[88–90]. Candidates that

perform well in 2D—for example by target knockdown or measurable phenotypic effects—are then tested in spheroids to determine whether that activity persists under basic 3D constraints. Typical readouts include spheroid formation, growth, viability, cross-sectional area, and live/dead staining or imaging **(Figure 6B)**. Taken together, tumor spheroids function best as first-pass clinically relevant potency filters: they test if the molecular and phenotypic potency defined in 2D persists once basic 3D architecture and diffusion limits are reintroduced.

Patient-derived tumor organoids (PDOs) and PDX-derived organoids (PDXOs)

PDOs, derived directly from patient resections, biopsies, or fine-needle aspiration samples, often preserve patient-specific genotypes, epithelial architectures, and intra-tumor heterogeneity[76]. PDX-derived organoids (PDXOs) offer a complementary route in which established patient-derived xenografts (PDXs) are re-cultured as 3D organoids for higher-throughput testing **(Figure 6A).** Both PDOs and PDXOs can be embedded in ECM-mimicking gels or replated into compatible 3D-supporting multiwell formats, while cultured with niche factor cocktails to generate self-organizing 3D structures[76,91]. These attributes make them natural candidates for organoid-based viability, imaging, and co-culture assays of RNA therapeutics. However, conventional PDOs primarily maintain epithelial compartments, while stromal and immune cells are either lost quickly or substantially depleted over time[7,50]. Together, PDOs and PDXOs are increasingly used for 3D viability and phenotypic assays to test whether RNA therapeutics and delivery systems retain activity in tumor-linked epithelial contexts that are more clinically relevant than 2D monolayers **(Figure 6B)**.

Organoid models with immune and stromal constraints

Building on PDOs and spheroids, multiple groups have created immune- and stromal-constrained organoids by incorporating autologous or allogeneic immune cells (T cells, NK cells, and macrophages)[42,72,92] and non-immune stromal cells (most commonly cancer-associated fibroblasts, and in some cases, endothelial cells)[93,94]. Importantly, in vitro ECM embedding or scaffold alone can mimic some

stromal-like constraints, but it does not by itself create a stromal-cell-containing organoid model [7]. Operationally, these advanced organoid models fall into two broad classes: 1) reconstituted systems, in which defined exogenous immune and/or stromal cells are added back to otherwise epithelial organoids, often using cell populations dissociated from tumor tissues[7]; and 2) native-architecture systems, such as Air-liquid-interface (ALI) organoids or selected microfluidic 3D culture formats, that transiently preserve endogenous non-epithelial compartments[7]. Their value for RNA potency testing lies in exposing cell-type-specific constraints—such as macrophage phagocytosis, T-cell-mediated killing, fibroblast-mediated protection, or cytokine-driven resistance—that are invisible in epithelial-only 2D assays[7] **(Figure 6B).** At present, their use in RNA potency testing is still concentrated in a limited number of centers and indications **(Figure 6C)**, but existing studies already illustrate how clinically relevant potency can be made experimentally accessible [42,72,93,95].

Organoid-on-chip (OOC) platforms and perfused microfluidic systems

Microfluidic devices that host organoids or spheroids under controlled flow can introduce more realistic exposure conditions—for example, perfusion, directional gradients, pulsatile dosing, or clearance under flow —and allow compartmentalization of tumor, stromal, and vascular-like components.[15,82] For RNA therapeutics, these microfluidic systems can conceptually make delivery-limiting transport constraints more explicit, including penetration through matrix-rich 3D tissues, heterogeneous local exposure, and loss of activity under flow **(Figure 6B)** [82,96]. This logic aligns well with clinically relevant potency as defined in Box 1, because such transport constraints may become rate-limiting determinants of whether a therapeutic mechanism remains functional in 3D tissue. In practice, however, they remain technically demanding and are not yet standardized for routine RNA therapeutic potency testing, and most reported applications still remain proof-of-concept and small-scale.[15,82,96]

Stem-cell derived organoids

Pluripotent stem cell-derived organoids, such as brain, lung, and liver organoids, are widely used to model development, organ physiology, infection, and certain genetic diseases[97]. For cancer and RNA therapeutics, their current roles are more niche: they appear in feasibility studies for delivery to specific tissues, in toxicity or safety assessments, or as "normal" reference epithelia to compare with tumor organoids[98,99]. At present, they are rarely used as workhorse potency platforms for oncologic RNA agents, but they will become increasingly relevant in sections on on-target/off-tumor effects and safety-oriented clinically relevant potency[97–99].

5.3 Readouts used in organoid-based potency assays

Molecular, delivery, and pathway readouts

In organoid-based RNA potency assays, mechanistic readouts often sit between bulk viability endpoints and more integrated functional measures. Across spheroids, PDOs, and selected immune-constrained organoid systems, investigators quantify target engagement and proximal pathway modulation in 3D using RT-qPCR, western blotting, immunofluorescence or immunohistochemistry, flow-cytometric surface-marker analysis, and, in selected antisense or splice-switching settings, transcript- or isoform-specific PCR assays **(Figure 6B)**[42,65,88–90,100–107]. In parallel, imaging-based measurements are layered onto these assays to assess uptake, penetration depth, spatial distribution, or outer-layer sequestration of RNA formulations within 3D tissues[65,89,95,101]. These delivery-sensitive readouts are especially relevant for RNA therapeutics, because apparent activity in 2D can fail in organoids when carriers do not penetrate efficiently through 3D tissues or do not achieve sufficient intracellular exposure across heterogeneous regions of the tissue[22–24].

In this sense, organoid-based molecular and delivery readouts do not replace phenotypic potency endpoints, but help determine whether clinically relevant 3D barriers alter the ability of an RNA therapeutic to reach the right cells and engage its target under clinically relevant constraints[7,22–24]. However, these assays are most often used as mechanistic support or confirmation layers rather than as fully parameterized

3D pharmacology[57]. Compared with viability, growth, or immune-killing readouts, molecular and distribution-focused measurements are still less frequently integrated into standardized 3D dose-response workflows.

Viability and growth metrics

The most common readouts in organoid-based potency assays are bulk viability and growth metrics. In spheroids, PDOs, and PDXOs, viability is often quantified with ATP-based assays such as CellTiter-Glo or related luminescent and colorimetric kits, adapted to 3D cultures by optimizing lysis and reading conditions **(Figure 6B)** [65,76,89,91,102–106,108]. These assays can yield plate-based dose-response curves analogous to 2D IC_{50}/EC_{50} measurements, but now under 3D architecture[11,64,89,104]. Complementary imaging-based growth metrics—such as spheroid or organoid cross-sectional area, volume estimates from z-stacks, and counts of viable organoids per well—are extracted from brightfield or fluorescence images using semi-automated or fully automated pipelines[65,88,101]. Some groups have proposed growth-rate-normalized metrics, such as the Normalized Organoid Growth Rate (NOGR), to correct for heterogeneity in baseline growth across patient-derived samples.[37] However, in the RNA-focused organoid literature, readouts remain dominated by relatively coarse viability and size changes, with limited adoption of standardized growth-corrected metrics **(Figure 6C)**.

Morphology, invasion, and structural phenotypes

Beyond bulk viability, organoid systems capture morphological and structural responses that are largely invisible in 2D[10]. Quantitative imaging can track changes in organoid or spheroid size, compactness, fragmentation, and live/dead spatial patterning, as well as the emergence of necrotic or hypoxic cores[106–112]. More broadly, matrix-embedded organoid assays can also be used to evaluate radial outgrowth, invasive dissemination, and other ECM-interacting phenotypes after perturbation. These readouts are well established in the wider organoid field for studying invasion, metastasis-related programs, and microenvironment-dependent response phenotypes[113,114] **(Figure 6B)**. However, in the RNA-focused

organoid literature we analyze in this review, potency readouts remain dominated by relatively coarse viability and size changes. More invasion- or metastasis-related phenotypes are still more often evaluated in conventional 2D assays than in organoid-based models. Systematic use of richer morphological or invasion metrics as quantitative potency endpoints for siRNA, ASO, or other RNA therapeutics in organoid-based models is still rare **(Figure 6C)**[21,72,115].

Immune and stromal functional readouts

In Immune- and stromal-constrained cancer organoid platforms, functional readouts extend beyond tumor-cell intrinsic viability to include immune-cell killing, phagocytosis, cytokine signaling, and stromal protection or matrix remodeling[7,17]. Tumor-immune organoids can be categorized into 1) models reconstituted from dissociated patient tissues, and 2) tissues partially minced to preserve some natural tumor phenotype[7]. In these immune-constrained organoids and natural tumor-immune explants, lymphocyte-dominant tumor killing is measured by longitudinal live/dead imaging, loss of tumor markers, or reporter constructs in tumor cells, while immune effector activity is quantified by flow cytometry (activation markers, exhaustion markers, proliferation), cytokine staining, and, in some cases, TCR sequencing responding lymphocyte populations[7,50,109,116,117]. For myeloid-derived cell populations such as macrophages and DCs, their readouts from the immune-constrained organoids can include macrophage phagocytosis as well as DC activation or antigen-presentation state, measured by uptake assays, surface phenotype, cytokine output, and T-cell priming capacity[116–121] **(Figure 6B)**. For stromal-constrained organoids, their readouts are distinct and include fibroblast activation, matrix remodeling, and other ECM-associated protective signatures[110,116,117] **(Figure 6B)**. For RNA therapeutics, these immune and stromal readouts are beginning to appear in siRNA-PDO-macrophage co-cultures that probe "don't-eat-me" signalling and phagocytosis[42]. Cytokine readouts are also used in emerging RNA-enabled immunotherapy contexts (e.g., circRNA-derived neoepitope studies) that couple immune activation assays to tumor organoid killing[72]. However, most RNA organoid assays still remain tumor-cell-focused, and immune- or stromal-functional endpoints are used far less often than viability, growth, or size readouts **(Figure 6C)**.

High-content multi-omics and spatial profiling

Finally, a subset of organoid and tumor explant studies layer single-cell and spatial multi-omic profiling on top of functional assays **(Figure 6B)**. Single-cell RNA sequencing, sometimes combined with V(D)J/TCR repertoire analysis, is used to map cell states and clonal expansions before and after treatment[117,120–123]. Spatially resolved and multiplexed imaging approaches are increasingly being adapted to tumor organoid systems, where they can capture how treatment-associated phenotypes are organized within 3D tissue architecture; direct spatial transcriptomic applications are emerging, but remain less routine than confocal/whole-mount imaging and single-cell multi-omic workflows[120,124–127]. Emerging 'digitalized organoid' pipelines—AI-assisted 3D segmentation and feature extraction—can further convert imaging and spatial assays into scalable, quantitative phenotypes and facilitate integration with multi-omics[128]. This approach has been particularly informative for dissecting mechanisms of response and resistance to immuno-checkpoint blockade (ICB) and T-cell therapies in immune-competent organoids and explants, revealing shifts in T-cell exhaustion programs, myeloid polarization, and tumor-intrinsic adaptation[113,121,123]. To date, such high-content readouts are not yet commonly applied to RNA therapeutics in organoid systems, and most current examples come instead from immune-competent organoid or explant studies of ICB, T-cell therapies, or related biologic comparators, or from mechanistic organoid studies focused on ECM context, invasion, and TME architecture[57,93,113,114,127] **(Figure 6C)**. However, in principle they are directly applicable: the same pipelines can be used to quantify how siRNA/ASO, mRNA, or circRNA agents reprogram tumor and immune compartments in 3D, and to define clinically relevant potency metrics that integrate molecular, cellular, and tissue-level changes.

5.4 Advantages and Limitations of Organoid-based potency platforms

Organoid-based 3D systems offer several advantages for potency testing that 2D monolayers cannot easily provide. By restoring three-dimensional architecture, ECM, and more tumor-relevant diffusion barriers than 2D, organoid-based 3D systems generate spatial gradients of oxygen, nutrients, and

drugs that more closely resemble solid tumors[10,16]. PDOs preserve at least a subset of patient-specific genotypes, epithelial architecture, and phenotypic heterogeneity, providing a more faithful context for testing whether an RNA therapeutic maintains activity across diverse subpopulations[7,76]. At a practical level, different organoid-based formats contribute different kinds of contextual information: standardized spheroids are most useful for early 3D delivery and phenotypic filtering, PDOs and PDXOs add patient-linked epithelial relevance, and immune- or stromal-constrained systems can expose cell-type-specific constraints that are invisible in epithelial-only 2D assays. When immune and stromal compartments are added, selected reconstituted or native-architecture systems can also recreate basic features of the TME—such as partial immune exclusion, myeloid polarization, or fibroblast-mediated protection—rendering it possible in principle to read out not only molecular and cellular potency but also clinically relevant potency in the sense defined in Box 1[7,17,93].

At the same time, organoid-based platforms introduce practical and conceptual limitations that constrain their use as standardized potency assays. Establishment and maintenance of organoids are more labor-intensive and costly than 2D culture, and success rates, growth kinetics, and baseline phenotypes can vary substantially between patients and tissue sources. Experimental variables such as initial organoid size distribution, matrix composition, passage number, and co-culture conditions are difficult to harmonize at scale, complicating quantitative comparisons across studies or centers. Throughput is inherently lower than in 2D: while miniaturized and semi-automated formats are emerging, most organoid assays cannot yet support the same breadth of sequence, chemistry, and formulation screening that is routine in monolayer systems. Importantly, the main limitation in the current RNA-organoid literature is not only platform variability, but also assay design: many studies use organoids as downstream confirmation layers after 2D potency screening rather than as primary potency-defining systems[17,76,82].

Finally, readouts in organoid and explant assays are often less standardized than their 2D counterparts. Many studies rely on semi-quantitative endpoints—changes in organoid size, number, morphology, or live/dead staining—without consistently reporting dose-response metrics that could serve

as formal potency parameters, and high-content imaging or single-cell profiling pipelines remain technically demanding, all of which were elaborated in the previous section. Across the current RNA-focused literature, 3D assays are frequently single-dose or otherwise sparsely parameterized, and many measure viability, growth, or imaging phenotypes without paired 3D target-engagement data or pathway readouts in the organoids themselves. In some workflows, organoids are also dissociated, re-seeded, or transfected under conditions that partly bypass the intact 3D delivery barriers that clinically relevant potency assays are meant to test . Together, these factors mean that organoid-based systems are currently best viewed as complementary potency platforms: they are well suited to probing delivery, spatial heterogeneity, and microenvironment-dependent effects that 2D cannot capture, but they do not yet replace monolayer assays as the primary, scalable workhorse for defining molecular and cellular potency across large RNA libraries. In the next section, we use this framework to compare how 2D and organoid assays are actually deployed in current RNA studies, and to identify where organoids add clear value versus where 2D remains sufficient.

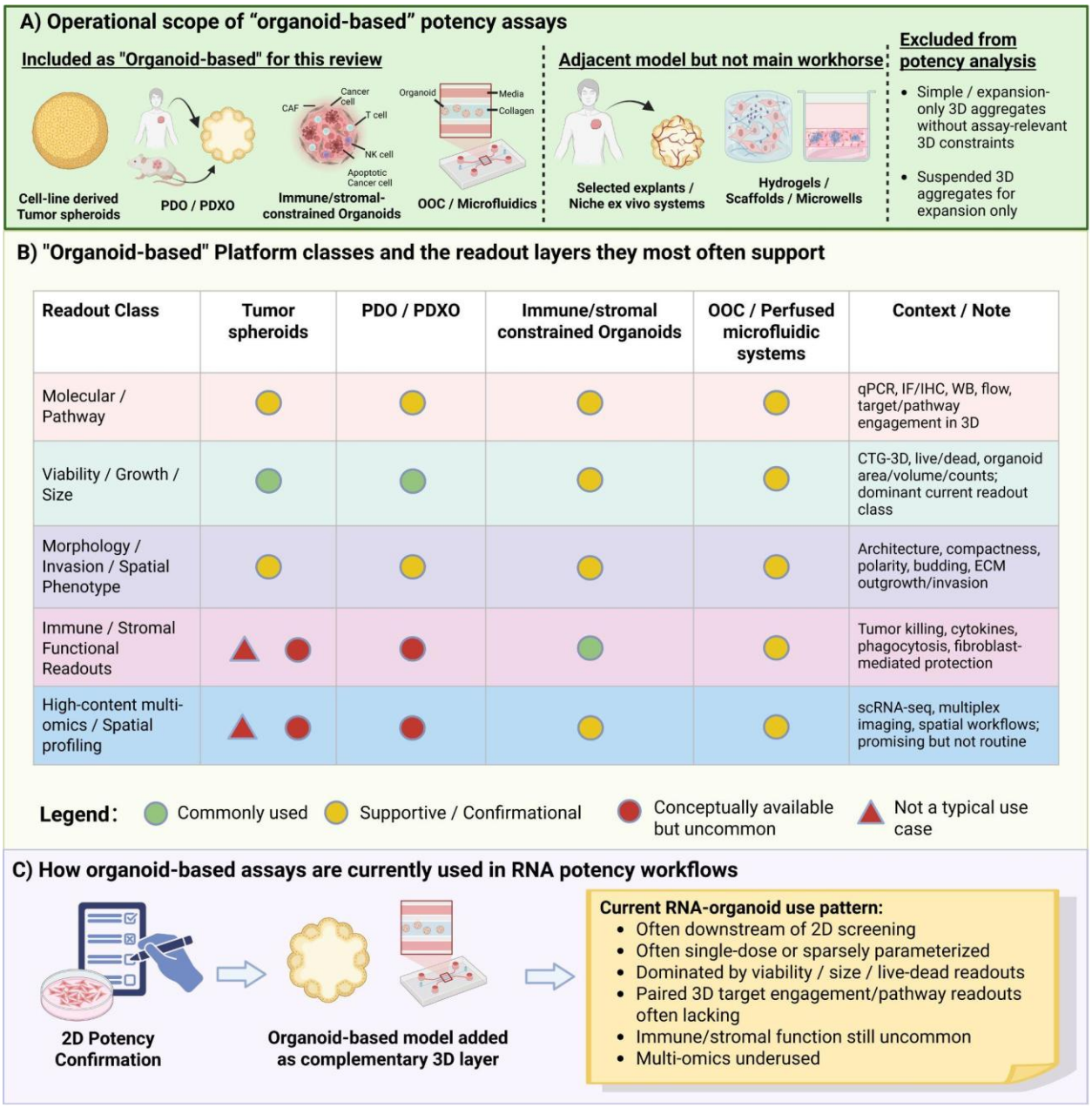

Figure 6. Operational scope, platform classes, readout layers, and current deployment of organoid-based assays for clinically relevant potency testing of RNA therapeutics in solid tumors.

(A) In this review, "organoid-based" is used as an operational umbrella term for 3D tumor systems that deliberately reintroduce assay-relevant architectural, diffusion, and microenvironmental constraints. Included platforms comprise cell-line-derived tumor spheroids, PDOs/PDXOs, immune- and/or stromal-constrained organoids, and organoid-on-chip or perfused microfluidic systems. Selected explants and

enabling 3D methods such as hydrogels, scaffolds, or microwells are shown as adjacent models rather than main workhorse potency platforms. **(B)** These platform classes differ in the readout layers they most often support. Molecular/pathway measurements and delivery-sensitive imaging are commonly used as supportive or confirmatory mechanistic layers; viability/growth readouts remain the dominant current class; morphology/invasion phenotypes are informative but less routinely used in RNA-focused studies; and immune/stromal functional and high-content multi-omic or spatial readouts remain concentrated in more specialized systems. Across the platform axis, contextual complexity and patient/TME relevance generally increase from spheroids to immune-constrained and microfluidic systems, whereas throughput and standardization generally decrease. **(C)** In current RNA therapeutic workflows, organoid-based assays are most often deployed downstream of 2D potency screening as complementary 3D layers to test whether molecular and phenotypic activity persists under tumor architecture, delivery barriers, patient-linked heterogeneity, and, where incorporated, immune or stromal constraints. Thus, organoid-based models currently function mainly as clinically relevant potency platforms rather than as primary high-throughput potency-defining systems. Figure made using BioRender.

6. Evaluation of potency assays for RNA therapeutics in 2D in vitro models versus 3D/organoid-based models

In this section, we compare how 2D and organoid-based 3D platforms are actually deployed to evaluate potency across RNA therapeutic modalities in solid tumors. Building on the potency layers defined in Box 1 and the modality-specific potency logic in Section 3, we organize the comparison by RNA class (RNAi/ASO and related inhibitory RNAs; mRNA / circRNA vaccines and payloads), and for each we identify (i) which potency components are efficiently parameterized in 2D, (ii) which failure modes and constraints are missed in 2D but become apparent under 3D architecture and microenvironmental context, and (iii) the specific experimental situations in which spheroids, PDOs/PDXOs, immune-constrained organoids, or microphysiological systems provide more informative or clinically relevant readouts. Our goal is not to position organoids as replacements for 2D assays, but to define when they add decision-relevant information about clinically relevant potency—particularly for delivery, penetration, heterogeneity, and microenvironment-dependent mechanisms—and what practical limitations currently prevent them from serving as routine, standardized potency platforms.

6.1 siRNAs, ASOs, and related inhibitory RNAs

For these inhibitory and antisense RNA modalities, 2D assays efficiently parameterize molecular potency and early phenotypic consequences, whereas organoid-based assays are mainly used to test whether these activities survive 3D architectural and microenvironmental constraints. Particularly in 2D assays, molecular potency readouts evaluate how efficiently the RNA agent—whether a siRNA duplex, a gapmer or splice-switching ASO, or a therapeutic miRNA mimic/inhibitor—suppresses or rewires its intended mRNA and protein targets, such as KRAS, PRDM2, MYC, or specific noncoding RNAs . By contrast, 2D phenotypic readouts reveal how those changes in tumor cells translate into quantifiable outputs such as viability, proliferation, apoptosis, migration, invasion, and response to other therapies such as paclitaxel or platinum chemotherapy (sensitization or resistance reversal) . In most of the siRNA-focused studies

considered here, this is implemented as a cascade: target knockdown in tumor cell lines is quantified by RT-PCR and western blot, then functional effects on tumor-cell viability, proliferation, and apoptosis are measured in 2D monolayer cultures using colorimetric assays, and only after that are 3D or organoid models and in vivo tumor models brought in as additional layers of testing[64,95,101–103,129]. This structure reflects both practicality and what 2D assays already do well: monolayer cultures of tumor cells are the most efficient stage to parameterize molecular potency and to derive classical pharmacometrics such as IC_{50}, EC_{50}, and GR under controlled exposure conditions[64,101,103].

At the same time, monolayer cultures remove many of the obstacles that make these inhibitory RNA therapies challenging in solid tumors. In 2D dishes, tumor cells are arranged as a thin sheet with short diffusion distances and minimal extracellular matrix or stromal barriers. Vascular geometry and tissue architecture are absent. Many of the oligonucleotide formulations highlighted in this review—tumor-penetrating peptide nanocomplexes[42,64,89], triblock polymer nanoparticles[101], ionizable supramolecular dendrimers[102,103], engineered exosomes[65]—all engineered specifically to overcome 3D delivery and distribution problems. What 2D cannot answer well is whether that same molecular potency survives through the 3D architecture and heterogeneity of a solid tumor, where diffusion, matrix, and stromal configuration all modulate exposure.

Organoid and organoid-based assays begin to address this gap, but in several distinct use cases. First, tumor cell-line derived 3D spheroids, cultured in Matrigel or ULA plates, are the simplest early 3D phenotype tests. In these spheroid models, siRNA formulations are judged by their effects on spheroid formation and growth, which are quantified by counting spheroids and measuring their cross-sectional area in images[88,129]. These assays reveal how siRNA delivery performs once tumor cells are arranged in clusters rather than as a sheet, and they can show obvious diffusion limits, but they are still single-line models and often do not report standardized 3D dose-response metrics[95,129]. Second, more advanced studies use PDOs, in which tumor cells from patient tissue are cultured as 3D organoids and then replated into standardized multi-well plates (e.g., 96-well or 384-well formats in specific studies) for viability assays such as CellTiter-

Glo or MTT. Here, organoids act as a quantitative 3D filter on top of the 2D data: they preserve at least some patient-specific genotypes and heterogeneity while yielding a scalable ATP-based viability metric **(Table 3)**. A third, emerging use case treats organoids as delivery- and context-aware potency platforms. Instead of seeking answers from tumor viability metrics, these platforms ask "does this siRNA formulation reach the relevant parts of a 3D tumor model and produce the expected functional effect in that context?" Examples include organoid-macrophage co-culture assays in which anti-CD47 siRNA nanocomplexes and calreticulin-modulating payloads increase phagocytosis of labeled PDOs[42], tumor-penetrating siRNA nanocomplexes evaluated in pancreatic PDOs for penetration and growth inhibition[89,95], and exosome-based siRNA delivery tested in metastatic colorectal cancer organoids to reverse chemoresistance[65] **(Table 3)**.

A similar ladder is apparent for ASOs, but the relevant targets are heterogeneous rather than confined to one RNA class. Splice-switching ASOs have been optimized in 2D and then advanced into patient-derived pancreatic organoids, where exon inclusion, PKM isoform switching, pyruvate-kinase activity, and organoid viability can all be quantified.[104] Other ASO studies extend this logic into distinct 3D settings: TRA2β poison-exon ASOs induce the expected splice-switching event and reduce growth in breast-cancer organoids and glioblastoma neurospheres[107], whereas SNORD14E-targeting ASOs suppress growth in endometrial PDOs[108]. STAT3-targeting ASOs have also been evaluated in HCC PDXOs, although their study's 3D arm is limited mainly to live/dead staining and ATP-based viability[105]. Across these studies, organoids mainly function as a 3D confirmation and stratification layer: they demonstrate that the ASO-driven splice-state or gene-expression changes can suppress growth in heterogeneous, patient-like 3D tissues, sometimes in combination with chemotherapy, but do not consistently provide formal 3D IC_{50}/GR curves or direct measurements of target knockdown inside the organoids themselves.

Therapeutic miRNA mimics and inhibitors occupy a related niche, with an added layer of network complexity. Bioengineered miRNA mimics designed to restore tumor-suppressive miRNAs, and anti-miR agents aimed at cancer-associated-miRs (OncomiRs) such as miR-21, are first characterized in 2D for target-network modulation together with basic antitumor phenotypes such as proliferation, cell-cycle arrest,

apoptosis, and growth inhibition[45,67]. A subset of these programs then climbs the same ladder into PDOs: Gem-modified miRNA mimics suppress growth in PDAC organoids, and anti-miR-21 nanocomplexes reduce growth and survival in PDAC PDO avatars. They show that the network-level reprogramming observed in monolayers can also suppress growth and reverse chemoresistance in 3D[64,89]. Here again, organoids are used as contextual filters rather than as primary potency platforms: they confirm that multi-target miRNA interventions can overcome the architecture and heterogeneity of patient-derived tumors, but with viability, size, and invasion readouts that are mostly qualitative or semi-quantitative.

By contrast, piRNA-based therapeutics remain at an earlier stage. One recent ovarian-cancer study extended a piRNA mimic into PDOs and reported molecular and antitumor effects in 3D, but systematic PDO-based potency work is still lacking[100]. At present, organoid-based clinically relevant potency for piRNA remains a conceptual opportunity rather than an established practice. Across these classes—siRNA duplexes, ASOs, therapeutic miRNAs, and early piRNA programs—organoid assays clearly add value for inhibitory RNA drug development, but their limitations as potency assays are also visible. In 3D, potency is often described qualitatively or semi-quantitatively—smaller organoids, fewer organoids, more cell death by live/dead staining—without consistently reporting standardized IC_{50}, EC_{50}, or GR metrics in organoids. In many studies, a weak or heterogeneous effect in organoids could reflect poor penetration or distribution of the RNA formulation rather than inadequate intrinsic silencing activity, yet only a minority of assays explicitly measure target knockdown or pathway rewiring inside organoids alongside the 3D phenotypic readout[88,100,104,107]. Assay standardization is also limited: seeding density, initial organoid size distribution, matrix composition, treatment duration, and image-analysis pipelines vary substantially between groups. Finally, most RNAi organoid assays are still tumor-cell-intrinsic. Immune-competent 3D assays, where siRNA- or ASO-induced changes in immune visibility (e.g., “don’t-eat-me” signaling and macrophage phagocytosis) or T-cell killing are measured in organoids, remain rare.

Despite clear conceptual advantages, organoid-based potency strategies for siRNA, ASOs, and related inhibitory RNAs are currently used mainly as 3D phenotypic confirmation platforms rather than as

fully standardized potency assays. Most studies still derive molecular pharmacometrics and target engagement in 2D, using organoids to test whether that potency survives 3D architecture and delivery barriers, but without routinely quantifying 3D knockdown or network rewiring, dose-response IC_{50}/GR values in organoids, or delivery-aware and immune-aware functional endpoints.

RNA agents and tumor types	**Selected 3D model**	**Key 3D readout(s)**	**What 3D adds beyond 2D**
1. A nanocomplex that contains anti-CD47 siRNA and calreticulin-inducing polymer; **Tumor type:** CRC [42]	CRC PDOs from one patient cocultured with human monocyte-derived macrophages	CFSE-labelled PDO phagocytosis; flow cytometry (%CFSE+ macrophages); phagocytosis assays	Extends 2D phagocytosis data into a patient-derived 3D tumor-macrophage context.
2. CD44-targeted LNPs delivering siYAP + siTAZ; **Tumor type:** TNBC; prostate cancer [88]	TNBC cell-line spheroids in 96-well ULA plates; prostate PDXO model	**Spheroid:** apoptosis reporter and volume change; **PDXO:** siRNA's effect on diameter over time	Adds 3D phenotypic confirmation after 2D potency testing and delivery studies.
3. RIZ2-targeting siRNA (via CaP nanoparticles, ± carboplatin); **Tumor type:** NSCLC [129]	A549 NSCLC 3D spheroids embedded in Matrigel	Spheroid size/shape readout, with or without Wnt agonist rescue	Links the 2D Wnt signature to a 3D growth phenotype beyond flat-culture MTT alone.
4. Anti-tumoral piRNA mimic: cholesterol-modified ago-piRNA28846; **Tumor type:** Ovarian cancer [100]	Ovarian cancer PDOs embedded in Matrigel	PDO growth plus NSUN2-linked molecular/IF readouts	Confirms anti-tumor activity in 3D PDOs from multiple patients and shows reduced NSUN2 signal consistent with the proposed mechanism.

5. Gemcitabine-modified miRNA mimics; **Tumor type:** PDAC [64]	PDAC PDO lines in Matrigel, 96-well format	CellTiter-Glo viability curves with PDO IC_{50} values	A clear organoid potency example with explicit 3D dose-response and IC_{50} values across PDO lines.
6. Anti–miR-21 nanocomplex; **Tumor type**: PDAC [89]	PANC-1/BxPC3 spheroids; multiple PDAC PDOs grown in Matrigel	PDO/spheroid MTT; organoid number and area; PDO miR-21 profiling; one PDO dose-response curve	Uses PDOs as functional avatars; includes a clear PDO dose-response example and links PDO response to matched PDX response.
7. iRGD-guided anti-KRAS siRNA tumor-penetrating nanocomplex; **Tumor type:** PDAC [95]	Human PDAC PDOs and mouse KPC-derived PDAC organoids in GFR Matrigel	Confocal penetration imaging and IF with image quantification	Provides a delivery-aware 3D readout by visualizing siRNA penetration across tumor architecture.
8. siKRAS delivered by triblock polymer nanoparticles; **Tumor type:** PDAC [101]	PDAC PDOs in Matrigel droplets	KRAS IHC/WB in PDOs; PDO number, morphology, and diameter	Confirms KRAS knockdown and anti-tumor effect in patient-derived PDOs beyond monolayer data.
9. siRNA dendrimer nanosystem that targets Myc/AKT2; **Tumor type:** PDAC [103]	PDO-derived PDAC spheroids formed in 96-well ULA plates	Myc qRT-PCR/WB in PDO spheroids; CellTiter-Glo viability	Shows that the siRNA dendrimer still knocks down Myc and reduces viability in 3D patient-derived tumor models.

10. anti-DDIT4-AS1 siRNA co-delivered with paclitaxel; **Tumor type:** TNBC [106]	Breast cancer PDOs (including TNBC) in Matrigel/type-I collagen 384-well platform	CellTiter-Glo viability; bright-field PDO number and size	Provides an elementary 3D confirmation that the combined gene-drug strategy outperforms paclitaxel alone.
11. Exosome-delivered siRNA targeting CCDC80; **Tumor type:** CRC [65]	Chemoresistant CRC tumorspheres; chemoresistant CRC PDOs in Matrigel	Tumorsphere number/size; PDO CellTiter-Glo viability under oxaliplatin + engineered exosomes	Adds 3D tumorsphere and PDO data showing reversal of oxaliplatin chemoresistance in a 3D context.
12. Splice-switching ASO targeting PKM pre-mRNA (PKM1/PKM2 switch); **Tumor type:** PDAC [104]	Human PDAC PDOs in Matrigel	RT-PCR splice switching, PKM1/2 protein, pyruvate kinase activity, and CellTiter-Glo viability	Directly links ASO splice correction in PDOs to downstream protein/enzyme change and reduced organoid viability.
13. SNORD14E-targeting ASO; **Tumor type:** Endometrial Cancer (EC) [108]	Human EC PDOs in Matrigel; transfection-free ASO uptake	Bright-field PDO growth/size; 3D luminescent viability	Extends efficacy into patient-derived EC organoids and provides a patient-linked 3D confirmation layer.
14. Both KRAS-targeting ASO and RIG-I agonist immRNA loaded in extracellular vesicles; **Tumor type:** PDAC; KRAS-mutant lung/PDAC/CRC models [90]	PDAC PDOs in Matrigel; 3D cancer spheroids for PBMC infiltration assay	AO/PI live-dead imaging in PDOs; PBMC infiltration into spheroids	Adds a 3D immune- and context-aware layer for a combined tumor-intrinsic plus immunomodulatory RNA strategy.

15. Modified STAT3 ASO (lead: STAT3-ASO2); **Tumor type:** HCC [105]	HCC PDXOs cultured in Matrigel, 96-well format	Live/dead imaging; CellTiter-Glo viability	Provides a patient-/tumor-linked 3D confirmation layer for antitumor activity after 2D and xenograft work.
16. Splice-switching ASO-1570 targeting the TRA2β-poison exon (PE); **Tumor type:** Breast cancer and Glioblastoma [107]	MDA-MB231 Matrigel organoids; U87MG neurospheres	TRA2β-PE inclusion RT-PCR; live/dead imaging; 3D growth/size quantification	Shows that splice-switching activity persists in preclinical 3D cancer models and links poison-exon inclusion to reduced 3D growth.

Table 3. Representative organoid-based studies of inhibitory RNA therapeutics (siRNAs, ASOs, miRNA therapeutics, and piRNA mimics) in solid tumors.

Summary of the RNA modality, tumor indication, 3D model platform, key 3D readouts, and the specific information added by the 3D system beyond conventional 2D monolayer testing. Across these studies, organoids are used primarily as complementary 3D confirmation or clinically relevant context platforms rather than as fully standardized primary potency assays. RNA agents' names are underlined. ***Assay acronyms***: ATP, Adenosine Triphosphate; GFR: Growth Factor Reduced; IF, Immunofluorescence; PI, Propidium Iodide; RT-PCR, Reverse-transcription Polymerase Chain Reaction; WB: Western-blotting. ***Delivery acronyms:*** immRNA, immuno-modulating RNA; LNP, Lipid Nanoparticle. ***Tumor- or Immune-cell acronyms***: CRC, Colorectal Cancer; HCC, Hepatocellular Carcinoma; NSCLC, Non-Small Cell Lung Cancer; PBMC, Peripheral Blood Mononuclear Cells; PDAC, Pancreatic Ductal Adenocarcinoma; TNBC, Triple-Negative Breast Cancer.

6.2 Exogenous mRNA and limitations of testing their clinically relevant potency in cancer organoids.

It is useful to distinguish two functional lanes for exogenous mRNA in oncology. The two lanes are cancer mRNA vaccines, which deliver antigen-encoding mRNA to professional APCs to prime T-cell responses, and local payload constructs, which deliver mRNA directly into tumors to express cytokines, costimulatory ligands, or other effector proteins within the lesion. Detailed distinctions between them have been discussed previously.

mRNA cancer vaccines—priming lives outside tumor organoids.

For mRNA cancer vaccines, molecular and phenotypic potency are dominated by events in APCs and lymphoid: mRNA uptake and translation in DCs, co-stimulation and innate sensing, and the magnitude and quality of antigen-specific T-cell responses[21,46]. Those readouts are naturally captured in 2D APC/T-cell assays, including DC maturation, cross-presentation, cytokine profiles, T-cell proliferation and killing, and downstream in vivo models that provide more complete lymphoid architecture[21,46]. In contrast, classical epithelial tumor organoids do not reproduce lymph node microanatomy, APC trafficking, or clonal expansion dynamics, and therefore do not offer a cleaner priming readout than well-designed 2D immune assays plus carefully chosen in vivo animal studies. Tumor organoids also do not, by themselves, address where vaccine-elicited cells are generated or how they home to tumors. Of note, immune organoid and secondary lymphoid organ-like systems are being developed to model APC-lymphocyte priming events and, in some scenarios, germinal-center-like responses[130,131]; engineered lymph node-tumor hybrid organoid systems are also a notable but specialized exception[110]. But these models are still early, not standardized for RNA vaccine potency, and largely decoupled from patient-specific epithelial 3D tumor models. Microfluidic and OOC systems can add controlled flow, compartmentalization, and physiological immune-cell interactions, but they remain specialized and difficult to standardize and scale for routine mRNA vaccine potency[15,132].

However, tumor organoids can still enter the picture downstream, as effector-phase challenge systems. Given primed T cells or other effector populations—whether elicited by an mRNA vaccine or expanded ex vivo—PDOs can be used to ask tumor-centric clinically relevant potency questions. These questions include: *Is the target antigen expressed across patient subclones? Does HLA dysfunction limit recognition? Do 3D architecture and local stromal organization impose immune-exclusion barriers?* Early proof-of-concept studies with epitope-focused mRNA vaccines illustrate this pattern: vaccine-induced immune responses have been evaluated in engineered human immune-organoid/tumor-organoid interaction systems, where tumor organoids function mainly as downstream 3D challenge targets for antitumor activity rather than as the primary site where vaccine priming potency is measured[73]. In this sense, organoids are most valuable when the question is not "can we prime T cells?" but "given primed T cells, does this patient's tumor permit infiltration and killing, and what combinations unmask response?"

Local mRNA payloads—first steps toward clinically relevant potency in PDOs.

For intratumoral or local mRNA payloads, the logic is different and more compatible with tumor organoids. Here, molecular potency is the efficiency of payload expression in the tumor and, when modeled, the tumor's local immune or stromal compartments; cellular and clinically relevant potency are defined by how that local expression reshapes viability, immunogenicity, and immune/stromal behavior in 3D. These are precisely the constraints that 2D under-represents. Accordingly, a small but growing number of programs now use PDOs to check whether mRNA payloads can achieve tumor-restricted expression and functional effects in a 3D architecture. For example, self-replicating IL-12 mRNA constructs with programmable genetic circuitry have been tested in patient-derived tumor organoids to confirm preserved tumor-side expression, while parallel in vivo studies assessed de-targeting of off-target tissues and improved tolerability[133]. At present, however, these organoid assays for mRNA payloads are still qualitative or semi-quantitative. They typically focus on expression, basic viability, or binary immune activation rather than standardized 3D dose-response metrics, spatial killing profiles, or delivery-aware potency parameters.

They also remain technically demanding and program-specific, limiting their use as routine release or comparability assays.

Taken together, this means that organoid-based potency strategies for exogenous mRNA are underdeveloped and split by lane. For mRNA cancer vaccines, organoids are not yet well suited to model the priming cascade and are better viewed as downstream human 3D platforms for tumor-side validation, such as antigen/HLA competence, infiltration and killing patterns, and rational vaccine-ICB combinations. For local mRNA payloads, organoid-based 3D tumor systems offer a more natural clinically relevant potency platform; they are able to report tumor-restricted expression and 3D functional effects, but current use is confined to early proof-of-concept studies rather than standardized, quantitative potency assays.

6.3 Exogenous circRNA and limitations of testing their clinically relevant potency in cancer organoids.

Exogenous circRNA therapeutics enter the solid-tumor space as a close cousin of mRNA therapeutics. As outlined in Section 2.3, most current exogenous circRNA constructs are designed either as vaccines, which encode tumor-associated or neoantigenic epitopes, often with adjuvant motifs[53–55]; or as local payloads that express cytokines, costimulatory ligands, or other therapeutic proteins within the tumor or its microenvironment[47,55,56]. At the molecular and cellular levels, their potency logic largely mirrors mRNA: for vaccines, the critical biology lies in antigen expression and innate sensing in professional APCs and the quality of the antigen-specific T-cell response; for local payloads, it lies in efficient translation in target cells and the downstream reprogramming of tumor, immune, and stromal compartments. CircRNAs differ mainly in stability and translation control, not in where these key biological steps happen, so clinically relevant potency constraints are analogous to those already discussed for mRNA vaccines and intratumoral payloads.

For circRNA vaccines, this means that priming potency is fundamentally an APC/lymphoid problem. Molecular potency depends on circRNA uptake and cap-independent translation in DCs and related APCs, together with innate sensing and costimulatory programs; phenotypic potency is reflected in

the magnitude, breadth, and functional quality of antigen-specific T-cell responses. These readouts are naturally obtained in 2D APC/T-cell systems and in vivo models that supply proper lymphoid architecture[53–56]. Classical epithelial tumor organoids do not reproduce lymph node microanatomy, APC trafficking, or clonal expansion dynamics, and therefore do not offer a cleaner or more mechanism-appropriate priming readout than well-designed 2D immune assays plus carefully chosen animal studies[7,76]. Recent related circRNA-neoepitope work illustrates the same division of labor: predicted circRNA-derived peptides were first used in conventional immune assays to stimulate and expand antigen-specific CD8+ T cells, and the resulting effectors were then tested against PDOs as downstream 3D challenge targets[72,134]. Even immune-competent organoid models and secondary lymphoid organoids, while conceptually attractive, remain technically heterogeneous and are not yet standardized as routine potency assays for circRNA vaccines. Under this lens, tumor organoids are best deployed downstream of priming: as human 3D challenge systems that receive vaccine-elicited T cells (or other effectors) and report tumor-side determinants of killing, rather than as primary platforms to quantify circRNA vaccine potency itself.

For local circRNA payloads, tumor organoids would in principle be well suited to probe clinically relevant potency, because the key questions are local expression, spatial distribution, and downstream 3D effects within tumor tissue, but most studies to date still optimize circRNA constructs in 2D monolayers for expression and proximal phenotypes; when more complex validation is added, it is often through in vivo models rather than organoids[23]. By contrast, we could not identify a robust primary literature base in which engineered circRNA payloads were systematically tested in cancer organoids as 3D validation platforms. The closest related studies instead involve endogenous tumor-suppressive circRNAs, such as circ_0007379 in colorectal cancer or circANAPC7 in pancreatic cancer, whose re-expression suppresses growth in 2D and in organoid-based models. These studies suggest that organoids could serve as useful 3D confirmation layers for future circRNA payload programs, but they do not yet establish a mature organoid-based payload-potency framework[115,135].

At present, explicit circRNA organoid potency frameworks remain underdeveloped. Most circRNA-organoid applications report qualitative or semi-quantitative changes—smaller or fewer organoids, altered invasion, or pathway markers—without systematically defining organoid-specific dose-response metrics (e.g., IC_{50}/GR values in PDOs) or directly measuring target expression and pathway modulation inside organoids in parallel with 3D phenotypic readouts. As with mRNA, organoids are rarely used to dissect where circRNA constructs are expressed across tumor subclones, how 3D architecture shapes diffusion and uptake, or how local immune and stromal compartments modulate functional impact. We therefore view circRNA payloads as an area where organoid-based clinically relevant potency assays are conceptually compelling but still in an early "case study" stage. Taken together, this keeps circRNA organoid potency work at a proof-of-concept stage rather than a standardized assay framework. **7. Implementation, fit-for-purpose standardization, and translational positioning**

Across the earlier sections, we argued that organoid-based assays are most informative when matched to the contextual barrier or interaction they are meant to test. The implementation challenge is therefore not universal standardization of a single "organoid potency assay," but fit-for-purpose qualification of distinct assay classes[136]. PDOs, cell-line-derived spheroids, immune- or stromal-constrained organoids, and microphysiological systems preserve different barriers and compartments, and within each class reproducibility depends on tissue handling, biopsy quality, tumor cellularity, prior treatment, matrix and media formulation, passage history, organoid size distribution, and readout design[7,76,97,137]. Even when nominal protocols are similar, inter-laboratory variation in success rates, growth kinetics, and drug-response behavior remains substantial[76,136,138]. Before organoid-based potency can influence decisions reliably, these variables need explicit SOPs, inclusion/exclusion rules, and routine QC anchors such as genotyping, histology, growth behavior, and metadata capture over time[136,139].

On the readout side, most organoid drug screens still report relatively coarse endpoint metrics such as ATP-based viability or simple size measurements at a single endpoint[76,137]. Analogous efforts to standardize potency quantification now exist across 2D and 3D systems: GR and related 2D response

metrics reduce bias caused by differences in untreated growth rate across models, while NOGR was developed to quantify organoid responses using baseline growth and imaging-based changes over time[35,37]. These approaches show that more standardized, growth-aware qualification of potency metrics is feasible in organoids, but they are far from universally adopted. For RNA therapeutics in particular, only a minority of studies pair organoid-side target knockdown or pathway measurements with the 3D phenotypic readout, and formal organoid dose-response parameterization remains inconsistent[88,100,104,107]. As a result, clinically relevant potency is often inferred indirectly from "smaller organoids" or "more cell death" without knowing whether failures result from biology or delivery.

Practical constraints also shape how far organoid potency assays can be pushed. Deriving and expanding PDOs is slower and more labor-intensive than seeding 2D lines; many clinical biopsies never yield stable cultures, and even successful lines may require weeks before they are assay-ready[76,137]. High-content imaging, single-cell sequencing, or spatial profiling on organoids adds substantial cost and analysis time[124,128,137]. Because organoid assays remain slower, costlier, and less standardized than 2D systems, they are most realistically positioned at selective decision points—such as translational confirmation, patient-linked resistance mapping, or indication-specific combination testing—rather than as universal first-pass screens[76,137,140]. In this sense, their value is not throughput for its own sake, but the ability to answer high-value clinically relevant questions that simpler models systematically miss.

Within this landscape, RNA therapeutics are still at an earlier stage than small molecules and many antibody-based therapeutic programs in terms of organoid integration. Most published RNA-organoid studies still follow a "2D-first, 3D-confirmation" ladder: basic target-modulation or expression are optimized in 2D culture models, and only then are a limited number of PDOs or other 3D models used to test whether those effects survive tissue architecture and patient heterogeneity **(Table 3)**[64,89,104,108]. Formal IC_{50}/EC_{50} or GR-style parameterization is modality-dependent and remains inconsistent across RNA studies [64]. For immunomodulatory RNAs, such as mRNA/circRNA vaccines, local immunomodulatory

mRNA/circRNA payloads, or siRNAs against myeloid checkpoints, immune-competent 3D assays are particularly sparse, so potency remains largely defined by APC/T-cell assays and in vivo models[21,46,50,68].

Translationally, organoids already show value in selected non-RNA settings, particularly chemotherapy, chemoradiation, and some precision-oncology workflows[117,125,141,142]. For RNA therapeutics, however, the evidence base is still much narrower: we could not identify a robust prospective clinical literature in which organoid potency data were formally validated as treatment-selection or development-defining surrogates for RNA modalities. The near-term translational role is therefore more modest but still meaningful. For solid-tumor RNA therapeutics, organoids are best positioned as patient-linked clinically relevant platforms to test whether delivery-sensitive activity persists under 3D architecture, to map resistance niches that might explain clinical heterogeneity, and to prioritize combinations or escalation into more expensive preclinical studies[136].

Taken together, these constraints suggest a realistic near-term role for organoid-based potency assays rather than an idealized one. For solid-tumor RNA therapeutics, organoid assays fit best as (i) secondary platforms that test whether well-characterized 2D potency survives tissue architecture and delivery barriers in a small panel of PDOs, (ii) translational tools that help interpret clinical variability or design combinations by mapping resistance niches in patient-matched organoids, and (iii) specialized immune-competent systems used to address concrete questions about myeloid or T-cell engagement. In the near term, they are therefore better viewed as selective, decision-influencing clinically relevant assays than as generalized, first-pass potency assays for every RNA sequence entering a pipeline. Critically, for organoid-based potency testing of RNA therapeutics, fit-for-purpose standardization efforts should prioritize five concrete benchmarks: (1) consensus minimum reporting standards for 3D assays, including organoid type and passage, matrix composition, size distribution at treatment, dose range, and readout modalities; (2) parallel measurement of target knockdown or payload expression inside organoids alongside viability or growth endpoints, so that biological failure can be distinguished from delivery failure; (3) adoption of growth-rate-corrected metrics such as NOGR or GR-adjusted IC_{50} values where mechanism-

appropriate, rather than reliance on single-timepoint viability percentages; (4) prospective co-registration of PDO drug-response profiles with patient clinical outcomes, where feasible, to begin building the translational evidence base for regulatory acceptance; and (5) explicit documentation of whether and how intact 3D delivery barriers are preserved in each assay design, to prevent conflation of "3D confirmation" studies that bypass delivery constraints with genuine clinically relevant potency measurements. Progress on these benchmarks will determine whether organoid-based potency data can eventually mobilize from explanatory and translational use toward more formal roles in product characterization, indication-specific decision-making, and eventually, where validated, regulatory or clinical-development workflows.

8. Future directions: from exploratory organoid assays to qualified potency platforms

The central challenge emerging from this review is not whether organoid-based systems are biologically richer than 2D monolayers, but how that added complexity can be converted into assays that are reproducible, interpretable, and worth deploying at specific decision points in RNA therapeutic development. The most important future direction is therefore not maximal complexity, but fit-for-purpose assay qualification. Different RNA modalities fail at different rate-limiting steps: inhibitory RNAs are often constrained by delivery, penetration, and heterogeneous intracellular exposure; mRNA and circRNA vaccines are constrained largely by APC uptake, lymphoid priming, and downstream tumor recognition; and local mRNA or circRNA payloads are constrained by the localization, persistence, and cell-type specificity of transgene expression. Future organoid work will be most useful when each assay is explicitly designed around the barrier or interaction most likely to determine success or failure for that modality, rather than treating all 3D models as interchangeable.

A second priority is to expand the biological range of organoid-based potency assays without losing mechanistic discipline. In practice, this effort will likely depend on three enabling developments. First, immune- and stromal-constrained organoid systems, including reconstituted co-cultures and selected native-architecture or microfluidic platforms, may make it possible to define potency in terms of multicellular response rather than tumor-cell viability alone[7,17,32]. Second, advances in miniaturized culture formats, semi-automated handling, and higher-throughput organoid workflows may gradually narrow the operational gap between organoids and 2D systems[9,143]. Third, imaging-rich and AI-assisted analysis may help convert organoid assays from single-endpoint readouts into higher-dimensional phenotypic platforms capable of distinguishing delivery failure, partial response in resistant subclones, and broader target engagement in 3D tissues[37,128,144].

A third priority is translational anchoring. In non-RNA settings, organoids are already beginning to show value as patient-linked platforms for response prediction and resistance mapping in selected indications. For RNA therapeutics, the analogous opportunity is to build carefully chosen co-clinical

workflows in which organoid data are prospectively linked to patient response, resistance, or combination benefit in defined modality-indication pairs. These studies do not need to prove that organoids replace conventional potency assays across the board; rather, they need to show where organoid-based measurements add unique value that simpler systems cannot provide. For newer RNA modalities with especially sparse organoid literature, including circRNA therapeutics, high-value next steps include: 1) standardized 2D-to-organoid escalation pipelines linked to in vivo or translational-validation studies, with matched molecular and phenotypic readouts across stages; 2) organoid-immune co-cultures that accept vaccine-elicited effectors; and 3) delivery-aware assays that relate spatial expression patterns in organoids to functional outcomes.

Taken together, the future of organoid-based RNA potency testing lies in selective depth, not universal adoption. The field will advance most effectively by matching each organoid platform to a concrete mechanistic question, integrating molecular and functional 3D readouts, and building translational evidence in the specific contexts where clinically relevant barriers truly determine therapeutic performance. Under those conditions, organoids will not simply make potency assays more complicated; they will make them more informative.

9. Conclusions

The central argument of this review can be stated simply: for RNA therapeutics in solid tumors, what a drug candidate does in a two-dimensional monolayer under idealized exposure conditions and what it does when it must traverse the full biological complexity of a human tumor are not the same question. The gap between them is not a technical artifact to be corrected by better cell lines or longer time-points; it is a fundamental consequence of the architecture, heterogeneity, and microenvironmental dynamics that define solid tumor biology. Conventional 2D potency assays are excellent tools for the questions they can answer, such as sequence-dependent target engagement, early pharmacology, and dose-response parameterization under controlled conditions, and they should continue to form the primary stage of RNA therapeutic characterization. But they are structurally blind to the delivery, penetration, and resistance mechanisms that most often determine whether an RNA drug succeeds or fails in patients. Organoid-based potency assays have the potential to make these failure modes experimentally visible and quantitatively tractable, but that potential has not yet been consistently realized in the current literature.

Our analysis across RNA modalities reveals a consistent pattern: organoid-based assays are most often deployed as downstream confirmation layers after 2D potency has been established, rather than as primary platforms designed to interrogate the specific contextual barriers that are rate-limiting for each modality. For siRNA and ASO-based strategies, where delivery through 3D architecture is frequently the dominant failure mode, organoids are used primarily for spheroid growth inhibition and PDO viability confirmation, but rarely to measure target knockdown inside the 3D tissue itself or to derive formal 3D dose-response metrics. For local mRNA payloads, and more tentatively for emerging circRNA payload concepts, the potential to test tumor-restricted expression, cell-type specificity, and local immune activation in PDOs exists and is beginning to be realized, but current use remains confined to early proof-of-concept studies. For mRNA and circRNA vaccines, classical tumor organoids are not the appropriate primary potency platform, because the critical biology of antigen presentation and T-cell priming occurs in lymphoid architecture that organoids do not recapitulate; their proper role is as downstream tumor-

challenge systems that test whether vaccine-elicited effectors can infiltrate and kill in patient-specific 3D contexts.

The practical implementation gaps identified in this review are substantial but tractable. Most organoid-based RNA potency assays still fail to report standardized 3D dose-response metrics, pair viability readouts with parallel target-engagement data inside the organoids, use immune-competent or stromal co-culture systems, or adequately address the bypass problem such as the common practice of dissociating, re-seeding, or directly lipofecting organoid cells under conditions that circumvent the very 3D delivery barriers that clinically relevant potency assays are designed to interrogate. Addressing these gaps requires not only technical standardization, but a deliberate shift in assay design philosophy: organoids should be configured to impose the specific clinically relevant constraints that are rate-limiting for the modality under evaluation, and the readouts should be selected to report whether the therapeutic mechanism survives those constraints, not merely whether some phenotypic change is detectable in 3D culture.

We propose that the field adopt a deliberately layered potency strategy with explicit decision criteria for when each model system contributes non-redundant information. Two-dimensional assays should remain the primary stage for molecular potency characterization, lead optimization, and large-scale screening across sequences and chemistries. Tumor spheroids and PDOs should be deployed as a second-stage clinically relevant potency layer when delivery, 3D penetration, or patient-specific heterogeneity are plausible failure modes, not as a routine confirmation step for every candidate, but as targeted experimental probes applied to a smaller number of leading candidates with well-defined contextual questions. Immune- and stromal-constrained organoid systems should be reserved for programs where the therapeutic mechanism depends on modulating non-epithelial compartments, for instance, siRNA strategies targeting macrophage checkpoints, mRNA payloads encoding immunomodulatory proteins, or combinatorial approaches pairing RNA agents with checkpoint inhibitors. Organoid-on-chip and microphysiological systems, while not yet routine, are the appropriate platform for programs where vascular barriers or convective transport are specific mechanistic concerns. In all cases, the critical discipline is to pair

phenotypic readouts with concurrent target-engagement measurements inside the 3D system, and to report dose-response relationships rather than single-concentration snapshots.

The scientific and clinical stakes are high. Multiple RNA therapeutic programs are already in clinical development for solid tumors, but their maturity is uneven across modalities. Among direct exogenous RNA platforms, mRNA platforms are currently furthest advanced, whereas selected siRNA and ASO programs have reached early-to-mid clinical development, and circRNA remains at a much earlier stage. Representative clinical-stage exogenous RNA therapeutic programs in solid tumors and the potency-testing questions they foreground, are summarized in **Table 4**. At the same time, the organoid technology infrastructure is simultaneously maturing: high-throughput PDO screening formats, automated imaging, AI-enhanced phenotypic analysis, and immune co-culture systems are all becoming more widely accessible. The regulatory environment is evolving, with increasing agency interest in human-relevant in vitro models that can reduce reliance on poorly predictive animal studies. The convergence of these forces creates a narrow but important window in which the field can establish rigorous, standardized, and mechanistically grounded organoid-based potency frameworks for RNA therapeutics, before clinical programs scale and before suboptimal assay designs become entrenched as industry practice. This review aims to provide the conceptual foundation and practical guidance needed to seize that opportunity, advancing RNA therapeutics development from a field characterized by unexplained preclinical-to-clinical gaps toward one in which clinically relevant potency is measured, understood, and acted upon at every stage of the development pipeline.

Representative program & Core therapeutic strategy	Tumor type	Clinical development stage	Key clinically relevant potency question
siRNA—siG12D-LODER Local KRAS-targeting siRNA implant (combined with chemotherapy) [145]	Pancreatic adenocarcinoma	Phase 2	Does local siRNA delivery remain effective across dense 3D tumor tissue and heterogeneous intratumoral distribution?
siRNA—STP707 Systemic dual-target siRNA (TGF-β1 / COX-2) [146]	Advanced / metastatic or unresectable solid tumors	Phase 1	Can systemic RNAi maintain delivery, penetration, and functional activity across heterogeneous solid-tumor tissues?
siRNA—EphA2-DOPC siRNA Liposomal siRNA targeting EphA2 [147]	Advanced or recurrent solid tumors	Phase 1	Does nanoparticle-mediated siRNA reach relevant tumor compartments and retain target-modulating activity under clinically relevant transport barriers?
ASO—Danvatirsen (AZD9150) STAT3-targeting ASO [148–150]	Advanced solid tumors, including NSCLC and recurrent / metastatic SCCHN	Phase 1b/2 and Phase 2 clinical development	Can transcript-targeted activity remain functionally meaningful in heterogeneous tumor and immune contexts, especially in combination regimens?

ASO—AZD8701 FOXP3-targeting ASO [151]	Advanced solid tumors	Phase 1	Can ASO-mediated modulation of immunoregulatory targets achieve clinically relevant effects in non-epithelial compartments?
ASO—OT-101 (trabedersen) TGF-β2-targeting ASO [152,153]	Metastatic NSCLC; advanced unresectable or metastatic pancreatic cancer	Phase 1/2 (NSCLC) and Phase 2b/3 (pancreatic cancer)	Does antisense-mediated pathway modulation remain effective under stromal and microenvironmental resistance constraints?
mRNA—V940 / mRNA-4157 (intismeran autogene) Personalized neoantigen mRNA vaccine [154,155]	Melanoma	Phase 2b, and Phase 3	Because primary potency depends on APC uptake and lymphoid priming, where should tumor organoids enter as downstream challenge systems for infiltration and killing?
mRNA—autogene cevumeran Personalized neoantigen mRNA vaccine (combined with anti-PD-L1 and chemotherapy) [156,157]	PDAC	Phase 1, Phase 2	In a tumor type with immunosuppressive TME such as PDAC, how should potency be partitioned between lymphoid priming assays and downstream tumor-side challenge systems rather than primary organoids?

mRNA—mRNA-2752 Intratumoral mRNA payload encoding immune modulators [158]	Advanced / metastatic solid tumors	Phase 1	Can local payload expression remain spatially restricted and functionally effective within 3D tumor and TME architecture?
circRNA-based dendritic-cell vaccine (CirFAM53B-219aa) Ex vivo circRNA-loaded dendritic-cell vaccine with camrelizumab [159]	HER2-negative advanced breast cancer	Phase 1	For emerging exogenous circRNA vaccines, how should potency be partitioned between priming-focused immune assays and downstream tumor-organoid challenge systems?

Table 4. Representative clinical-stage exogenous RNA therapeutic programs in solid tumors and the potency-testing questions they foreground.

Acronyms: ASO, antisense oligonucleotide; NSCLC, non-small cell lung cancer; PDAC, pancreatic ductal adenocarcinoma; SCCHN, squamous cell carcinoma of head and neck.

10. References:

1. Bray, F. *et al.* Global cancer statistics 2022: GLOBOCAN estimates of incidence and mortality worldwide for 36 cancers in 185 countries. *CA A Cancer J Clinicians* **74**, 229–263 (2024).

2. Hendriks, H. Advancing oncology drug development: Innovative approaches to enhance success rates while reducing animal testing. *Biochimica et Biophysica Acta (BBA) - Reviews on Cancer* **1880**, 189467 (2025).

3. Atkins, J. T. *et al.* Pre-clinical animal models are poor predictors of human toxicities in phase 1 oncology clinical trials. *Br J Cancer* **123**, 1496–1501 (2020).

4. Yan, Y. *et al.* Advances in RNA-based cancer therapeutics: pre-clinical and clinical implications. *Mol Cancer* **24**, 251 (2025).

5. Appleton, E., Chiocca, E. A., Ungerechts, G., Melcher, A. & Vile, R. Oncolytic viruses as anticancer agents: clinical progress and remaining challenges. *The Lancet* **406**, 1295–1312 (2025).

6. Tichet, M. *et al.* Bispecific PD1-IL2v and anti-PD-L1 break tumor immunity resistance by enhancing stem-like tumor-reactive CD8+ T cells and reprogramming macrophages. *Immunity* **56**, 162-179.e6 (2023).

7. Polak, R., Zhang, E. T. & Kuo, C. J. Cancer organoids 2.0: modelling the complexity of the tumour immune microenvironment. *Nat Rev Cancer* **24**, 523–539 (2024).

8. Ye, P. *et al.* TIM-3 blockade reverses oncolytic vaccinia virus-induced DCs inactivation and T cells exhaustion to improve antitumor immunity and therapeutic efficacy. *J Exp Clin Cancer Res* **44**, 333 (2025).

9. Loewa, A., Feng, J. J. & Hedtrich, S. Human disease models in drug development. *Nat Rev Bioeng* **1**, 545–559 (2023).

10. Jubelin, C. *et al.* Three-dimensional in vitro culture models in oncology research. *Cell Biosci* **12**, 155 (2022).

11. Berrouet, C., Dorilas, N., Rejniak, K. A. & Tuncer, N. Comparison of Drug Inhibitory Effects ($$\hbox {IC}_{50}$$) in Monolayer and Spheroid Cultures. *Bull Math Biol* **82**, 68 (2020).

12. Ireson, C. R., Alavijeh, M. S., Palmer, A. M., Fowler, E. R. & Jones, H. J. The role of mouse tumour models in the discovery and development of anticancer drugs. *Br J Cancer* **121**, 101–108 (2019).

13. Eguren-Santamaria, I. *et al.* Preclinical ex vivo and in vivo models to study immunotherapy agents and their combinations as predictive tools toward the clinic. *J Immunother Cancer* **13**, e011279 (2025).

14. Proietto, M. *et al.* Tumor heterogeneity: preclinical models, emerging technologies, and future applications. *Front. Oncol.* **13**, 1164535 (2023).

15. Ingber, D. E. Human organs-on-chips for disease modelling, drug development and personalized medicine. *Nat Rev Genet* **23**, 467–491 (2022).

16. Luo, Z. *et al.* Reconstructing the tumor architecture into organoids. *Advanced Drug Delivery Reviews* **176**, 113839 (2021).

17. Wang, Q., Yuan, F., Zuo, X. & Li, M. Breakthroughs and challenges of organoid models for assessing cancer immunotherapy: a cutting-edge tool for advancing personalised treatments. *Cell Death Discov.* **11**, 222 (2025).

18. Colombo, R., Tarantino, P., Rich, J. R., LoRusso, P. M. & De Vries, E. G. E. The Journey of Antibody–Drug Conjugates: Lessons Learned from 40 Years of Development. *Cancer Discovery* **14**, 2089–2108 (2024).

19. Keri, D., Walker, M., Singh, I., Nishikawa, K. & Garces, F. Next generation of multispecific antibody engineering. *Antibody Therapeutics* **7**, 37–52 (2024).

20. Walsh, G. & Walsh, E. Biopharmaceutical benchmarks 2022. *Nat Biotechnol* **40**, 1722–1760 (2022).

21. Liu, C. *et al.* mRNA-based cancer therapeutics. *Nat Rev Cancer* **23**, 526–543 (2023).

22. Gonzalez, J. C. *et al.* Nano Approaches to Nucleic Acid Delivery: Barriers, Solutions, and Current Landscape. *WIREs Nanomed Nanobiotechnol* **17**, e70010 (2025).

23. Kulkarni, J. A. *et al.* The current landscape of nucleic acid therapeutics. *Nat. Nanotechnol.* **16**, 630–643 (2021).

24. Grau, M. & Wagner, E. Strategies and mechanisms for endosomal escape of therapeutic nucleic acids. *Current Opinion in Chemical Biology* **81**, 102506 (2024).

25. Paul, S. *et al.* Cancer therapy with antibodies. *Nat Rev Cancer* **24**, 399–426 (2024).

26. Bordeau, B. M., Yang, Y. & Balthasar, J. P. Transient Competitive Inhibition Bypasses the Binding Site Barrier to Improve Tumor Penetration of Trastuzumab and Enhance T-DM1 Efficacy. *Cancer Research* **81**, 4145–4154 (2021).

27. Galvez-Cancino, F. *et al.* Fcγ receptors and immunomodulatory antibodies in cancer. *Nat Rev Cancer* **24**, 51–71 (2024).

28. Murciano-Goroff, Y. R., Warner, A. B. & Wolchok, J. D. The future of cancer immunotherapy: microenvironment-targeting combinations. *Cell Res* **30**, 507–519 (2020).

29. Wu, B., Zhang, B., Li, B., Wu, H. & Jiang, M. Cold and hot tumors: from molecular mechanisms to targeted therapy. *Sig Transduct Target Ther* **9**, 274 (2024).

30. Maute, R., Xu, J. & Weissman, I. L. CD47–SIRPα-targeted therapeutics: status and prospects. *Immuno-Oncology and Technology* **13**, 100070 (2022).

31. Williams, H. L. *et al.* The current landscape of spatial biomarkers for prediction of response to immune checkpoint inhibition. *npj Precis. Onc.* **8**, 178 (2024).

32. Sun, C.-P., Lan, H.-R., Fang, X.-L., Yang, X.-Y. & Jin, K.-T. Organoid Models for Precision Cancer Immunotherapy. *Front. Immunol.* **13**, 770465 (2022).

33. Mu, P. *et al.* Newly developed 3D in vitro models to study tumor–immune interaction. *J Exp Clin Cancer Res* **42**, 81 (2023).

34. Q6B Specifications: Test Procedures and Acceptance Criteria for Biotechnological/Biological Products | FDA. https://www.fda.gov/regulatory-information/search-fda-guidance-documents/q6b-specifications-test-procedures-and-acceptance-criteria-biotechnologicalbiological-products.

35. Hafner, M., Niepel, M., Chung, M. & Sorger, P. K. Growth rate inhibition metrics correct for confounders in measuring sensitivity to cancer drugs. *Nat Methods* **13**, 521–527 (2016).

36. Gupta, A., Gautam, P., Wennerberg, K. & Aittokallio, T. A normalized drug response metric improves accuracy and consistency of anticancer drug sensitivity quantification in cell-based screening. *Commun Biol* **3**, 42 (2020).

37. Deben, C. *et al.* Development and validation of the Normalized Organoid Growth Rate (NOGR) metric in brightfield imaging-based assays. *Commun Biol* **7**, 1612 (2024).

38. Hao, J. *et al.* Smart Nanoarchitectures for Precision RNA Delivery: Harnessing Endogenous and Exogenous Stimuli in Cancer Treatment. *Theranostics* **15**, 7747–7778 (2025).

39. Lv, X. *et al.* Targeting RNA splicing modulation: new perspectives for anticancer strategy? *J Exp Clin Cancer Res* **44**, 32 (2025).

40. Garcia-Borja, E. *et al.* Critical appraisal of the piRNA-PIWI axis in cancer and cancer stem cells. *Biomark Res* **12**, 15 (2024).

41. Yang, M. *et al.* Synchronous targeted delivery of TGF-β siRNA to stromal and tumor cells elicits robust antitumor immunity against triple-negative breast cancer by comprehensively remodeling the tumor microenvironment. *Biomaterials* **301**, 122253 (2023).

42. Huang, H. *et al.* Phagocytosis-Activating Nanocomplex Orchestrates Macrophage-Mediated Cancer Immunotherapy. *Advanced Materials* **37**, 2500982 (2025).

43. DeFranciscis, V., Amabile, G. & Kortylewski, M. Clinical applications of oligonucleotides for cancer therapy. *Molecular Therapy* **33**, 2705–2718 (2025).

44. Diener, C., Keller, A. & Meese, E. The miRNA–target interactions: An underestimated intricacy. *Nucleic Acids Research* **52**, 1544–1557 (2024).

45. Seyhan, A. A. Trials and Tribulations of MicroRNA Therapeutics. *IJMS* **25**, 1469 (2024).

46. Van Hoecke, L. *et al.* mRNA in cancer immunotherapy: beyond a source of antigen. *Mol Cancer* **20**, 48 (2021).

47. Yang, J. *et al.* Intratumoral delivered novel circular mRNA encoding cytokines for immune modulation and cancer therapy. *Molecular Therapy - Nucleic Acids* **30**, 184–197 (2022).

48. Jacob, E. M., Huang, J. & Chen, M. Lipid nanoparticle-based mRNA vaccines: a new frontier in precision oncology. *Precision Clinical Medicine* **7**, pbae017 (2024).

49. Lorentzen, C. L., Haanen, J. B., Met, Ö. & Svane, I. M. Clinical advances and ongoing trials of mRNA vaccines for cancer treatment. *The Lancet Oncology* **23**, e450–e458 (2022).

50. Magré, L. *et al.* Emerging organoid-immune co-culture models for cancer research: from oncoimmunology to personalized immunotherapies. *J Immunother Cancer* **11**, e006290 (2023).

51. Kim, Y. *et al.* Physiological Barriers to Nucleic Acid Therapeutics and Engineering Strategies for Lipid Nanoparticle Design, Optimization, and Clinical Translation. *Pharmaceutics* **17**, 1309 (2025).

52. Liu, J.-Q. *et al.* Intratumoral delivery of IL-12 and IL-27 mRNA using lipid nanoparticles for cancer immunotherapy. *Journal of Controlled Release* **345**, 306–313 (2022).

53. Gong, Z. *et al.* Recent advances and perspectives on the development of circular RNA cancer vaccines. *npj Vaccines* **10**, 41 (2025).

54. Das, U. *et al.* Circular RNA vaccines: Pioneering the next-gen cancer immunotherapy. *Cancer Pathogenesis and Therapy* **3**, 309–321 (2025).

55. Niu, D., Wu, Y. & Lian, J. Circular RNA vaccine in disease prevention and treatment. *Sig Transduct Target Ther* **8**, 341 (2023).

56. Yu, L.-L. *et al.* CircRNAs in tumor immunity and immunotherapy: Perspectives from innate and adaptive immunity. *Cancer Letters* **564**, 216219 (2023).

57. Oliver, P. L. & Hill, A. C. Model selection in preclinical nucleic acid therapeutics research. *Commun Biol* **9**, 200 (2026).

58. Larrue, R. *et al.* miR-92a-3p regulates cisplatin-induced cancer cell death. *Cell Death Dis* **14**, 603 (2023).

59. Lee, S. J. *et al.* hsa-miR-CHA2, a novel microRNA, exhibits anticancer effects by suppressing cyclin E1 in human non-small cell lung cancer cells. *Biochimica et Biophysica Acta (BBA) - Molecular Basis of Disease* **1870**, 167250 (2024).

60. Han, X. & Lv, C. MiRNA-21 promotes the migration and proliferation of prostate cancer cells via activating the JAK/STAT pathway. *Discov Onc* **16**, 162 (2025).

61. Yahya, S. M. M. *et al.* Restoring microRNA-34a overcomes acquired drug resistance and disease progression in human breast cancer cell lines via suppressing the ABCC1 gene. *Breast Cancer Res Treat* **204**, 133–149 (2024).

62. Ni, N. *et al.* Antisense oligonucleotide targeting TARDBP-EGFR splicing axis inhibits progression of oral squamous cell carcinoma through ABCA1-regulated cholesterol efflux. *Int J Oral Sci* **18**, 10 (2026).

63. Arshad, M. *et al.* Neratinib could be effective as monotherapy or in combination with trastuzumab in HER2-low breast cancer cells and organoid models. *Br J Cancer* **130**, 1990–2002 (2024).

64. Yuen, J. G. *et al.* Development of gemcitabine-modified miRNA mimics as cancer therapeutics for pancreatic ductal adenocarcinoma. *Molecular Therapy: Oncology* **32**, 200769 (2024).

65. Huang, C. *et al.* Delivery of Engineered Primary Tumor-Derived Exosomes Effectively Suppressed the Colorectal Cancer Chemoresistance and Liver Metastasis. *ACS Nano* **17**, 10313–10326 (2023).

66. Khojastehpour, S. *et al.* Reduced Cish expression by siRNA knockdown in Natural Killer cells promotes anti-tumor effects against gastric cancer cell lines. *Discov Onc* **16**, 1004 (2025).

67. Di Martino, M. T., Tagliaferri, P. & Tassone, P. MicroRNA in cancer therapy: breakthroughs and challenges in early clinical applications. *J Exp Clin Cancer Res* **44**, 126 (2025).

68. Peng, K., Zhao, X., Fu, Y.-X. & Liang, Y. Eliciting antitumor immunity via therapeutic cancer vaccines. *Cell Mol Immunol* **22**, 840–868 (2025).

69. Yaremenko, A. V., Khan, M. M., Zhen, X., Tang, Y. & Tao, W. Clinical advances of mRNA vaccines for cancer immunotherapy. *Med* **6**, 100562 (2025).

70. Lin, Y.-X. *et al.* Reactivation of the tumor suppressor PTEN by mRNA nanoparticles enhances antitumor immunity in preclinical models. *Sci. Transl. Med.* **13**, eaba9772 (2021).

71. Deng, Z. *et al.* An OX40L mRNA vaccine inhibits the growth of hepatocellular carcinoma. *Front. Oncol.* **12**, 975408 (2022).

72. Ren, Y. *et al.* Circular RNA as a source of neoantigens for cancer vaccines. *J Immunother Cancer* **12**, e008402 (2024).

73. Wang, R. *et al.* An epitope-directed mRNA vaccine inhibits tumor metastasis through the blockade of MICA/B α1/2 shedding. *Cell Reports Medicine* **6**, 101981 (2025).

74. Aksoy, S. A. *et al.* Organoids, tissue slices and organotypic cultures: Advancing our understanding of pancreatic ductal adenocarcinoma through in vitro and ex vivo models. *Seminars in Cancer Biology* **109**, 10–24 (2025).

75. Tieu, T. *et al.* Patient-Derived Prostate Cancer Explants: A Clinically Relevant Model to Assess siRNA-Based Nanomedicines. *Adv Healthcare Materials* **10**, 2001594 (2021).

76. Tong, L. *et al.* Patient-derived organoids in precision cancer medicine. *Med* **5**, 1351–1377 (2024).

77. Sokolova, V., Rojas-Sánchez, L., Białas, N., Schulze, N. & Epple, M. Calcium phosphate nanoparticle-mediated transfection in 2D and 3D mono- and co-culture cell models. *Acta Biomaterialia* **84**, 391–401 (2019).

78. Nayak, P., Bentivoglio, V., Varani, M. & Signore, A. Three-Dimensional In Vitro Tumor Spheroid Models for Evaluation of Anticancer Therapy: Recent Updates. *Cancers* **15**, 4846 (2023).

79. Abolhassani, H. *et al.* Nanobiotechnological approaches for breast cancer Management: Drug delivery systems and 3D In-Vitro models. *Coordination Chemistry Reviews* **508**, 215754 (2024).

80. Lu, H. & Stenzel, M. H. Multicellular Tumor Spheroids (MCTS) as a 3D In Vitro Evaluation Tool of Nanoparticles. *Small* **14**, 1702858 (2018).

81. Shi, H. *et al.* 3-Dimensional mesothelioma spheroids provide closer to natural pathophysiological tumor microenvironment for drug response studies. *Front. Oncol.* **12**, 973576 (2022).

82. Park, B. *et al.* Advances in organoid-on-a-chip for recapitulation of human physiological events. *Materials Today* **84**, 75–94 (2025).

83. Wang, T., Wang, L., Wang, G. & Zhuang, Y. Leveraging and manufacturing in vitro multicellular spheroid-based tumor cell model as a preclinical tool for translating dysregulated tumor metabolism into clinical targets and biomarkers. *Bioresour. Bioprocess.* **7**, 35 (2020).

84. Lopez-Vince, E., Simon-Yarza, T. & Wilhelm, C. A polysaccharide-based hydrogel platform for tumor spheroid production and anticancer drug screening. *Sci Rep* **15**, 4213 (2025).

85. Tahara, S. *et al.* Comparison of three-dimensional cell culture techniques of dedifferentiated liposarcoma and their integration with future research. *Front. Cell Dev. Biol.* **12**, 1362696 (2024).

86. Flörkemeier, I. *et al.* Multicellular ovarian cancer spheroids: novel 3D model to mimic tumour complexity. *Sci Rep* **14**, 23526 (2024).

87. Nazari, S. S. Generation of 3D Tumor Spheroids with Encapsulating Basement Membranes for Invasion Studies. *CP Cell Biology* **87**, e105 (2020).

88. Zhao, G. *et al.* Peptide-Modified Lipid Nanoparticles Boost the Antitumor Efficacy of RNA Therapeutics. *ACS Nano* **19**, 13685–13704 (2025).

89. Gilles, M.-E. *et al.* Personalized RNA Medicine for Pancreatic Cancer. *Clinical Cancer Research* **24**, 1734–1747 (2018).

90. Phung, C. D. *et al.* Combination of KRAS ASO and RIG-I agonist in extracellular vesicles transforms the tumor microenvironment towards effective treatment of KRAS-dependent cancers. *Theranostics* **15**, 6818–6838 (2025).

91. Guillen, K. P. *et al.* A human breast cancer-derived xenograft and organoid platform for drug discovery and precision oncology. *Nat Cancer* **3**, 232–250 (2022).

92. Mercadante, M. *et al.* Large scale quantification of natural killer cell-induced apoptosis in patient-derived organoids reveals intratumoral response heterogeneity. *npj Precis. Onc.* **10**, 48 (2025).

93. Sharpe, B. P. *et al.* Patient-derived tumor organoid and fibroblast assembloid models for interrogation of the tumor microenvironment in esophageal adenocarcinoma. *Cell Reports Methods* **4**, 100909 (2024).

94. Lee, M. *et al.* Modeling the metastatic tumor microenvironment: a co-culture platform of lung cancer and blood vessel organoids for drug evaluation. *Sci Rep* **15**, 45252 (2025).

95. Lo, J. H. *et al.* iRGD-guided Tumor-penetrating Nanocomplexes for Therapeutic siRNA Delivery to Pancreatic Cancer. *Molecular Cancer Therapeutics* **17**, 2377–2388 (2018).

96. Liu, L., Wang, G., Zhang, Y., Shi, B. & Li, M. High-Throughput Generation of Tumor Spheroids via Droplet Microfluidics for siRNA-Loaded Nanomedicine Assessment. *Adv Healthcare Materials* e03604 (2026) doi:10.1002/adhm.202503604.

97. Tang, X.-Y. *et al.* Human organoids in basic research and clinical applications. *Sig Transduct Target Ther* **7**, 168 (2022).

98. Küstermann, C. *et al.* iPSC-derived lung and lung cancer organoid model to evaluate cisplatin encapsulated autologous iPSC-derived mesenchymal stromal cell-isolated extracellular vesicles. *Stem Cell Res Ther* **15**, 246 (2024).

99. Xu, S. *et al.* Lung-targeted RNA delivery systems: strategies and therapeutic applications. *J Nanobiotechnol* **24**, 142 (2026).

100. Qin, H. *et al.* piRNA28846 has the potential to be a novel RNA nucleic acid drug for ovarian cancer. *npj Precis. Onc.* **9**, 65 (2025).

101. Cao, L. *et al.* Triblock polymer PDMAEMA-co-PNIPAM-co-PMPC to deliver siKRAS for gene therapy in pancreatic cancer. *Chemical Engineering Journal* **485**, 149884 (2024).

102. Xiong, Y. *et al.* Small Activating RNA Modulation of the G Protein-Coupled Receptor for Cancer Treatment. *Advanced Science* **9**, 2200562 (2022).

103. Dhumal, D. *et al.* An ionizable supramolecular dendrimer nanosystem for effective siRNA delivery with a favorable safety profile. *Nano Res.* **14**, 2247–2254 (2021).

104. Wan, L. *et al.* Screening Splice-Switching Antisense Oligonucleotides in Pancreas-Cancer Organoids. *Nucleic Acid Therapeutics* **34**, 188–198 (2024).

105. Zhang, Q. *et al.* Novel STAT3 oligonucleotide compounds suppress tumor growth and overcome the acquired resistance to sorafenib in hepatocellular carcinoma. *Acta Pharmacol Sin* **45**, 1701–1714 (2024).

106. Jiang, T. *et al.* Targeting lncRNA DDIT4-AS1 Sensitizes Triple Negative Breast Cancer to Chemotherapy via Suppressing of Autophagy. *Advanced Science* **10**, 2207257 (2023).

107. Leclair, N. K. *et al.* Antisense oligonucleotide-mediated TRA2β poison exon inclusion induces the expression of a lncRNA with anti-tumor effects. *Nat Commun* **16**, 1670 (2025).

108. Chen, X. *et al.* A patient-derived organoid-based study identified an ASO targeting SNORD14E for endometrial cancer through reducing aberrant FOXM1 Expression and β-catenin nuclear accumulation. *J Exp Clin Cancer Res* **42**, 230 (2023).

109. Hsu, J. *et al.* A T cell receptor β chain–directed antibody fusion molecule activates and expands subsets of T cells to promote antitumor activity. *Sci. Transl. Med.* **15**, eadi0258 (2023).

110. Votanopoulos, K. I. *et al.* Model of Patient-Specific Immune-Enhanced Organoids for Immunotherapy Screening: Feasibility Study. *Ann Surg Oncol* **27**, 1956–1967 (2020).

111. Grebenyuk, S. *et al.* Large-scale perfused tissues via synthetic 3D soft microfluidics. *Nat Commun* **14**, 193 (2023).

112. Beckers, C., Vasilikos, L., Moor, L. & Pruschy, M. Live-cell imaging and analysis of 3D spheroids in hypoxia- and radiotherapy-related research. *Clinical and Translational Radiation Oncology* **51**, 100920 (2025).

113. Lee, H. J. *et al.* Single-cell multiomic modelling of early metastatic events promoted by the extracellular matrix. *Br J Cancer* **133**, 1708–1719 (2025).

114. Haughton, P. D. *et al.* Differential transcriptional invasion signatures from patient derived organoid models define a functional prognostic tool for head and neck cancer. *Oncogene* **43**, 2463–2474 (2024).

115. Long, F. *et al.* Intergenic CircRNA *Circ_0007379* Inhibits Colorectal Cancer Progression by Modulating *miR-320a* Biogenesis in a KSRP-Dependent Manner. *Int. J. Biol. Sci.* **19**, 3781–3803 (2023).

116. Zhou, T. *et al.* CD64^{+} fibroblast-targeted vilanterol and a STING agonist augment CLDN18.2 BiTEs efficacy against pancreatic cancer by reducing desmoplasia and enriching stem-like CD8^{+} T cells. *Gut* **73**, 1984–1998 (2024).

117. Ding, S. *et al.* Patient-derived micro-organospheres enable clinical precision oncology. *Cell Stem Cell* **29**, 905-917.e6 (2022).

118. Subtil, B. *et al.* Dendritic cell phenotype and function in a 3D co-culture model of patient-derived metastatic colorectal cancer organoids. *Front. Immunol.* **14**, 1105244 (2023).

119. Reischer, A. *et al.* Targeted CD47 checkpoint blockade using a mesothelin-directed antibody construct for enhanced solid tumor-specific immunotherapy. *Cancer Immunol Immunother* **74**, 214 (2025).

120. Plebanek, M. P. *et al.* A lactate-SREBP2 signaling axis drives tolerogenic dendritic cell maturation and promotes cancer progression. *Sci. Immunol.* **9**, eadi4191 (2024).

121. Turpin, R. *et al.* Respiratory complex I regulates dendritic cell maturation in explant model of human tumor immune microenvironment. *J Immunother Cancer* **12**, e008053 (2024).

122. Neal, J. T. *et al.* Organoid Modeling of the Tumor Immune Microenvironment. *Cell* **175**, 1972-1988.e16 (2018).

123. Li, K. *et al.* An organoid co-culture model for probing systemic anti-tumor immunity in lung cancer. *Cell Stem Cell* **32**, 1218-1234.e7 (2025).

124. Elhanani, O., Ben-Uri, R. & Keren, L. Spatial profiling technologies illuminate the tumor microenvironment. *Cancer Cell* **41**, 404–420 (2023).

125. Mo, S. *et al.* Patient-Derived Organoids from Colorectal Cancer with Paired Liver Metastasis Reveal Tumor Heterogeneity and Predict Response to Chemotherapy. *Advanced Science* **9**, 2204097 (2022).

126. Ma, S. *et al.* Lamination-based organoid spatially resolved transcriptomics technique for primary lung and liver organoid characterization. *Proc. Natl. Acad. Sci. U.S.A.* **121**, e2408939121 (2024).

127. Abdullah, H. *et al.* Kidney tumoroid characterisation by spatial mass spectrometry with same-section multiplex immunofluorescence uncovers tumour microenvironment lipid signatures associated with aggressive tumour phenotypes. *npj Imaging* **3**, 43 (2025).

128. Ong, H. T. *et al.* Digitalized organoids: integrated pipeline for high-speed 3D analysis of organoid structures using multilevel segmentation and cellular topology. *Nat Methods* **22**, 1343–1354 (2025).

129. Kumar, S. *et al.* siRNA-based therapeutic candidate targeting PRDM2 for inhibition of lung cancer progression. *Biomedicine & Pharmacotherapy* **193**, 118807 (2025).

130. Moll, M. & Baumjohann, D. Boosting human immunology: harnessing the potential of immune organoids. *EMBO Mol Med* **17**, 385–394 (2025).

131. Wagar, L. E. *et al.* Modeling human adaptive immune responses with tonsil organoids. *Nat Med* **27**, 125–135 (2021).

132. Jeger-Madiot, R. *et al.* Modeling memory B cell responses in a lymphoid organ-chip to evaluate mRNA vaccine boosting. *Journal of Experimental Medicine* **221**, e20240289 (2024).

133. Shenoy, G. N. *et al.* Abstract 3472: STX-003: cancer immunotherapy with systemic delivery of mRNA utilizing programmable genetic circuits for precise regulation of IL-12 expression and reduced toxicity. *Cancer Research* **85**, 3472–3472 (2025).

134. Wang, W. *et al.* Tumor-Specific CircRNA-Derived Antigen Peptide Identification for Hepatobiliary Tumors. *Engineering* **22**, 159–170 (2023).

135. Shi, X. *et al.* Circular RNA ANAPC7 Inhibits Tumor Growth and Muscle Wasting via PHLPP2–AKT–TGF-β Signaling Axis in Pancreatic Cancer. *Gastroenterology* **162**, 2004-2017.e2 (2022).

136. Xiang, D. *et al.* Building consensus on the application of organoid-based drug sensitivity testing in cancer precision medicine and drug development. *Theranostics* **14**, 3300–3316 (2024).

137. Song, X. *et al.* Organoids in drug development: from predictive models to regulatory integration. *Drug Discovery Today* **31**, 104608 (2026).

138. Planchak, S., Hernandez Moyers, A., Chen, Y., Lockwood, O. & Tripathi, A. Comparative Evaluation of HepG2 Spheroid Generation Methods for Toxicology. *Cel. Mol. Bioeng.* https://doi.org/10.1007/s12195-026-00894-1 (2026) doi:10.1007/s12195-026-00894-1.

139. Zhou, C. *et al.* Standardization of organoid culture in cancer research. *Cancer Medicine* **12**, 14375–14386 (2023).

140. Aksoy, E. K. *et al.* Abstract 87: Integrated pipeline for immuno-oncology drug testing: from patient-derived organoid assays with reconstituted TME to fresh ex vivo patient tissue cultures. *Cancer Research* **84**, 87–87 (2024).

141. Yao, Y. *et al.* Patient-Derived Organoids Predict Chemoradiation Responses of Locally Advanced Rectal Cancer. *Cell Stem Cell* **26**, 17-26.e6 (2020).

142. Smabers, L. P. *et al.* Patient-Derived Organoids Predict Treatment Response in Metastatic Colorectal Cancer. *Clinical Cancer Research* **31**, 5015–5026 (2025).

143. Zuo, J., Fang, Y., Wang, R. & Liang, S. High-throughput solutions in tumor organoids: from culture to drug screening. *Stem Cells* **43**, sxae070 (2025).

144. Betge, J. *et al.* The drug-induced phenotypic landscape of colorectal cancer organoids. *Nat Commun* **13**, 3135 (2022).

145. Alagesan, B. *et al.* A Phase II Trial of an Extended-Release siRNA Implant Targeting *KRAS* G12D/V in Locally Advanced Pancreatic Cancer. *Clinical Cancer Research* **32**, 1059–1067 (2026).

146. US National Library of Medicine. *Ph. 1, Evaluation of Safety, Tolerability, PK, Anti-Tumor Activity of STP707 IV in Subjects With Solid Tumors*. https://clinicaltrials.gov/study/NCT05037149 (2024).

147. Reddy, R. A. *et al.* EphA2 siRNA in DOPC nanoliposomes (EPHARNA): A phase I clinical trial in patients with solid tumors. *JCO* **43**, 3086–3086 (2025).

148. US National Library of Medicine. *AZD9150 Plus Durvalumab Alone or in Combination With Chemotherapy in Patients With Advanced, Solid Tumours and in Patients With Non-Small-Cell Lung Cancer*. https://clinicaltrials.gov/study/NCT03421353 (2024).

149. Tang, C. *et al.* Preclinical study and parallel phase II trial evaluating antisense STAT3 oligonucleotide and checkpoint blockade for advanced pancreatic, non-small cell lung cancer and mismatch repair-deficient colorectal cancer. *bmjonc* **3**, e000133 (2024).

150. US National Library of Medicine. *Study to Assess MEDI4736 With Either AZD9150 or AZD5069 in Advanced Solid Tumors & Relapsed Metastatic Squamous Cell Carcinoma of Head & Neck*. https://clinicaltrials.gov/study/NCT02499328 (2025).

151. Siu, L. L. *et al.* AZD8701, an Antisense Oligonucleotide Targeting FOXP3 mRNA, as Monotherapy and in Combination with Durvalumab: A Phase I Trial in Patients with Advanced Solid Tumors. *Clinical Cancer Research* **31**, 1449–1462 (2025).

152. Trabedersen (OT-101) With Pembrolizumab for Newly Diagnosed PD-L1–Positive Metastatic NSCLC. *ONCOLOGY* 436–437 (2025) doi:10.46883/2025.25921056.

153. US National Library of Medicine. *A Study of OT-101 With mFOLFIRINOX in Patients With Advanced and Unresectable or Metastatic Pancreatic Cancer (STOP-PC)*. https://clinicaltrials.gov/study/NCT06079346 (2024).

154. Weber, J. S. *et al.* Individualised neoantigen therapy mRNA-4157 (V940) plus pembrolizumab versus pembrolizumab monotherapy in resected melanoma (KEYNOTE-942): a randomised, phase 2b study. *The Lancet* **403**, 632–644 (2024).

155. Weber, J. S. *et al.* INTerpath-001: Pembrolizumab with V940 (mRNA-4157) versus pembrolizumab with placebo for adjuvant treatment of high-risk stage II-IV melanoma. *JCO* **42**, TPS9616–TPS9616 (2024).

156. Sethna, Z. *et al.* RNA neoantigen vaccines prime long-lived CD8+ T cells in pancreatic cancer. *Nature* **639**, 1042–1051 (2025).

157. US National Library of Medicine. *A Study of the Efficacy and Safety of Adjuvant Autogene Cevumeran Plus Atezolizumab and mFOLFIRINOX Versus mFOLFIRINOX Alone in Participants With Resected PDAC (IMCODE003)*. https://clinicaltrials.gov/study/NCT05968326 (2026).

158. US National Library of Medicine. *Dose Escalation Study of mRNA-2752 for Intratumoral Injection to Participants in Advanced Malignancies*. https://clinicaltrials.gov/study/NCT03739931 (2025).

159. US National Library of Medicine. *A Single Arm Clinical Study of Dendritic Cell Vaccine Loaded With Circular RNA Encoding Cryptic Peptide for Patients With HER2-Negative Advanced Breast Cancer*. https://clinicaltrials.gov/study/NCT06530082 (2024).

Chapter 4. Integrated Discussion: From Model Architecture to Mechanistic Relevance

The central conclusion of this thesis is that three-dimensional in vitro models should not be treated as interchangeable technical upgrades over two-dimensional culture, but as experimental systems whose architecture directly shapes biological readout and translational interpretation. The two chapters approach this conclusion from different directions. Chapter 2 addresses the issue experimentally through a controlled comparison of HepG2 spheroid-generation methods, showing that distinct 3D platforms produce different morphological and functional outcomes even when built from the same cell line. Chapter 3 addresses the issue conceptually by examining organoid-based potency assays for RNA therapeutics in solid tumors and by defining clinically relevant potency as the measurement of dose-response behavior under the barriers and interactions that are rate-limiting for therapeutic performance. Together, these chapters argue that the value of a model lies not in its nominal complexity, but in whether its architecture captures the specific biological constraint that matters for the question being asked.

One of the clearest messages from the HepG2 study is that 3D model design itself is an independent experimental variable. The comparison of agarose gels, microwell and single-well ULA plates, and hanging drops showed that morphology, reproducibility, throughput, and hepatocyte-like output do not move together as a single package. In particular, 35-microwell agarose gels yielded the most circular spheroids and, among the multi-spheroid formats functionally assessed, produced the strongest albumin and ATP outputs, yet no method simultaneously optimized repeatability, throughput, and functional robustness. The practical consequence is important: if different formation methods generate measurably different biological states, then “using a spheroid model” is not a sufficient methodological description. The platform is part of the biological result. This is especially relevant in liver toxicology and disease modeling, where the predictive value of a model depends on architecture-dependent properties such as diffusion behavior, compaction, and maintenance of hepatocyte-like function.

The RNA-organoid review from Chapter 3 extends this logic beyond hepatic spheroid culture and places it in a broader framework for therapeutic evaluation. In that chapter, potency is separated into molecular potency, cellular/phenotypic potency, and clinically relevant potency. This distinction is more than semantic. It clarifies that different models answer different parts of the same therapeutic cascade. Conventional 2D assays remain highly effective for questions of target engagement, proximal pathway modulation, and early phenotypic effects under controlled exposure. However, they are structurally poor at capturing the barriers that dominate many failures in solid tumors, including 3D diffusion distances, extracellular matrix, heterogeneous local exposure, and immune or stromal context. The review therefore argues that organoid-based systems are most valuable not because they are "closer to in vivo" in a vague sense, but because they can preserve exactly those human-biology-relevant constraints that determine whether an observed molecular effect remains functionally meaningful under more realistic conditions.

When considered together, chapters 2 and 3 support a common principle: biological relevance depends on mechanistic alignment between model architecture and experimental purpose. In the HepG2 chapter (Chapter 2), this means recognizing that a platform chosen for accessibility or throughput may not be the one that best preserves function, while a platform chosen for more favorable biological output may be limited by assay compatibility, technical burden, or scale. In the RNA potency chapter (Chapter 3), the same principle appears in a more general form. Some questions are best answered in 2D, particularly when the limiting step is sequence-dependent target modulation under uniform exposure. Other questions require escalation into 3D because the limiting step is not target engagement itself, but whether activity survives delivery barriers, matrix constraints, tissue heterogeneity, or multicellular microenvironmental interactions. In both cases, the mistake is the same: assuming that model class alone determines relevance. It does not. Relevance emerges when the model is matched to the bottleneck.

This thesis therefore argues for a strategy of selective complexity rather than reflexive complexity. The goal should not be to replace all 2D assays with organoids or to treat every 3D culture system as intrinsically

superior. Such a position would be neither practical nor scientifically disciplined. 2D systems remain indispensable because they are standardized, scalable, and well suited for early pharmacology. At the same time, the review shows clearly that organoid-based RNA potency assays are still often underdeveloped: many remain single-dose, qualitative, or semi-quantitative; 3D dose-response metrics are rare; and target knockdown or pathway modulation is frequently confirmed only in 2D rather than inside the 3D tissue itself. That means the appropriate future direction is not universal organoid adoption, but a more rigorous escalation logic in which each platform is introduced because it reveals a failure mode or mechanistic constraint that simpler systems cannot.

A major implication of this work is methodological. Across both Chapter 2 and Chapter 3, the challenge is not only biological fidelity but also standardization without conceptual oversimplification. The HepG2 study demonstrates the need for more explicit reporting and benchmarking of formation method, geometry, assay compatibility, and functional output in 3D liver models. The review similarly argues that organoid-based potency workflows need better alignment across stages, including matched molecular and functional readouts, more formal 3D dose-response parameterization, and clearer definitions of what the model is intended to test. In this sense, standardization should not mean forcing all systems into one universal template. Instead, it should mean making model choice explicit, justified, and comparable. A standardized field is not one in which every model is the same; it is one in which differences are understood, measured, and connected to the scientific question.

These findings also point toward a more disciplined translational philosophy for preclinical bioengineering. In vitro systems have often been evaluated according to an implicit hierarchy in which additional complexity is assumed to bring a model closer to truth. This thesis suggests a different view. Complexity is useful only when it makes the right variable experimentally visible. For HepG2 spheroids, that variable may be geometry-dependent function, compaction, or future xenobiotic-response competence. For RNA therapeutics in solid tumors, it may be penetration, spatial distribution, cell-type-specific expression, or

local immune and stromal response. A model that captures the wrong complexity may be more expensive, harder to interpret, and no more informative than a simpler assay. Conversely, a deliberately chosen 3D system that preserves the rate-limiting barrier may provide uniquely decision-relevant information even if it remains incomplete as a representation of the whole organism.

Several limitations remain. The HepG2 study (Chapter 2) was necessarily bounded by available readouts, assay cost, and technical constraints, including limited functional replication and incomplete visualization of internal spheroid architecture. The review chapter (Chapter 3) likewise shows that much of the current literature still consists of only partial implementations of clinically relevant potency testing. These limitations do not weaken the thesis-level argument; they sharpen it. In both chapters, the difficulty lies in moving from qualitative appreciation of 3D relevance to quantitatively interpretable, mechanism-matched workflows. That transition is still incomplete, but the evidence assembled here suggests that it is both necessary and tractable.

In conclusion, this thesis proposes a unified view of 3D in vitro systems across two seemingly different domains. The HepG2 chapter (Chapter 2) shows that platform choice changes what is measured. The review chapter on RNA-organoid-potency axis (Chapter 3) shows that potency itself must be interpreted in layers, and that the clinically relevant potency layer appears only when the model preserves the barriers that truly limit performance. The integrated lesson is straightforward but important: model architecture is not an accessory to biological interpretation; it is one of its determinants. More rigorous preclinical inference will therefore depend not on using more complex models by default, but on designing and selecting models whose architecture is explicitly matched to the mechanism, bottleneck, and translational question under study.